Volume 15, Number 4, 2015 ISSN 1562-8353

NONLINEAR DYNAMICS AND SYSTEMS THEORY
An International Journal of Research and Surveys

Volume 15 Number 4 2015

CONTENTS

© 2015, InforMath Publishing Group ISSN 1562-8353 Printed in Ukraine
To receive contents and abstracts by e-mail, visit our Website at: **http://www.e-ndst.kiev.ua**

NONLINEAR DYNAMICS & SYSTEMS THEORY

Volume 15, No. 4, 2015

Nonlinear Dynamics and Systems Theory

An International Journal of Research and Surveys

EDITOR-IN-CHIEF A.A.MARTYNYUK
S.P.Timoshenko Institute of Mechanics
National Academy of Sciences of Ukraine, Kiev, Ukraine

REGIONAL EDITORS

P.BORNE, Lille, France
Europe

M.BOHNER, Rolla, USA
North America

T.A.BURTON, Port Angeles, USA
C.CRUZ-HERNANDEZ, Ensenada, Mexico
USA, Central and South America

AI-GUO WU, Harbin, China
China and South East Asia

K.L.TEO, Perth, Australia
Australia and New Zealand

InforMath Publishing Group
http://www.e-ndst.kiev.ua

Nonlinear Dynamics and Systems Theory

An International Journal of Research and Surveys

EDITOR-IN-CHIEF A.A.MARTYNYUK

The S.P.Timoshenko Institute of Mechanics, National Academy of Sciences of Ukraine,
Nesterov Str. 3, 03680 MSP, Kiev-57, UKRAINE / e-mail: anmart@stability.kiev.ua
e-mail: amartynyuk@voliacable.com

MANAGING EDITOR I.P.STAVROULAKIS

Department of Mathematics, University of Ioannina
451 10 Ioannina, HELLAS (GREECE) / e-mail: ipstav@cc.uoi.gr

REGIONAL EDITORS

AI-GUO WU (China), e-mail: agwu@163.com
P.BORNE (France), e-mail: Pierre.Borne@ec-lille.fr
M.BOHNER (USA), e-mail: bohner@mst.edu
T.A.BURTON (USA), e-mail: taburton@olypen.com
C. CRUZ-HERNANDEZ (Mexico), e-mail: ccruz@cicese.mx
K.L.TEO (Australia), e-mail: K.L.Teo@curtin.edu.au

EDITORIAL BOARD

Ahmed N.U. (Canada)
Aleksandrov, A.Yu. (Russia)
Artstein, Z. (Israel)
Awrejcewicz J. (Poland)
Bajodah, A.H. (Saudi Arabia)
Benrejeb M. (Tunisia)
Bevilaqua, R. (USA)
Braiek, N.B. (Tunisia)
Chen Ye-Hwa (USA)
Corduneanu, C. (USA)
D'Anna, A. (Italy)
De Angelis, M. (Italy)
Dshalalow, J.H. (USA)
Eke, F.O. (USA)
Enciso G. (USA
Fabrizio, M. (Italy)
Georgiou, G. (Cyprus)
Guang-Ren Duan (China)
Honglei Xu (Australia)
Izobov, N.A. (Belarussia)
Karimi, H.R. (Norway)
Khusainov, D.Ya. (Ukraine)
Kloeden, P. (Germany)
Kokologiannaki, C. (Greece)
Kuznetsov, N.V. (Finland)
Lazar, M. (The Netherlands)
Leonov, G.A. (Russia)
Limarchenko, O.S. (Ukraine)
Lopez-Gutieres, R.M. (Mexico)
Nguang Sing Kiong (New Zealand)
Okninski, A. (Poland)
Peng Shi (Australia)
Peterson, A. (USA)
Rushchitsky, J.J. (Ukraine)
Shi Yan (Japan)
Siljak, D.D. (USA)
Sree Hari Rao, V. (India)
Stavrakakis, N.M. (Greece)
Vassilyev, S.N. (Russia)
Vatsala, A. (USA)
Wang Hao (Canada)

ADVISORY EDITOR

A.G.MAZKO, Kiev, Ukraine
e-mail: mazko@imath.kiev.ua

ADVISORY COMPUTER SCIENCE EDITORS

A.N.CHERNIENKO and L.N.CHERNETSKAYA, Kiev, Ukraine

ADVISORY LINGUISTIC EDITOR

S.N.RASSHYVALOVA, Kiev, Ukraine

© 2015, InforMath Publishing Group, ISSN 1562-8353 print, ISSN 1813-7385 online, Printed in Ukraine
No part of this Journal may be reproduced or transmitted in any form or by any means without permission from InforMath Publishing Group.

INSTRUCTIONS FOR CONTRIBUTORS

(1) General. Nonlinear Dynamics and Systems Theory (ND&ST) is an international journal devoted to publishing peer-refereed, high quality, original papers, brief notes and review articles focusing on nonlinear dynamics and systems theory and their practical applications in engineering, physical and life sciences. Submission of a manuscript is a representation that the submission has been approved by all of the authors and by the institution where the work was carried out. It also represents that the manuscript has not been previously published, has not been copyrighted, is not being submitted for publication elsewhere, and that the authors have agreed that the copyright in the article shall be assigned exclusively to InforMath Publishing Group by signing a transfer of copyright form. Before submission, the authors should visit the website:

http://www.e-ndst.kiev.ua

for information on the preparation of accepted manuscripts. Please download the archive Sample_NDST.zip containing example of article file (you can edit only the file Samplefilename.tex).

(2) Manuscript and Correspondence. Manuscripts should be in English and must meet common standards of usage and grammar. To submit a paper, send by e-mail a file in PDF format directly to

Professor A.A. Martynyuk, Institute of Mechanics,
Nesterov str.3, 03057, MSP 680, Kiev-57, Ukraine
e-mail: anmart@stability.kiev.ua; center@inmech.kiev.ua

or to one of the Regional Editors or to a member of the Editorial Board. Final version of the manuscript must typeset using LaTex program which is prepared in accordance with the style file of the Journal. Manuscript texts should contain the title of the article, name(s) of the author(s) and complete affiliations. Each article requires an abstract not exceeding 150 words. Formulas and citations should not be included in the abstract. AMS subject classifications and key words must be included in all accepted papers. Each article requires a running head (abbreviated form of the title) of no more than 30 characters. The sizes for regular papers, survey articles, brief notes, letters to editors and book reviews are: (i) 10-14 pages for regular papers, (ii) up to 24 pages for survey articles, and (iii) 2-3 pages for brief notes, letters to the editor and book reviews.

(3) Tables, Graphs and Illustrations. Each figure must be of a quality suitable for direct reproduction and must include a caption. Drawings should include all relevant details and should be drawn professionally in black ink on plain white drawing paper. In addition to a hard copy of the artwork, it is necessary to attach the electronic file of the artwork (preferably in PCX format).

(4) References. References should be listed alphabetically and numbered, typed and punctuated according to the following examples. Each entry must be cited in the text in form of author(s) together with the number of the referred article or in the form of the number of the referred article alone.

Journal: [1] Poincare, H. Title of the article. *Title of the Journal* **Vol. l** (No.l), Year, Pages. [Language]
Book: [2] Liapunov, A.M. *Title of the book.* Name of the Publishers, Town, Year.
Proceeding: [3] Bellman, R. Title of the article. In: *Title of the book.* (Eds.). Name of the Publishers, Town, Year, Pages. [Language]

(5) Proofs and Sample Copy. Proofs sent to authors should be returned to the Editorial Office with corrections within three days after receipt. The corresponding author will receive a sample copy of the issue of the Journal for which his/her paper is published.

(6) Editorial Policy. Every submission will undergo a stringent peer review process. An editor will be assigned to handle the review process of the paper. He/she will secure at least two reviewers' reports. The decision on acceptance, rejection or acceptance subject to revision will be made based on these reviewers' reports and the editor's own reading of the paper.

NONLINEAR DYNAMICS AND SYSTEMS THEORY
An International Journal of Research and Surveys
Published by InforMath Publishing Group since 2001

Volume 15 Number 4 2015

CONTENTS

Founded by A.A. Martynyuk in 2001.
Registered in Ukraine Number: KB 5267 / 04.07.2001.

NONLINEAR DYNAMICS AND SYSTEMS THEORY

An International Journal of Research and Surveys

Impact Factor from SCOPUS for 2013: SNIP – 1.108, IPP – 0.809, SJR – 0.496

Nonlinear Dynamics and Systems Theory (ISSN 1562–8353 (Print), ISSN 1813–7385 (Online)) is an international journal published under the auspices of the S.P. Timoshenko Institute of Mechanics of National Academy of Sciences of Ukraine and Curtin University of Technology (Perth, Australia). It aims to publish high quality original scientific papers and surveys in areas of nonlinear dynamics and systems theory and their real world applications.

AIMS AND SCOPE

Nonlinear Dynamics and Systems Theory is a multidisciplinary journal. It publishes papers focusing on proofs of important theorems as well as papers presenting new ideas and new theory, conjectures, numerical algorithms and physical experiments in areas related to nonlinear dynamics and systems theory. Papers that deal with theoretical aspects of nonlinear dynamics and/or systems theory should contain significant mathematical results with an indication of their possible applications. Papers that emphasize applications should contain new mathematical models of real world phenomena and/or description of engineering problems. They should include rigorous analysis of data used and results obtained. Papers that integrate and interrelate ideas and methods of nonlinear dynamics and systems theory will be particularly welcomed. This journal and the individual contributions published therein are protected under the copyright by International InforMath Publishing Group.

PUBLICATION AND SUBSCRIPTION INFORMATION

Nonlinear Dynamics and Systems Theory will have 4 issues in 2016, printed in hard copy (ISSN 1562–8353) and available online (ISSN 1813–7385), by InforMath Publishing Group, Nesterov str., 3, Institute of Mechanics, Kiev, MSP 680, Ukraine, 03057. Subscription prices are available upon request from the Publisher (`mailto:anmart@stability.kiev.ua`), EBSCO Information Services (`mailto:journals@ebsco.com`), or website of the Journal: `http://e-ndst.kiev.ua`. Subscriptions are accepted on a calendar year basis. Issues are sent by airmail to all countries of the world. Claims for missing issues should be made within six months of the date of dispatch.

ABSTRACTING AND INDEXING SERVICES

Papers published in this journal are indexed or abstracted in: Mathematical Reviews / MathSciNet, Zentralblatt MATH / Mathematics Abstracts, PASCAL database (INIST–CNRS) and SCOPUS.

Nonlinear Dynamics and Systems Theory, **15** (4) (2015) 334–343

Synchronization of Dumbbell Satellites: Generalized Hamiltonian Systems Approach

L.O. Arriaga-Camargo [1], R. Martínez-Clark [2], C. Cruz-Hernández [*2], A. Arellano-Delgado [2] and R.M. López-Gutiérrez [3]

[1] *Bonn-Rhein-Sieg University of Applied Sciences, von-Liebig-Straße 20 53359 Rheinbach, Germany.*
[2] *Electronics and Telecommunications Department, Scientific Research and Advanced Studies of Ensenada (CICESE), Km 107, Carretera Tijuana-Ensenada, 22860 Ensenada, BC, Mexico.*
[3] *Engineering Faculty, Baja California Autonomous University (UABC), km 103, Carretera Tijuana-Ensenada, 22860, Ensenada, BC, México.*

Received: July 6, 2015; Revised: October 28, 2015

Abstract: In this paper, the attitude synchronization problem of two dumbbell satellite models is addressed. To achieve this purpose, a synchronization approach based on generalized Hamiltonian systems and state observer design reported in literature, is applied. Potential applications of attitude synchronization are multi-satellites arrays for self assembly structures, and resolution enhancement. Numerical results of the synchronization behavior achievement are presented.

Keywords: *dumbbell satellites; attitude synchronization; generalized Hamiltonian systems; nonlinear observers.*

Mathematics Subject Classification (2010): 34D06, 93B07, 93C10.

1 Introduction

Modern space missions involve the use of multiple small satellites, this scheme introduces several advantages compared to single satellite missions. An interesting topic regarding these missions, is the attitude synchronization of the satellites. This allows to handle larger structures than what can be launched. Some interesting applications include: resolution enhancement, interferometry or, super-sized focal length [1], this behavior is also useful for in-orbit-self-assembly operations [2].

* Corresponding author: mailto:ccruz@cicese.mx

© 2015 InforMath Publishing Group/1562-8353 (print)/1813-7385 (online)/http://e-ndst.kiev.ua

The mathematical model considered in this paper is reported in [3] and corresponds to a dumbbell satellite. This model represents a simple structure consisting of two point masses connected by a mass-less rod. This dumbbell satellite model is suitable for a straightforward investigation of the general properties of the rigid body motion in a gravity field and has attracted the attention of scientists since the middle of the past century [4].

For attitude synchronization of two dumbbell satellites, the approach used in this paper is the generalized Hamiltonian systems and design of nonlinear observer presented in [5] which has been successfully applied in synchronization of chaotic systems, see e.g. [6–11].

The paper is arranged as follows: Section 2 describes briefly the mathematical preliminaries on synchronization of nonlinear oscillators from the perspective of generalized Hamiltonian systems and design of nonlinear observer. Section 3 describes the dumbbell satellite mathematical model used for attitude synchronization purposes. Then, Section 4 presents the attitude synchronization of two dumbbell satellites in master-slave coupling via generalized Hamiltonian forms and state observer design approach. In Section 5, numerical results are discussed and finally some conclusions are given in Section 6.

2 Synchronization Via Generalized Hamiltonian Forms and Observer Design

In this section, briefly we describe the synchronization for two nonlinear dynamical systems via generalized Hamiltonian forms and nonlinear observer design approach, for details see [5].

2.1 Generalized Hamiltonian Systems

Consider the following nonlinear dynamical system described by the state equation

$$\dot{x} = f(x), \qquad x \in \mathbb{R}^n. \tag{1}$$

Following the approach provided in [5], many physical nonliner systems described by equation (1) can be written in the following generalized Hamiltonian canonical form,

$$\dot{\boldsymbol{x}} = \mathcal{J}(\boldsymbol{x}) \frac{\partial H}{\partial x} + \mathcal{S}(\boldsymbol{x}) \frac{\partial H}{\partial x}, \quad x \in \mathbb{R}^n, \tag{2}$$

where $H(x)$ denotes a smooth energy function which is globally positive definite in $\mathbb{R}^n$. The column *gradient vector* of H, denoted by $\partial H/\partial x$, is assumed to exist everywhere. One of the most frequently used functions $H(x)$ is the quadratic energy function of the form

$$H(\boldsymbol{x}) = \frac{1}{2}\boldsymbol{x}^T \mathcal{M} \boldsymbol{x} \tag{3}$$

with $\mathcal{M}$ being a symmetric, positive definite, constant matrix. In such case, $\partial H/\partial x = \mathcal{M}\boldsymbol{x}$**.** The square matrices $\mathcal{J}(\boldsymbol{x})$ and $\mathcal{S}(\boldsymbol{x})$, present in (2), satisfy, for all $x \in \mathbb{R}^n$, the following properties, which represent the energy managing structure of the system:

$$\mathcal{J}(\boldsymbol{x}) + \mathcal{J}^T(\boldsymbol{x}) = 0, \qquad \mathcal{S}(\boldsymbol{x}) = \mathcal{S}^T(\boldsymbol{x}). \tag{4}$$

The vector field $\mathcal{J}(\boldsymbol{x}) \frac{\partial H}{\partial x}$ exhibits the *conservative* part of the system and it is also referred to as the *work-less part*, or *work-less forces* of the system. The matrix $\mathcal{S}(\boldsymbol{x})$

is, in general, a symmetric matrix describing the *working* or *nonconservative* part of the system. For certain systems, the symmetric matrix $\mathcal{S}(\boldsymbol{x})$ is *negative definite* or *negative semidefinite*, in such cases the vector field is known as the *dissipative* part of the system.

Sometimes, specially in the contex of state observer design, the system under observation will be written in the special form

$$\dot{\boldsymbol{x}} = \mathcal{J}(\boldsymbol{x}) \frac{\partial H}{\partial x} + \mathcal{S}(\boldsymbol{x}) \frac{\partial H}{\partial x} + \mathcal{F}(x), \tag{5}$$

where $\mathcal{F}(x)$ represents a locally destabilizing vector field and $\mathcal{S}(\boldsymbol{x})$ is a symmetric matrix, not necesarily of definite sign. However, many physical systems are already in the generalized Hamitlonian canonical form (2).

2.2 Nonlinear Observer Design for a Class of Systems in Generalized Hamiltonian Form

For a complete description of the synchronization method, the reader is encouraged to see [5]. A special class of generalized Hamiltonian systems with destabilizing vector field and linear output map y is given by

$$\begin{aligned} \dot{x} &= \mathcal{J}(y) \tfrac{\partial H}{\partial x} + (\mathcal{I} + \mathcal{S}) \tfrac{\partial H}{\partial x} + \mathcal{F}(y), \qquad x \in \mathbb{R},^n \\ y &= \mathcal{C} \tfrac{\partial H}{\partial x}, \qquad y \in \mathbb{R}^m, \end{aligned} \tag{6}$$

where $\mathcal{S}$ is a *constant symmetric matrix*, not necessarily of definite sign. The matrix $\mathcal{I}$ is a *constant skew symmetric matrix*. The vector variable y is referred to as the *system output*. The matrix $\mathcal{C}$ is a constant matrix.

The estimate of the state vector x is denoted by ξ, and consider the Hamiltonian energy function $H(\xi)$ to be the particularization of H in terms of ξ, similarly, η is the estimated output computed in terms of the estimated state ξ. The gradient vector $\partial H(\xi)/\partial \xi$ is, naturally, of the form $\mathcal{M}\xi$ with $\mathcal{M}$ being a constant symmetric positive definite matrix.

A dynamic nonlinear state observer for the system (6) is obtained as

$$\begin{aligned} \dot{\xi} &= \mathcal{J}(y) \tfrac{\partial H}{\partial \xi} + (\mathcal{I} + \mathcal{S}) \tfrac{\partial H}{\partial \xi} + \mathcal{F}(y) + K(y - \eta), \\ \eta &= C \tfrac{\partial H}{\partial \xi}, \end{aligned} \tag{7}$$

where K is a constant vector, known as the *observer gain*. The *state estimation error*, defined as $e = x - \xi$ and the *output estimation error*, defined as $e_y = y - \eta$, are governed by

$$\begin{aligned} \dot{e} &= \mathcal{J}(y) \tfrac{\partial H}{\partial e} + (\mathcal{I} + \mathcal{S} - \mathcal{K}\mathcal{C}) \tfrac{\partial H}{\partial e}, \qquad e \in \mathbb{R}^n, \\ e_y &= C \tfrac{\partial H}{\partial e}, \qquad e_y \in \mathbb{R}^m, \end{aligned} \tag{8}$$

where the vector $\partial H(e)/\partial e$ with some abuse of notation, stands for the gradient vector of the modified energy function, $\partial H(e)/\partial e = \partial H(x)/\partial x - \partial H(\xi)/\partial \xi = \mathcal{M}(x - \xi) = \mathcal{M}e$. In the rest of this work, when needed, it is set that $\mathcal{I} + \mathcal{S} = \mathcal{W}$.

2.3 Synchronization of dynamical systems

Definition 2.1 Synchronization problem ([12]): We say that the slave satellite (7) synchronizes with the master satellite (6), if

$$\lim_{t\to\infty} \|x(t) - \xi(t)\| = 0, \tag{9}$$

no matter which initial conditions $x(0)$ and $\xi(0)$ hold. Here the state estimation error $e(t) = x(t) - \xi(t)$ represents the synchronization error.

Theorem 2.1 ([5]) *The state $x(t)$ of the nonlinear system (6) can be globally, exponentially, asymptotically estimated by the state $\xi(t)$ of an observer of the form (7), if the pair of matrices $(\mathcal{C}, \mathcal{W})$, or the pair $(\mathcal{C}, \mathcal{S})$, is either observable or, at least, detectable.*

An observability condition on either of the pairs $(\mathcal{C}, \mathcal{W})$ or $(\mathcal{C}, \mathcal{S})$ is clearly a sufficient but not necessary condition for asymptotic state reconstruction. A necessary and sufficient condition for global asymtotic stability to zero of the state estimation error $e(t)$ is given by the following theorem.

Theorem 2.2 ([5]) *The state $x(t)$ of the nonlinear system (6) can be globally, exponentially, asymptotically estimated by the state $\xi(t)$ of an observer of the form (7) if and only if there exists a constant matrix $\mathcal{K}$ such that the symmetric matrix*

$$\begin{aligned}[\mathcal{W} - \mathcal{K}\mathcal{C}] + [\mathcal{W} - \mathcal{K}\mathcal{C}]^T &= [\mathcal{S} - \mathcal{K}\mathcal{C}] + [\mathcal{S} - \mathcal{K}\mathcal{C}]^T \\ &= 2\left[\mathcal{S} - \tfrac{1}{2}\left(\mathcal{K}\mathcal{C} + \mathcal{C}^T\mathcal{K}^T\right)\right]\end{aligned}$$

is negative definite.

The application of this method on the field of synchronization of chaotic circuits implies the design of a state observer of the form (7) to act as the receiver of the chaotic system in the form (6) considered as the emitter.

Several advantages of generalized Hamiltonian systems approach over other synchronization techiniques are reported in the literature, the following advantages are enumerated in [5] and [12] and reproduced below:

- It enables synchronization be achieved in a systematic way and clarifies the issue of deciding on the nature of the output signal to be transmitted.
- It can be successfully applied to several well-known chaotic systems.
- It does not require the computation of any Lyapunov exponent.
- It does not require initial conditions belonging to the same basin of attraction.

3 Dumbbell Satellite Model

Typical models of a dumbbell satellite are given in [3] and [4]. In Figure 1 a graphical interpretation can be observed. This model consists of two point masses coupled by a mass-less rod. In this case, θ represents the attitude of the satellite and the (r, ϕ)-tuple represents the position of the satellite with respect to a reference point.

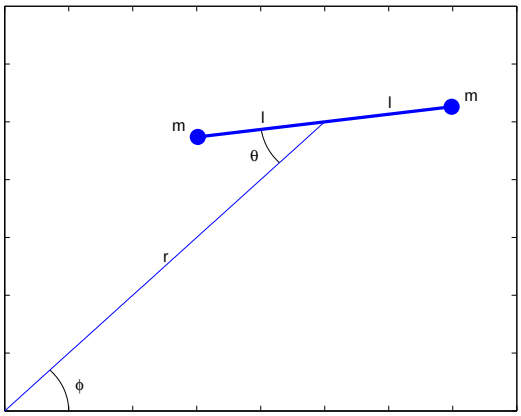

Figure 1: Dumbbell satellite representation.

In this model, the Lagrangian of the system with a normalized universal gravitational constant (G), is given by

$$L = m(\dot{r}^2 + r^2\dot{\phi}^2 + l^2(\dot{\theta} - \dot{\phi})^2) + \frac{m}{\sqrt{l^2 + r^2 - 2lrcos\theta}} + \frac{m}{\sqrt{l^2 + r^2 + 2lrcos\theta}}. \tag{10}$$

Applying the Euler-Lagrange equation for θ, we can obtain the following differential equation

$$2l^2(\ddot{\theta} - \ddot{\phi}) + \frac{lrsin\theta}{(l^2 + r^2 + 2lrcos\theta)^{3/2}} - \frac{lrsin\theta}{(l^2 + r^2 - 2lrcos\theta)^{3/2}} = 0 \tag{11}$$

by using a binomial approximation for both denominators, and taking into account that $r \gg l$, one can derive the differential equation of the attitude dynamics of a dumbbell satellite

$$\ddot{\theta} + \frac{3sin(2\theta)}{2r^3} = \ddot{\phi}. \tag{12}$$

By using a similar procedure for r and ϕ, the differential equations are:

$$\ddot{r} - r\dot{\phi}^2 = -\frac{1}{r^2}, \tag{13}$$

$$\frac{d}{dt}(r^2\dot{\phi}) = 0. \tag{14}$$

Equations (13) and (14) describe the Keplerian motion. By using the well-known solutions, $\ddot{\phi}$ can be computed. The equation (12) for the attitude dynamics of a dumbbell satellite is given by

$$\ddot{\theta} + \frac{3}{2}\frac{\sin(2\theta)}{r^3} = -\frac{2\varepsilon\sqrt{1-\varepsilon^2}\sin E}{a^3(1-\varepsilon\cos E)^4}. \tag{15}$$

Here a and ε refer to the semi-major axis and the eccentricity of the dumbbell satellite's orbital motion, respectively. E denotes the so-called eccentric anomaly and is

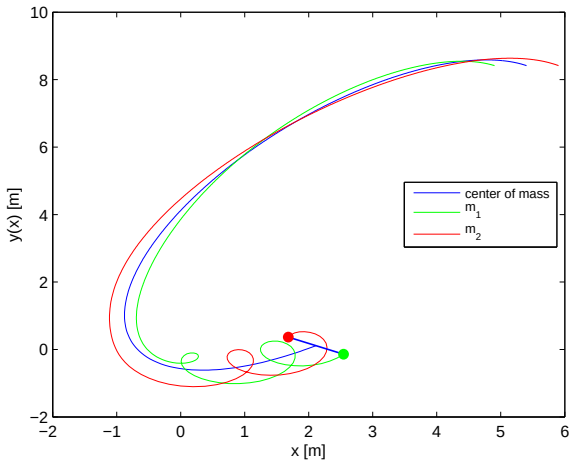

Figure 2: Motion trajectory of a single dumbbell satellite.

related to time t via Kepler's equation. If E is used eventually as an independent variable rather than t [3], the second order differential equation for $\ddot{\theta}$ can be obtained as follows

$$\frac{d^2\theta}{dE^2} - \frac{d\theta}{dE}\frac{\varepsilon \sin E}{1-\varepsilon\cos E} + \frac{3}{2}\frac{\sin(2\theta)}{1-\varepsilon\cos E} = -\frac{2\varepsilon\sqrt{1-\varepsilon^2}\sin E}{(1-\varepsilon\cos E)^2}. \tag{16}$$

Figure 2 shows the motion trajectory governed by the dynamics of the dumbbell satellite model (13)-(15). Recasting the second order equation as a first order system and writing x and t rather than θ and E, respectively, the attitude of the dumbbell satellite is described in the state space as

$$\dot{x_1} = x_2, \tag{17a}$$

$$\dot{x_2} = -\frac{3}{2}\frac{\sin(2x_1)}{1-\varepsilon\cos t} + \frac{\varepsilon\sin t}{1-\varepsilon\cos t}x_2 - \frac{2\varepsilon\sqrt{1-\varepsilon^2}\sin t}{(1-\varepsilon\cos t)^2}. \tag{17b}$$

In this case, x_1 represents the attitude (angular motion) while x_2 represents the angular velocity of the dumbbell satellite.

4 Synchronization of Two Dumbbell Satellites

As seen in the previous section, the equations (17) govern the attitude dynamics of the dumbbell satellite. Therefore, take the state vector as $x^T = [x_1, x_2]$ and define an energy function as $H(\boldsymbol{x}) = \frac{1}{2}\boldsymbol{x}^T\mathcal{I}\boldsymbol{x}$ where $\mathcal{I}$ is the 2×2 identity matrix. The system (17) can be rewritten in its generalized Hamiltonian form, according to equation (6), so in this way

the *master dummbell satellite* in generalized Hamiltonian form is given by

$$\begin{bmatrix} \dot{x}_1 \\ \dot{x}_2 \end{bmatrix} = \frac{1}{2}\begin{bmatrix} 0 & 1 \\ -1 & 0 \end{bmatrix}\frac{\partial H}{\partial x} + \frac{1}{2}\begin{bmatrix} 0 & 1 \\ 1 & 0 \end{bmatrix}\frac{\partial H}{\partial x} + \begin{bmatrix} 0 \\ -\frac{3}{2}\frac{\sin(2x_1)}{(1-\varepsilon\cos(t))} + \frac{\varepsilon\sin(t)}{1-\varepsilon\cos(t)}x_2 - \frac{2\varepsilon\sqrt{1-\varepsilon^2}\sin(t)}{(1-\varepsilon\cos(t))^2} \end{bmatrix}. \quad (18)$$

If we select $y = x_1$ as the output, then the $\mathcal{J}$, $\mathcal{S}$, and $\mathcal{C}$ matrices are given by

$$\mathcal{J} = \frac{1}{2}\begin{bmatrix} 0 & 1 \\ -1 & 0 \end{bmatrix}, \quad \mathcal{S} = \frac{1}{2}\begin{bmatrix} 0 & 1 \\ 1 & 0 \end{bmatrix}, \quad \mathcal{C} = \begin{bmatrix} 1 & 0 \end{bmatrix}. \quad (19)$$

From equation (19) it can be seen that the pair $(\mathcal{C}, \mathcal{S})$ is observable. Therefore the observer for the system (18) according to equation (7) (*slave dumbbell satellite*) has the following form

$$\begin{bmatrix} \dot{\xi}_1 \\ \dot{\xi}_2 \end{bmatrix} = \frac{1}{2}\begin{bmatrix} 0 & 1 \\ -1 & 0 \end{bmatrix}\frac{\partial H}{\partial \xi} + \frac{1}{2}\begin{bmatrix} 0 & 1 \\ 1 & 0 \end{bmatrix}\frac{\partial H}{\partial \xi} + \begin{bmatrix} 0 \\ -\frac{3}{2}\frac{\sin(2y)}{(1-\varepsilon\cos(t))} + \frac{\varepsilon\sin(t)}{1-\varepsilon\cos(t)}\xi_2 - \frac{2\varepsilon\sqrt{1-\varepsilon^2}\sin(t)}{(1-\varepsilon\cos(t))^2} \end{bmatrix} + \begin{bmatrix} k_1 \\ k_2 \end{bmatrix}(x_1 - \xi_1), \quad (20)$$

where k_1 and k_2 are the observer gains. If the synchronization error is defined as $\boldsymbol{e}(t) = \boldsymbol{x}(t) - \boldsymbol{\xi}(t)$, then the dynamics of this error are described as

$$\begin{bmatrix} \dot{e}_1 \\ \dot{e}_2 \end{bmatrix} = \frac{1}{2}\begin{bmatrix} -k_1 & 1+k_2 \\ -(1+k_2) & 0 \end{bmatrix}\frac{\partial H}{\partial e} + \frac{1}{2}\begin{bmatrix} -k_1 & 1-k_2 \\ 1-k_2 & 0 \end{bmatrix}\frac{\partial H}{\partial e} + \begin{bmatrix} 0 & 0 \\ 0 & \frac{\varepsilon\sin(t)}{1-\varepsilon\cos(t)} \end{bmatrix}\frac{\partial H}{\partial e}. \quad (21)$$

Next, we examine the stability of the synchronization error (21) between the master dumbbel satellite (18) in Hamiltonian form and slave dumbbell satellite (20) state observer. Invoking to Theorem 2.2, we have that

$$2\left[\mathcal{S} - \frac{1}{2}\left(\mathcal{K}\mathcal{C} + \mathcal{C}^T\mathcal{K}^T\right)\right] < 0,$$

and

$$\begin{bmatrix} -2k_1 & 1-k_2 \\ 1-k_2 & 0 \end{bmatrix} < 0 \quad (22)$$

by applying the Sylvester's criterion – which provides a test for negative definiteness of a matrix – thus, we have the mentioned 2×2 matrix will be negative definite matrix, if we choose k_1 and k_2 such that the condition (22) holds. In the following numerical results, we have used k_1, $k_2 > 0$ to satisfy the stability condition (22).

5 Numerical Results

In this section, numerical results are reported for synchronization of the attitude and angular velocity of two dumbbell satellites, by using generalized Hamiltonian forms and

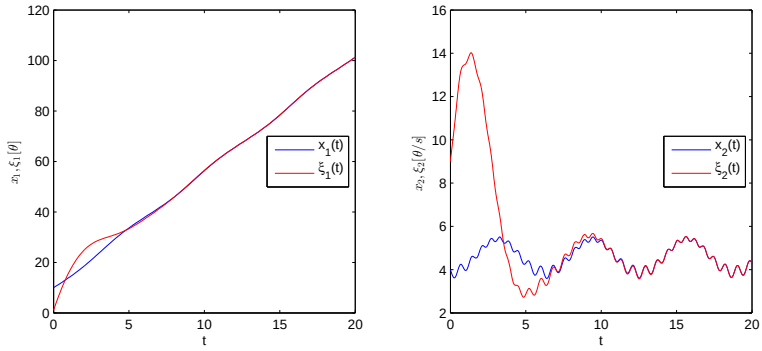

Figure 3: State attitudes $x_1(t)$, $\xi_1(t)$ (left) and state angular velocities $x_2(t)$, $\xi_2(t)$ (right) for master and slave dumbbell satellites.

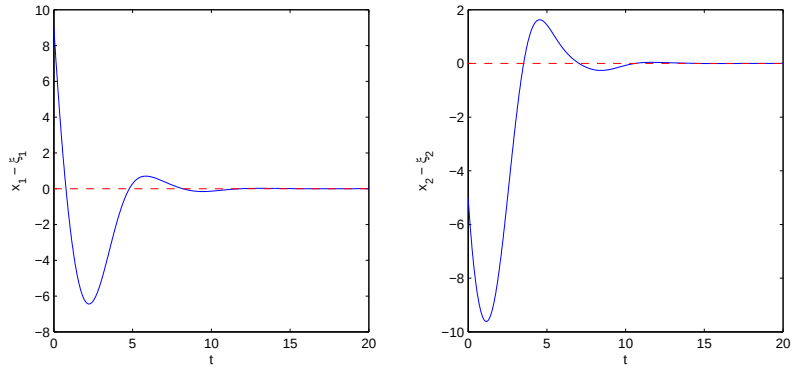

Figure 4: Error dynamics of the attitude (left) and its angular velocity (right) for the numerical simulation in Figure 3.

observer design (equations (18) and (20), respectively). Figure 3 shows the state trajectories of master and slave satellites for the following values: initial conditions $x_1(0) = 10$, $x_2(0) = 4$, $\xi_1(0) = 1$, and $\xi_2(0) = 9$, the eccentricity of the dumbell satellites $\varepsilon = 0.3$, and the gains for slave satellite dumbbell $k_1 = k_2 = 1$.

The synchronization error dynamics between the master dumbbell satellite (18) and its slave dumbbell satellite (20) are shown in Figure 4.

Figure 5 illustrates the synchronization between two dumbbell satellites x_i vs ξ_i, $i = 1, 2$.

6 Conclusion

In this paper, we have presented synchronization between two dumbbell satellites, in particular for the attitude and for the angular velocity, from the perspective of generalized Hamiltonian forms and state nonlinear observer design, an approach that has proven its

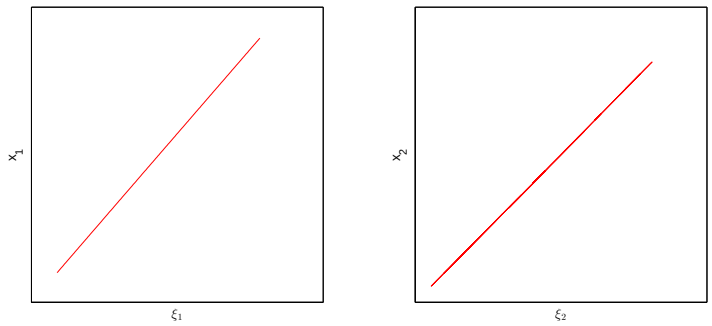

Figure 5: Synchronization of two dumbbell satellites for x_i vs ξ_i, $i = 1, 2$.

efficiency in the literature. The numerical results reported support the control laws designed for attitude synchronization of two dumbbell satellites.

Attitude synchronization for satellites is intended to serve as a first control loop for large array satellite missions; in which a large number of small satellites forms a bigger system functioning as a whole for capabilities enhancement. Thus, in future, a formation controller and the one presented above, can be used together for this type of synchronization space missions with small dumbbell satellites, via synchronization approach used in this paper.

Acknowledgment

This work was supported by the CONACyT, México under Resarch Grant 166654.

References

[1] Sarlette, A., Sepulchre, R. and Leonard, N. Cooperative attitude synchronization in satellite swarms: a consensus approach. In: *17th IFAC Symposium on Automatic Control in Aerospace*, 2007.

[2] Okasha, M., Park, C. and Park, S.-Y. Guidance and control for satellite in-orbit-self-assembly proximity operations. *Aerospace Science and Technology* **41** (2015) 289–302.

[3] Kirchgraber, U., Manz, U. and Stoffer, D. Rigorous Proof of Chaotic Behaviour in a Dumbbell Satellite Model. *Journal of Mathematical Analysis and Applications* **251** (2000) 897–911.

[4] Celletti, A. and Sidorenko, V. Some properties of the dumbbell satellite attitude dynamics. *Celestial Mechanics and Dynamical Astronomy* **101** (1-2) (2008) 105–126.

[5] Sira-Ramírez, H. and Cruz-Hernández, C. Synchronization of Chaotic Systems: a Generalized Hamiltonian Systems Approach. *International Journal of Bifurcation and Chaos* **11** (5) (2001) 1381–1395.

[6] Cruz-Hernández, C. Synchronization of time-delay chuas oscillator with application to secure communication. *Nonlinear Dynamics and Systems Theory* **4** (1) (2004) 1–13.

[7] Posadas-Castillo, C., Cruz-Hernández, C. and Nuñez-Pérez, R. Experimental realization of binary signals transmission based on synchronized lorenz circuits. *J. Appl. Res. Technol.* **2** (2) (2004) 127–137.

[8] Gámez-Guzmán, L., Cruz-Hernández, C., López-Gutiérrez, R. and García-Guerrero, E. Synchronization of chuas circuits with multi-scroll attractors: Application to communication. *Communications in Nonlinear Science and Numerical Simulation* **14** (6) (2009) 2765–2775.

[9] Gámez-Guzmán, L., Cruz-Hernández, C., López-Gutiérrez, R. M. and García-Guerrero, E. E. Synchronization of Chua's circuits with multi-scroll attractors: Application to communication. *Communications in Nonlinear Science and Numerical Simulation* **14** (6) (2009) 2765–2775.

[10] Trejo-Guerra, R., Tlelo-Cuautle, E., Muñoz Pacheco, J. M., Sánchez-López, C. and Cruz-Hernández, C. On the Relation between the Number of Scrolls and the Lyapunov Exponents in PWL-functions-based η-Scroll Chaotic Oscillators. *International Journal of Nonlinear Sciences and Numerical Simulation* **11** (11) (2010) 903–910.

[11] Muñoz Pacheco, J. M., Zambrano-Serrano, E., Félix-Beltrán, O., Gómez-Pavón, L. C., and Luis-Ramos, A. Synchronization of PWL function-based $2D$ and $3D$ multi-scroll chaotic systems. *Nonlinear Dynamics* **70** (2) (2012) 1633–1643.

[12] Cruz-Hernández, C. and Martynyuk, A. A. (Eds.) *Advances in Chaotic Dynamics and Applications*. London, Cambridge Scientific Publishers, 2010.

Nonlinear Dynamics and Systems Theory, **15** (4) (2015) 344–359

Fuzzy Modeling and Robust Pole Assignment Control for Difference Uncertain Systems

A. Aydi *, M. Djemel and M. Chtourou

Control and Energy Management Laboratory (CEM Lab),
University of Sfax, National school of engineering of Sfax, P.B. 1173, 3083 Sfax, Tunisia.

Received: June 29, 2015; Revised: November 4, 2015

Abstract: This paper deals with fuzzy modeling and robust control of nonlinear systems affected by bounded uncertainties. The proposed fuzzy model is composed of two parts: a linear uncertain part and a nonlinear one. The linear uncertain part is obtained by the nominal system linearization around some operating points. The nonlinear part is approximated by a Takagi-Sugeno fuzzy system whose parameters are estimated using the descent gradient method. A robust pole assignment called 'pole colouring' is used for the system control. This strategy of control is synthesized based only on the linear uncertain part of the decomposed model. Finally, two simulation examples are treated to illustrate the effectiveness of the proposed fuzzy modeling and control approaches.

Keywords: *uncertain nonlinear system; fuzzy modeling; Takagi-Sugeno system; linearization; robust pole assignment.*

Mathematics Subject Classification (2010): 03B52, 62K25.

1 Introduction

The modeling of an uncertain nonlinear system is an important step for the system analysis and control. It consists in developing a mathematical model ensuring the required accuracy and having a useful structure. In fact, a model must reproduce correctly the dynamics of the considered system even in the presence of nonlinearities, uncertainties and perturbations. These constraints make the classical modeling methods limited. So the evolutionist techniques, such as fuzzy systems [1] and neural networks [2] are considered as potential solutions for this problem. Indeed, they are considered as universal

* Corresponding author: mailto:aydi_amiraa@yahoo.fr

© 2015 InforMath Publishing Group/1562-8353 (print)/1813-7385 (online)/http://e-ndst.kiev.ua

approximators [3, 4]. So, they can reproduce any nonlinear dynamics with an arbitrary accuracy.

In this paper, fuzzy systems are considered for nonlinear uncertain systems modeling. They are classified as intelligent modeling tools. A fuzzy system is described by a set of IF-THEN fuzzy rules. According to fuzzy rules conclusions, two types of fuzzy systems are distinguished: Mamdani fuzzy systems [5] and Takagi-Sugeno fuzzy ones [6]. Mamadani fuzzy systems present linguistic conclusions. However, Takagi-Sugeno fuzzy systems possess numerical ones. Two types of fuzzy rules generation approaches are distinguished: manual and analytic ones.

Takagi-Sugeno fuzzy systems are considered as powerful modeling tools [7]. Their parameters are often identified using training algorithms such as descent gradient method [8–10], recursive least square algorithm [11], orthogonal least square algorithm [12], genetic algorithms [13, 14] and robust algorithms [15, 16]. There are several works about fuzzy modeling of nonlinear systems [17–20] and also uncertain ones [21, 22].

A real system is by nature uncertain. So, the use of classical control methods doesn′t guarantee the desired performance indexes. In fact, when the system parameters move from the nominal ones, the desired performances are not satisfied whence the necessity of the use of a robust control where uncertainties are explicitly taken into account. In the literature, there are several researches about the robust control such as the sliding mode [23,24], the gain scheduling [25], the H_2 performance [26], the H_∞ performance [27] and the robust tracking control [28, 29]. Also, there are some researches about robust control for linear uncertain discrete-time systems such as robust pole assignment. It is an interesting control method for linear uncertain systems. It consists of the location of the closed-loop system poles by considering the parameters variations. Nurges [30] proposed the location of the characteristic equation parameters in a stable polytope, also the uncertainties effects on characteristic equation coefficients could be minimized [31–33]. The minimization of the maximum distance between desired poles and obtained ones was proposed by Soylemez and Munro [34]. Discrete-time pole region was approximated by linear matrix inequality for robust pole assignment control design [35, 36].

These robust control techniques could be combined with fuzzy logic tools to benefit from those advantages [37–43]. For example Abid et al [37] used a robust fuzzy sliding mode controller for nonlinear discrete-time systems with parametric uncertainties. Also, Wu [38] proposed a robust H_2 fuzzy controller for the same purpose.

In this paper, fuzzy modeling and robust pole assignment control for uncertain nonlinear systems are considered. The proposed model involves two parts: (1) a linear uncertain one whose parameters are affected by bounded uncertainties and (2) a nonlinear one which is approximated by a Takagi-Sugeno fuzzy system. The linear uncertain part parameters are obtained by the nominal system linearization around some operating points. The Takagi-Sugeno fuzzy system synthesis needs two main phases: (1) the premises variables determination and (2) the conclusions parameters estimation. In fact, the premises variables determination consists essentially in input space partitioning and the conclusions parameters are estimated using the descent gradient method.

The robust pole assignment control proposed by Soylemez and Munro [34] is considered for the control of nonlinear uncertain systems. It is synthesized based only on the linear uncertain part of the developed fuzzy model. It consists in optimizing a cost function by varying the uncertain parameters. The nonlinear part of the model is supposed to be an additive perturbation.

This paper is organized as follows. In Section 2, the problem statement is presented.

The proposed fuzzy modeling approach is explained in Section 3. In Section 4, the used robust pole assignment control is detailed. In Section 5, two simulation examples are presented to illustrate the proposed modeling and control approaches. Finally, concluding remarks are given in Section 6.

2 Problem Statement

Consider the modeling and control problems of the class of nonlinear uncertain systems described by the following expression:

$$y(k+1) = F[y(k), \ldots, y(k-n+1), u(k), \ldots, u(k-m+1), p], \tag{1}$$

where u and y are the system input and the system output, respectively. F is a known nonlinear function and p is a parameters vector affected by additive uncertainties.

$$p = p_0 + \Delta p, \tag{2}$$

where p_0 is the nominal parameters vector and Δp is the uncertainties vector affecting the system.

The proposed modeling approach consists in dividing the behavior of the considered uncertain nonlinear system into two parts: a linear uncertain one y_l and a nonlinear one y_{nl} [44, 45]

$$y^m(k+1) = y_l(k+1) + y_{nl}(k+1), \tag{3}$$

where y^m is the model output.

This modeling approach needs two main steps:

- Step 1: the determination of the linear uncertain part parameters.
- Step 2: the approximation of the nonlinear part y_{nl} by a Takagi-Sugeno fuzzy system.

In this paper, a robust pole assignment control is used for the system control. It is synthesized considering only the linear uncertain part y_l of the model 3. The nonlinear part y_{nl} is considered as an additive perturbation. In the following, the proposed techniques for the model development will be presented. Also, the used approach for robust pole assignment control will be detailed.

3 Fuzzy Model Identification

In this section, the proposed fuzzy modeling approach is detailed. The system dynamics is decomposed into two terms: a linear uncertain expression and a nonlinear one. It will be compared with a global Takagi-Sugeno fuzzy model to demonstrate its interest.

3.1 Decomposed fuzzy model

The decomposed fuzzy model identification consists in determining the linear uncertain part y_l and estimating the nonlinear part y_{nl} by a Takagi-Sugeno fuzzy system. For each part computation, the structure and parameters determinations are necessary.

3.1.1 Linear uncertain part

The first part y_l is a linear expression with uncertain bounded parameters.

$$y_l(k+1) = -\sum_{i=1}^{n} a_{iu}(k)\, y(k-i+1) + \sum_{j=1}^{m} b_{ju}(k)\, u(k-j+1). \tag{4}$$

For a_{iu} and b_{ju} the index u indicates uncertain parameters. a_{iu},$i = \overline{1,n}$ and b_{ju},$j = \overline{1,m}$ are bounded uncertain parameters. It is to be noted that the coefficients a_{iu} and b_{ju} are obtained by the nominal system linearization around some operating points. In fact, around an operating point (U_l,Y_l) , the dynamics of the considered system is described by the expression

$$\delta y(k+1) = -\sum_{i=1}^{n} a_{il}\, \delta y(k-i+1) + \sum_{j=1}^{m} b_{jl}\, \delta u(k-j+1), \tag{5}$$

where

$$a_{il} = -\frac{\partial y(k+1)}{\partial y(k-i+1)}|_{(U_l,Y_l)}, \tag{6}$$

$$b_{jl} = \frac{\partial y(k+1)}{\partial u(k-j+1)}|_{(U_l,Y_l)}, \tag{7}$$

$$\delta y(k-i+1) = y(k-i+1) - Y_l,\ i = \overline{1,n}, \tag{8}$$

$$\delta u(k-j+1) = u(k-j+1) - U_l,\ j = \overline{1,m}, \tag{9}$$

$$l = \overline{1,L},$$

L is the considered operating points number. Using the expressions (8) and (9), the system dynamics is represented as follows:

$$y(k+1) = -\sum_{i=1}^{n} a_{il}\, y(k-i+1) + \sum_{j=1}^{m} b_{jl}\, u(k-j+1) + (Y_l + \sum_{i=1}^{n} a_{il}\, Y_l - \sum_{j=1}^{m} b_{jl}\, U_l). \tag{10}$$

So, the linear part y_l is given by the expression

$$y_l(k+1) = -\sum_{i=1}^{n} a_{il}\, y(k-i+1) + \sum_{j=1}^{m} b_{jl}\, u(k-j+1). \tag{11}$$

The nominal system must be linearized around some operating points to describe the dynamics of the considered nonlinear system for the global operating area. The operating points must be chosen properly. In fact, they have to be distributed on the global operating area. So, the obtained coefficients a_{iu},$i = \overline{1,n}$ and b_{ju},$j = \overline{1,m}$ are bounded uncertain parameters:

$$a_{iu} \in [min_{l=1\cdots L}\, a_{il}\ ;\ max_{l=1\cdots L}\, a_{il}], \quad b_{ju} \in [min_{l=1\cdots L}\, b_{jl}\ ;\ max_{l=1\cdots L}\, b_{jl}].$$

It is to be noted that the static terms $(Y_l + \sum_{i=1}^{n} a_{il}\, Y_l - \sum_{j=1}^{m} b_{jl}\, U_l)$ will be taken into account for the nonlinear part y_{nl} synthesis.

3.1.2 Nonlinear part

The nonlinear part y_{nl} in the expression (3) is approximated by a Takagi-Sugeno fuzzy system. It is described by a set of IF-THEN fuzzy rules having the following form:

$$if\ u(k)\ is\ A_r^1 \cdots and\ u(k-m+1)\ is\ A_r^m\ and\ y(k)\ is\ B_r^1 \cdots and\ y(k-n+1)\ is\ B_r^n,$$
$$then\ y_{nr}(k+1) = -\sum_{i=1}^{n} e_i^r\ y(k-i+1) + \sum_{j=1}^{m} f_j^r\ u(k-j+1), \quad (12)$$

where $r = \overline{1,R}$, R is the rules number. It is fixed after several simulations in order to get a compromise between a minimal error and a reasonable rules number. Consider x the premise variable vector such as: $x = [u(k),\ldots,u(k-m+1), y(k),\ldots,y(k-n+1)]$. The used membership function is the Gaussian

$$\mu_r(x_t) = \exp[-\frac{(x_t - c_t^r)^2}{2(\sigma_t^r)^2}], \quad t = \overline{1,n+m}. \quad (13)$$

The dynamics of the nonlinear part y_{nl} is described by the local models interpolation

$$y_{nl}(k+1) = \frac{\sum_{r=1}^{R}\ \alpha_r\ y_{nr}(k+1)}{\sum_{r=1}^{R}\ \alpha_r}, \quad (14)$$

where

$$\alpha_r = \prod_{t=1}^{n+m} \mu_r(x_t). \quad (15)$$

Consider $\theta_p = [c_t^r,\ \sigma_t^r,\ r = \overline{1,R},\ t = \overline{1,n+m}]$ the vector of the premises parameters of the fuzzy system. c_t^r and σ_t^r are, respectively, the center and the width of the Gaussian function relating to the r^{th} rule and the t^{th} member of the premise variable vector x. They are determined manually. In fact, the centers c_t^r are determined by the operating area partitioning and the widths σ_t^r are fixed such as there is neither discontinuity nor overlapping between the membership functions. However, the vector of the conclusions parameters is noted θ_c such as $\theta_c = [e_i^r,\ f_j^r,\ r = \overline{1,R},\ i = \overline{1,n},\ j = \overline{1,m}]$. The conclusions parameters are determined automatically. Indeed, they are estimated using the descent gradient method. The criterion to minimize is given by the expression (16). It is minimized through the minimization of the error corresponding to each example

$$J_c = \sum_{k=1}^{N} e(k), \quad (16)$$

where

$$e(k) = \frac{1}{2}[y^m(k) - y(k)]^2, \quad (17)$$

N is the size of the training data set.

The conclusions parameters are updated using the following expression

$$\theta_c(\tau) = \theta_c(\tau-1) - \epsilon\ \frac{\partial e(k)}{\partial\ \theta_c(\tau-1)}, \quad (18)$$

where τ is the iteration counter and ϵ is the learning rate. $\frac{\partial e(k)}{\partial\, \theta_c(\tau-1)}$ is given by the expression

$$\frac{\partial e(k)}{\partial\, \theta_c(\tau-1)} = [y^m(k) - y(k)]\, \frac{\partial y_{nl}(k)}{\partial\, \theta_c(\tau-1)}. \tag{19}$$

It should be noted that the linear part has been designed referring only to the nominal nonlinear system. So, the uncertain parameters must be taken into account for the design of the nonlinear part y_{nl}. It is done by varying these parameters to collect the training and the validation data sets.

3.2 Global Takagi-Sugeno fuzzy model

The Takagi-Sugeno fuzzy systems are usually used for the nonlinear systems description. They are described by a set of IF-THEN fuzzy rules having the following form:

$$\begin{aligned} &if\ u(k)\ is\ A_r^1 \cdots and\ u(k-m+1)\ is\ A_r^m\ and\ y(k)\ is\ B_r^1 \cdots and\ y(k-n+1)\ is\ B_r^n, \\ &\qquad then\ y_r^{mc}(k+1) = -\sum_{i=1}^{n} g_i^r\ y(k-i+1) + \sum_{j=1}^{m} h_j^r\ u(k-j+1) \end{aligned} \tag{20}$$

with $r = \overline{1, R}$.

The membership function is the Gaussian (13). The premises variables and the rules number are those used for the decomposed fuzzy model (3). The dynamic of the considered system is approximated by the local models interpolation

$$y^{mc}(k+1) = \frac{\sum_{r=1}^{R}\ \alpha_r\ y_r^{mc}(k+1)}{\sum_{r=1}^{R}\ \alpha_r}, \tag{21}$$

where α_r is given by expression (15) and y^{mc} is the global Takagi-Sugeno fuzzy model output.

The conclusions parameters are adjusted using the descent gradient method. The criterion to minimize is given by the expression (16) where $e(k)$ is the following:

$$e(k) = \frac{1}{2}[y^{mc}(k) - y(k)]^2. \tag{22}$$

The control of nonlinear uncertain systems (1) using the prescribed decomposed fuzzy model (3) is considered. But, the control synthesis will be based only on the linear uncertain part y_l. Otherwise, the nonlinear part y_{nl} will be considered as an additive perturbation. In this case, the linear robust controllers as a robust pole assignment one can be exploited.

4 Robust Pole Assignment Control

The robust pole assignment control proposed by Soylemez and Munro [34] is adopted for the control of linear uncertain systems. It can be used for continuous-time and also discrete-time linear systems affected by bounded uncertainties.

Consider a linear discrete-time system affected by bounded uncertainties and described by the following transfer function

$$G(q^{-1}) = \frac{B_u(q^{-1})}{A_u(q^{-1})} = \frac{b_{1u}q^{-1} + \cdots + b_{mu}q^{-m}}{1 + a_{1u}q^{-1} + \cdots + a_{nu}q^{-n}}, \tag{23}$$

where $b_{ju} \in [b_{ju}^{-}\ ;\ b_{ju}^{+}]$, $j = \overline{1,m}$ and $a_{iu} \in [a_{iu}^{-}\ ;\ a_{iu}^{+}], i = \overline{1,n}$.

The proposed controller is a PID one described by the expression

$$u(k) = u(k-1) + q_0\, e(k) + q_1\, e(k-1) + q_2\, e(k-2), \tag{24}$$

where

$$e(k) = y^d(k) - y(k), \tag{25}$$

y^d is the desired output.

When using a PID controller (24), the closed-loop system has the characteristic equation (26) which is also affected by uncertain parameters

$$W(q^{-1}, p) = \sum_i W_i(p)\, q^{-i}, \tag{26}$$

where p is the vector of uncertain parameters affecting the system.

The controller parameters θ are obtained through the minimization of the following cost function

$$J = \min_p\,(J_p), \tag{27}$$

$$\theta = [q_0;\ q_1;\ q_2]. \tag{28}$$

There are multiple choices for the criterion J_p. It can be related to desired performances like rise time, settling time $\cdots$ The simplest choice is the minimization of the maximum distance between the nominal poles and the corresponding perturbed ones of the closed-loop system. So, every pole takes one place in a disc centered on the corresponding nominal pole

$$J_p = \max_{i=1\cdots M}(|\lambda_i^0 - \lambda_i^p|), \tag{29}$$

where λ_i^0 and λ_i^p are the nominal pole and its corresponding perturbed one of the closed-loop system, respectively, M is the closed-loop system order. The controller synthesis corresponds to an optimization problem which is solved using the function *fminimax* from the Matlab toolbox.

5 Simulation Results

Two simulation examples are considered to show the effectiveness of the proposed modeling approach and the performances of the suggested control scheme. The first example is a chemical reactor and the second one is an academic system.

5.1 First example: Chemical reactor

Consider the modeling and the control problems of the chemical reactor [46] whose dynamics are described by the expression (30).

$$y(k+1) = A_1 + B_1\, u(k) + A_2\, y(k) + q(k)\, B_2\, u^3(k) + A_3\, y(k-1)\, u(k-1)\, u(k), \tag{30}$$

where $[A_1,\ A_2,\ A_3,\ B_1,\ B_2] = [0.558,\ 0.116,\ -0.034,\ 0.583,\ -0.127]$, q is an uncertain parameter supposed to be variable and bounded in an interval: $q(k) \in [0.9\,;\,1.1]$, u is the input flow of the product A and y is the concentration of the product B.

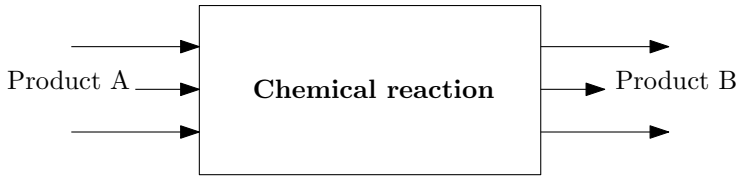

Figure 1: Chemical reactor.

5.1.1 Fuzzy modeling

The dynamics of the chemical reactor is decomposed as in equation (3). The linear uncertain part y_l is presented by the following expression

$$y_l(k+1) = -a_1\, y(k) - a_{2u}(k)\, y(k-1) + b_{1u}(k)\, u(k) + b_{2u}(k)\, u(k-1). \tag{31}$$

Since $\frac{\partial y(k+1)}{\partial y(k)}$ is constant, a_1 is a certain parameter. $a_{2u}(k)$, $b_{1u}(k)$ and $b_{2u}(k)$ are uncertain bounded parameters. They are obtained by the nominal system linearization around two operating points: $a_1 = -0.116$, $a_{2u}(k) \in [0.0014\,;\, 0.0218]$, $b_{1u}(k) \in [0.3103\,;\, 0.5626]$ and $b_{2u}(k) \in [-0.0288\,;\, -0.0052]$.

The nonlinear part y_{nl} in the expression (3) is presented by a set of IF-THEN fuzzy rules:

$$\begin{aligned} &if\ u(k)\ is\ A_r^1\ and\ u(k-1)\ is\ A_r^2\ and\ y(k)\ is\ B_r^1\ and\ y(k-1)\ is\ B_r^2 \\ &\quad then\ y_{nr}(k+1) = -e_1^r\, y(k) - e_2^r\, y(k-1) + f_1^r\, u(k) + f_2^r\, u(k-1). \end{aligned} \tag{32}$$

The obtained modeling results for the training set are given in Figure 2.

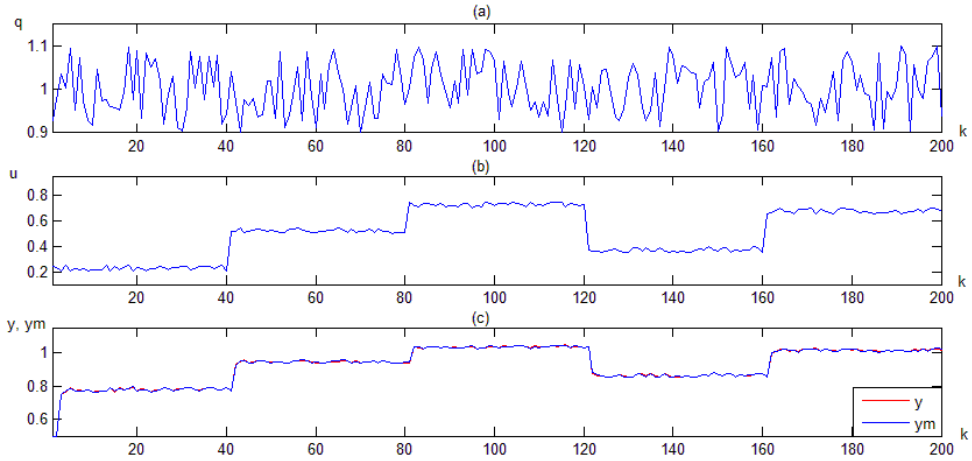

Figure 2: Evolution of the uncertain parameter (a), the input signal (b), the system and the model outputs for the training set.

The obtained results for the validation set are presented in Figure 3.

In order to compare the proposed fuzzy modeling method to the classical one, a global Takagi-Sugeno fuzzy model will be developed. It is described by a set of IF-THEN fuzzy

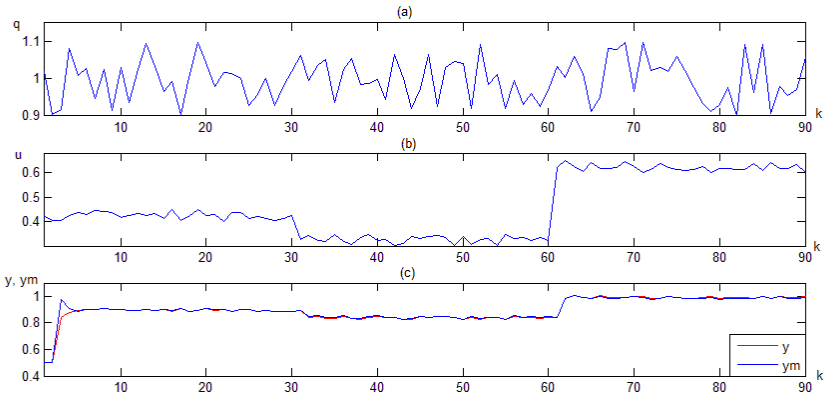

Figure 3: Evolution of the uncertain parameter (a), the input signal (b), the system and the model outputs for the validation set.

rules

$$\begin{aligned} &if\ u(k)\ is\ A_r^1\ and\ u(k-1)\ is\ A_r^2\ and\ y(k)\ is\ B_r^1\ and\ y(k-1)\ is\ B_r^2 \\ &then\ y_r^{mc}(k+1) = -g_1^r\, y(k) - g_2^r\, y(k-1) + h_1^r\, u(k) + h_2^r\, u(k-1). \end{aligned} \tag{33}$$

The conclusions parameters are estimated using the descent gradient method. The rules number is $R = 16$ and the learning rate is $\epsilon = 0.5$. For both models, the same system input and output partitioning are considered. In addition, the same training and validation sets are used.

The average value of the error committed by each model is evaluated in the validation set to demonstrate the effectiveness of the proposed modeling approaches

$$E = \frac{\sum_{k=1}^{N} |y(k) - y^m(k)|}{N}. \tag{34}$$

	Decomposed fuzzy model	Global Takgi-Sugeno fuzzy model
J (final)	0.0008	0.0008
Iteration number	6462	13740
E	0.0046	0.0049

Table 1: Comparison between the decomposed fuzzy model and the global Takagi-Sugeno fuzzy one.

According to this table, for the same criterion value the decomposed model requires less iterations number than the classical one. It is due to the system dynamics decomposition effect which accelerates the training.

5.1.2 Robust pole assignment control

The chemical reactor is controlled by the PID controller (24) whose parameters are determined using the described robust pole assignment and referring only to the linear

uncertain part (31) of the decomposed fuzzy model. The poles are located considering the parameter uncertainties of this part. The objective is to have a double pole $z_1 = z_2 = 0.2$ and two poles such as $z_3 = 0.1$ and $z_4 = 0.3$. The controller parameters are obtained through the minimization of the cost function (27). The results of the optimization problem resolution are the following: $q_0 = 0.2303$, $q_1 = 0.1906$ and $q_2 = 0.0118$.

For the uncertain parameter variations given in Figure 4, the results of the proposed control scheme are illustrated in Figure 5.

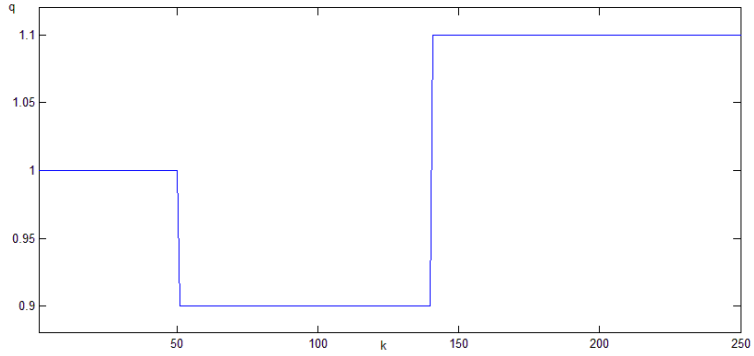

Figure 4: Evolution of the uncertain parameter $q(k)$.

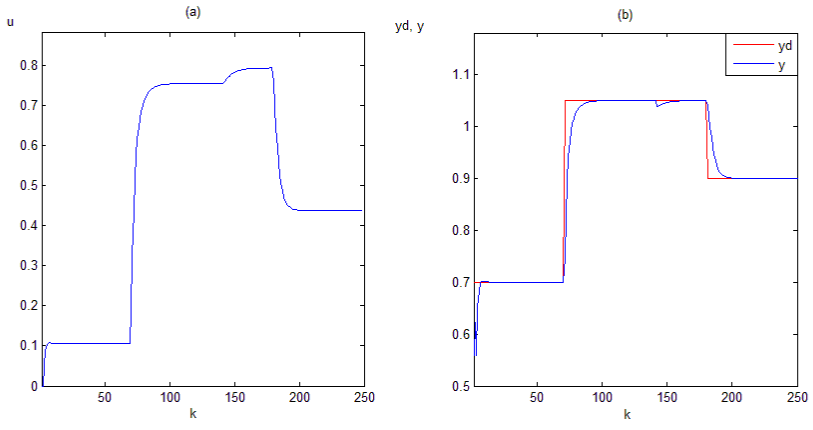

Figure 5: Evolution of the robust PID control action (a), desired output and system output (b).

For the chosen desired signal and uncertain parameter variations, the closed-loop system has acceptable performances.

5.2 Second example

Consider the nonlinear uncertain system described by the following expression [47]:

$$y(k+1) = \frac{y(k)\, y(k-1)\, y(k-2)\, u(k)\, [y(k-2)-1-q(k)]}{1+y^2(k-1)+y^2(k-2)} + \frac{u(k)}{1+y^2(k-1)+y^2(k-2)}, \tag{35}$$

where q is a bounded uncertain parameter such as: $q(k) \in [0\ ;\ 0.5]$, u and y are the system input and output, respectively.

5.2.1 Fuzzy modeling

The dynamics of the above system is described by the decomposed model (3). The linear uncertain part y_l is presented by the expression

$$y_l(k+1) = -a_{1u}(k)\, y(k) - a_{2u}(k)\, y(k-1) - a_{3u}(k)\, y(k-2) + b_{1u}(k)\, u(k), \tag{36}$$

where $a_{1u}(k)$, $a_{2u}(k)$, $a_{3u}(k)$ and $b_{1u}(k)$ are uncertain bounded parameters. They are obtained by the nominal system linearization around some operating points: $a_{1u}(k) \in [-0.0761\ ;\ 0.4003]$, $a_{2u}(k) \in [-0.4386\ ;\ 0]$, $a_{3u}(k) \in [-0.3516\ ;\ 0.0543]$ and $b_{1u}(k) \in [0.5924\ ;\ 1]$.

The nonlinear part y_{nl} in the expression (3) is described by a set of IF-THEN fuzzy rules

$$\begin{aligned} &if\ u(k)\ is\ A_r^1\ and\ y(k)\ is\ B_r^1\ and\ y(k-1)\ is\ B_r^2\ and\ y(k-2)\ is\ B_r^3 \\ &\quad then\ y_{nr}(k+1) = -e_1^r\, y(k) - e_2^r\, y(k-1) - e_3^r\, y(k-2) + f_1^r\, u(k). \end{aligned} \tag{37}$$

The rules number is $R = 16$ and the learning rate is $\epsilon = 0.2$. The obtained modeling results for the training set are given in Figure 6.

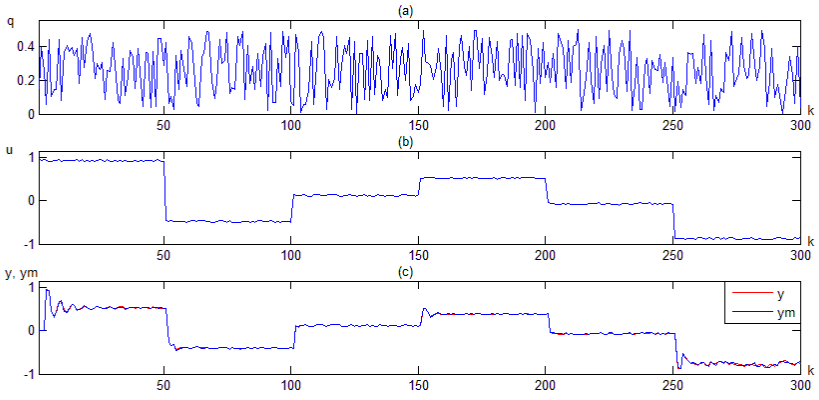

Figure 6: Evolution of the uncertain parameter (a), the input signal (b), the system and the model outputs for the training set.

The modeling results for the validation set are illustrated in Figure 7.

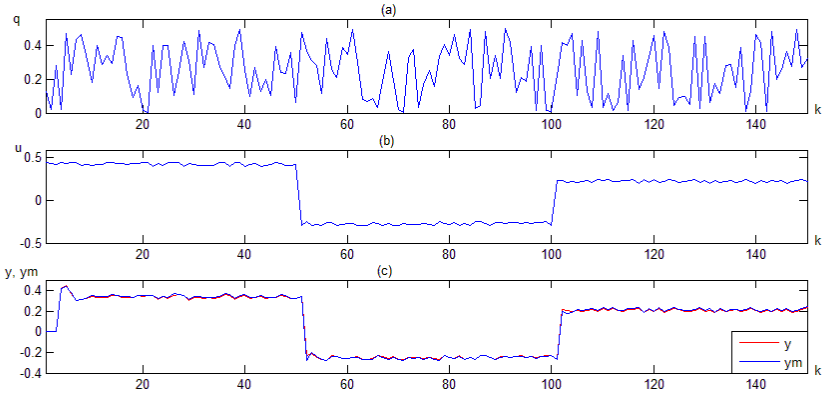

Figure 7: Evolution of the uncertain parameter (a), the input signal (b), the system and the model outputs for the validation set.

This system can be also approximated by a global Takagi-Sugeno fuzzy system composed of a set of IF-THEN fuzzy rules having the following form:

$$\begin{aligned} &if\ u(k)\ is\ A_r^1\ and\ y(k)\ is\ B_r^1\ and\ y(k-1)\ is\ B_r^2\ and\ y(k-2)\ is\ B_r^3 \\ &then\ y_r^{mc}(k+1) = -g_1^r\, y(k) - g_2^r\, y(k-1) - g_3^r\, y(k-2) + h_1^r\, u(k). \end{aligned} \tag{38}$$

The descent gradient method is applied for the estimation of the conclusions parameters. The rules number is $R = 16$ and the learning rate is $\epsilon = 0.2$. For both models, the same membership functions are used.

	Decomposed fuzzy model	Global Takgi-Sugeno fuzzy model
J (final)	0.025	0.025
Iteration number	4121	10999
E	0.0066	0.0079

Table 2: Comparison between the decomposed fuzzy model and the global Takagi-Sugeno fuzzy one.

According to this table, the decomposed fuzzy model is slightly more accurate and requires less time for the parameters training. It is due to the system dynamics decomposition.

5.2.2 Robust pole assignment control

The robust PID controller (24) is applied for the control of the system (35). The PID parameters are computed using the prescribed robust pole assignment and referring only to the linear uncertain part (36) of the decomposed fuzzy model. The objective is to have a double pole $z_1 = z_2 = 0.1$ and a double pole $z_3 = z_4 = 0.2$. The resulted PID parameters are the following ones: $q_0 = -0.5658$, $q_1 = 1.2047$ and $q_2 = -0.5586$.

For the uncertain parameter evolution given in Figure 8, the obtained control results are illustrated in Figure 9.

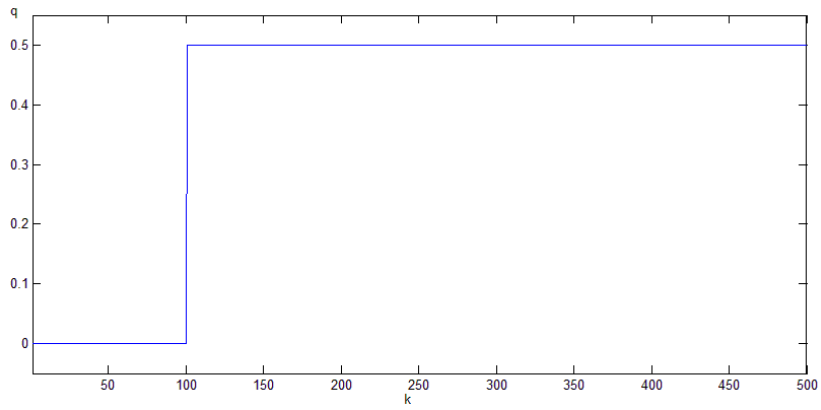

Figure 8: Evolution of the uncertain parameter $q(k)$.

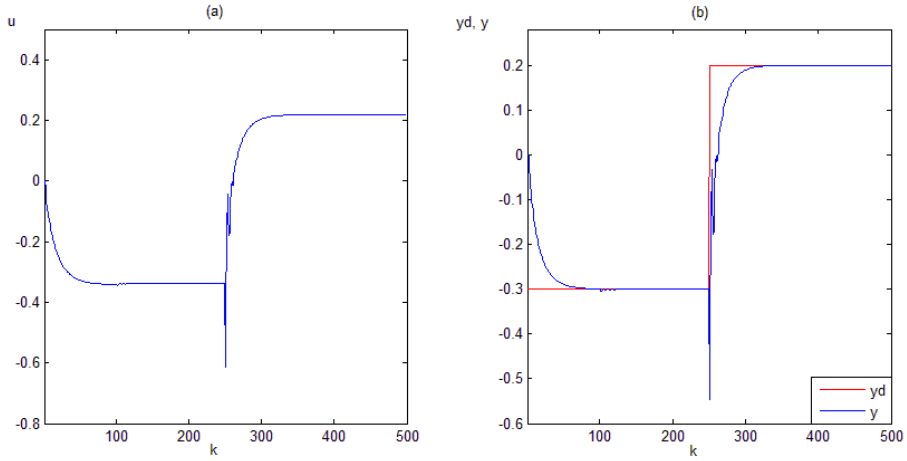

Figure 9: Evolution of the robust PID control (a), desired output and system output (b).

The resulted closed-loop system is stable and the static error is equal to zero for the chosen uncertain parameter values. But, the obtained results for the transient time are poor. So, the proposed control method is limited to the guarantee of desired performances. In addition, there is no guarantee for the closed-loop system stability. This may be caused by neglecting the nonlinear part of the model. So, in future works this control approach must be robustified and a stability study must be done to guarantee the performance and stability robustness of the closed-loop uncertain nonlinear system.

6 Conclusions

This study has developed new modeling and control schemes for nonlinear systems affected by bounded uncertainties. The proposed model consists in dividing the behavior of the considered system into two parts: a linear uncertain part and a nonlinear one. The used techniques for the system modeling have been explained. In fact, the linear uncer-

tain part has been obtained by the nominal system linearization around some operating points and the nonlinear part has been approximated by a Takagi-Sugeno fuzzy system whose parameters are estimated using the descent gradient method. A robust pole assignment control for the considered nonlinear system has been synthesized based only on the linear uncertain part of the decomposed fuzzy model. Two simulation examples have been treated to demonstrate the effectiveness of the suggested modeling approach and to experiment the proposed control scheme.

References

[1] Zadeh, L.A. Fuzzy Sets. *Information and control* **8** (1965) 338–353.

[2] Narendra, K.S. and Parthasarathy, K. Identification and control of dynamical systems using neural networks. *IEEE Transactions on Neural Networks* **1** (1) (1990) 4–27.

[3] Kosko, B. Fuzzy systems as universal approximators. *IEEE Transactions on Computers* **43** (11) (1994) 1329–1333.

[4] Hornik, K. Multilayer feedforward networks are universal approximators. *Neural Networks* **2** (5) (1989) 359–366.

[5] Mamdani, E.H. Application of Fuzzy Algorithms for control of a simple dynamic Plant. *Proc. of the IEE Control and Science* **121** (12) (1974) 1585–1588.

[6] Takagi, T. and Sugeno, M. Fuzzy identification of systems and its applications to modeling and control. *IEEE Transaction on Systems, Man and Cybernetics* **15** (15) (1985) 116–132.

[7] Cai, L., Cui, Z. and Liu, H. Universal approximation of T-S fuzzy systems. In: *Symposium on ICT and Energy Efficiency and Workshop on Information Theory and Security*. Dublin (2012) 166–171.

[8] Chen, M.Y. and Linkens, D.A. Rule-base-self-generation and simplification for data-driven fuzzy models. *Fuzzy Sets and Systems* **142** (2004) 243–265.

[9] Zhao, Z., Xie, W. and Hong, H. Identification of Takagi-Sugeno (TS) fuzzy model with evolutionary parallel gradient search. In: *Annual Meeting of the North American Fuzzy Information Processing Society (NAFIPS)*. New York City (2008) 1–6.

[10] Aflab, M.S. and Kadri, M.B. Parameter identification of Takagi-Sugeno fuzzy model of surge tank system. In: 3^{rd} *International Conference on Computer, Control & Communication*. Karachi (2013) 1–4.

[11] Xu, S. and Xuesong, X. Fuzzy identification base on cat swarm optimization algorithm. In: *The* 26^{th} *Chineese Control and Decision Conference*. Changsha (2014) 4264–4269.

[12] Soltani, M., Chaari, A., BenHmida, F. and Gossa, M. A new objective function for fuzzy c-regression model and its application to T-S fuzzy model identification. In: *International Conference on Communications, Computing and Control Applications*. Hammamet, Tunisia (2011) 1–5.

[13] Jin, Y. Fuzzy modeling of high-dimensional systems: complexity reduction and interpretability improvement. *IEEE Transactions on Fuzzy Systems* **8** (2) (2000) 212–221.

[14] Lavygina, A. and Hodashinsky, I. Hybrid algorithm for fuzzy model parameter estimation based on genetic algorithm and derivation based methods. In: *International Conference on Fuzzy Computation Theory and Applications (FCTA)* (2011) 513–515.

[15] Chuang, C.C., Su, S.F. and Chen, S.S. Robust TSK fuzzy modeling for function approximation with outliers. *IEEE Transactions on Fuzzy Systems* **9** (6) (2001) 810–821.

[16] Chuang, C.C., Jeng, J.T. and Tao, C.W. Hybrid robust approach for TSK fuzzy modeling with outliers. *Expert Systems with Applications* **36** (2009) 8925–8931.

[17] Rezaei Sadrabadi, M. and Fazel Zarandi, M.H. Identification of the linear parts of nonlinear systems for fuzzy modeling. *Applied Soft Computing* **11** (1) (2011) 807–819.

[18] Abdelazim, T. and Malik, O.P. Identification of nonlinear systems by Takagi-Sugeno fuzzy logic grey box modeling for real-time control. *Control Engineering Practice* **13** (12) (2005) 1489–1498.

[19] Sonbol, A.H., Fadali, M.S. and Jakarzadeh, S. TSK fuzzy function approximators: design and accuracy analysis. *IEEE Transactions on Systems Man Cybernetics, Part B: Cybernetics* **42** (3) (2012) 702–712.

[20] Hadjili, M.L. and Kara, K. Modelling and control using Takagi-Sugeno fuzzy models. In: *Saudi International Electronis, Communications and Photonics Conference*. Riyadh (2011) 1–6.

[21] Du, H. and Li, W. Model-based Takagi-Sugeno fuzzy approach for vehicle longitudinal velocity estimation during barking. In: *IEEE International Conference on Fuzzy Systems*. Beijing (2014) 1851–1858.

[22] Leite, D., Cominhas, W., Lemos, A. and Palhares, R. Parameter estimation of dynamic fuzzy models from uncertain data streams. In: *IEEE Conference on Norbert Wiener in the* 21^{st} *Century*. Boston MA (2014) 1–7.

[23] Khandekar, A.A., Malwatkar, G.M. and Patre, B.M. Discrete sliding mode control for robust tracking of high order delay time systems with experimental application. *ISA Transactions* **52** (1) (2013) 36–44.

[24] Xu, Q. Discrete-time second-order sliding mode control for a nanopositioning stage. In: *The* 33^{rd} *Chinese Control Conference*. Nanjing (2014) 7976–7981.

[25] Khansah, H., Mahout, V. and Bernussou, J. Scheduled robust control of nonlinear system by norm bounded approximation. In: 4^{th} *IEEE International Multi-Conference on Systems, Signals & Devices*, Hammamet, Tunisia (2007).

[26] Bedioui, N., Salhi, S. and Ksouri, M. H_2 performance via static output feedback for a class of nonlinear systems . In: 3^{rd} *International Conference on Signals, Circuits and Systems*. Medenine (2009) 1–6.

[27] Morais, C.F., Braga, M.F. Oliveira, R.C.L.F. and Peres, P.L.D. H_∞ static output feedback control of discrete-time Markov jump linear systems with uncertain transition probability matrix. In: *American Control Conference*. Portland OR (2014) 489–494.

[28] Yu, Y., Zhang, Q., Wang, J. and Sun, C.Y. Robust tracking control for the hypersonic flight vehicle via backstepping method. In: 33^{rd} *Chinese Control Conference*. Nanjing (2014) 4306–4311.

[29] Yu, J., Zhao, Y. and Wu, Y. Robust tracking control for a class of uncertain nonlinear systems. In: 33^{rd} *Chinese Control Conference*. Nanjing (2014) 2075–2079.

[30] Nurges, U. Robust pole assignment via reflection coefficients of polynomials. *Automatica* **42** (7) (2006) 1223–1230.

[31] Halpern, M.E., Evans, R.J. and Hill, R.D. Pole assignment with robust stability. *IEEE Transactions on Automatic Control* **40** (4) (1995) 725–729.

[32] Lordelo, A.D.S. and Ferreira, P.A.V. Interval analysis and design of robust pole assignment controllers. In: *proceedings of the* 41^{st} *IEEE Conference on Design and Control*. USA (2002) 1461–1466.

[33] Lordelo, A.D.S., Juzzo, E.A. and Ferreira, P.A.V. On the design of robust controller using the interval Diophantine equation. In: *IEEE International Symposium on Computer Aided Control Systems Design*. Taiwan (2004) 173–178.

[34] Soylemez, M.T. and Munro, N. Robust pole assignment in uncertain systems. *IEE Proceedings: Control Theory and Applications* **144** (3) (1997) 217–224.

[35] Risonova, D. and Holic, I. LMI approximation of pole-region for discrete-time linear dynamic systems. In: 15^{th} *International Carpathian Control Conference (ICCC)*. Velke Karlovice (2014) 497–502.

[36] Risonova, D. and Valach, P. Switched system robust control: pole placement LMI based approach. In: 15^{th} *International Carpathian Control Conference (ICCC)*. Velke Karlovice (2014) 491–496.

[37] Abid, H., Chtourou, M. and Toumi, A. Robust fuzzy sliding mode controller for discrete nonlinear systems. *International Journal of Computers, Communications & Control* **3** (1) (2008) 6–20.

[38] Wu, H.-N. Robust H_2 fuzzy output feedback control for discrete-time nonlinear systems with parametric uncertainties. *International Journal of Approximate Reasoning* **46** (1) (2007) 151–165.

[39] Aydi, A., Zaidi, I., Djemel, M. and Chtourou, M. Robust fuzzy PID controller for discrete-time uncertain nonlinear systems. In: 6^{th} *International Multi-conference on Systems, Signals and Devices, SSD'09*. Djerba, Tunisia (2009) 1–6.

[40] Yang, H., Shi, P., Zhang, J. and Qui, J. Robust H_∞ control for a class of discrete-time fuzzy systems via delta operator approach. *Information Sciences* **184** (1) (2012) 230–245.

[41] Hu, Y., Liu, J. and Lin, Z. LPV T-S fuzzy gain scheduling control of WTGS below rated wind speed . In: *the* 26^{th} *Chinese Control and Decision Conference*. Changsha (2014) 3328–3333.

[42] Chae, S., Ngung, S.K. and Wang, W. Robust H_∞ fuzzy control of discrete nonlinear networked control systems: a SOS approach. *Journal of the Franklin Institute* **351** (8) (2014) 4065–4083.

[43] Patkure, J., More, D.S. and Todkar, M. Fuzzy gain scheduling based control technique for the feed in the tool and cutter grinding machine. In: *International Conference on Circuit, Power and Computing Technologies*. Nagercoil (2014) 1090–1093.

[44] Aydi, A., Djemel, M. and Chtourou, M. On the fuzzy modeling of uncertain nonlinear systems. In: 15^{th} *International Conference on Sciences and Techniques of Automatic Control & Computer Engineering (STA)*. Hammamet, Tunisia (2014) 1055–1060.

[45] Chen, L. and Narendra, K.S. Identification and control of a nonlinear discrete-time system based on its linearization: a unified framework *IEEE Transactions on Neural Networks* **15** (3) (2004) 663–673.

[46] Hernandez, E. and Arkun, Y. Stability of nonlinear polynomial ARMA models and their inverse. *International Journal of Control* **63** (5) (1996) 885–906.

[47] Jin, L., Nikiforuk, P.N. and Gupta, M.M. Fast neural learning and control of discrete-time nonlinear systems. *IEEE Transactions on Systems, Man and Cybernetics* **25** (3) (1995) 478–488.

Nonlinear Dynamics and Systems Theory, **15** (4) (2015) 360–369

Direct Control of Matrix Converters Using Asymmetric Strategy (ASVM) to Feed the Double Star Induction Machine

F. Bettache [1], M. Tadjine [1], L. Nezli [1] and A. Tlemçani [2*]

[1] *Electrical Engineering Department, Process Control Laboratory LPC, National Polytechnic School ENP, 10 Avenue Pasteur, B. P. 182 El - Harrach, 16000, Algiers, Algeria*
[2] *Department of Electrical, Research Laboratory in Electrical Engineering and Automatic LREA, University of Medea, Ain D heb, 26001, Medea, Algeria*

Received: January 7, 2015; Revised: November 2, 2015

Abstract: Due to their distinct advantages, the variable speed multi-phase drive systems are seen as serious contender to the existing three-phase drives. However we present in this work the modeling and control of matrix converter feeding a double star induction machine. In order to achieve this goal we present the model of matrix converter, and its control strategy: based on the direct space vector modulation (DSVM). Then we perform simulation tests for the whole converter and machine using *Matlab–Simulink*. The results illustrate the proper functioning of the system.

Keywords: *matrix converter; double star induction machine; space vector; modulation; switching strategies.*

Mathematics Subject Classification (2010): 68Q05, 93B52, 93C25, 93C83.

1 Introduction

To introduce an electric motor in high power applications, such as traction or marine propulsion, it is often necessary to segment the power. To this end, we can intervene at the converter level through multi-level techniques or parallel converters [7].

Another solution is to apply the segmentation level to the set converter-machine using multiphase machines. Indeed, the total power is distributed over a larger number of inverter arms, each of which is fed with a decreased power, which allows for a higher switching frequency and a less important ripple current and torque [2, 11]. One of the

* Corresponding author: mailto:h_tlemcani@yahoo.fr

© 2015 InforMath Publishing Group/1562-8353 (print)/1813-7385 (online)/http://e-ndst.kiev.ua

most common examples of multiphase machines is the double star induction machine (DSIM).

Such a machine has the advantage of reducing the electromagnetic torque ripples and rotor losses significantly. The double star induction machine studied in this paper is a machine that has two systems of coupled three-phase windings in the stator fixed star and out of phase with each other at an γ ($\gamma = 30°$) and a mobile rotor similar to that of classical asynchronous machine. The two systems of stator phases are fed by two sources of power frequency and amplitude equal but out of phase with each other at an angle ($\delta = \gamma = 30°$). However, the machine AC (asynchronous) is traditionally controlled by a PWM inverter control, an alternative is the matrix converter. The main characteristics of MC are: Direct AC-AC polyphase power conversion, inherent bidirectional power flow capability, input/output sinusoidal waveforms with variable output voltage amplitude and frequency, input power factor control despite the load in the output side and a simple and compact power circuit because of the elimination of bulky reactive elements [1, 5, 6, 8]. Recently, the most popular control algorithm widely used in matrix converters is space vector modulation (SVM) that allows input current and output voltage to be independently controlled. The principal reason for this is the better harmonic performance that can be achieved using different switching strategies in each commutation period. Two versions for SVM are defined: the indirect modulation and the direct one. In this work, we adopt the direct modulation (DSVM) which is realized by asymmetrical switching strategy.

2 Modeling of the Double Star Asynchronous Machine

The DSIM consists of two three-phase windings in the stator shifted from each other by an angle of 30° and one three-phase rotor winding. The two stator windings are fed by two systems of voltage frequency and amplitude equal but out of phase with each other at an angle ($\delta = \gamma = 30°$). The windings are shown in the following (Figure 1):

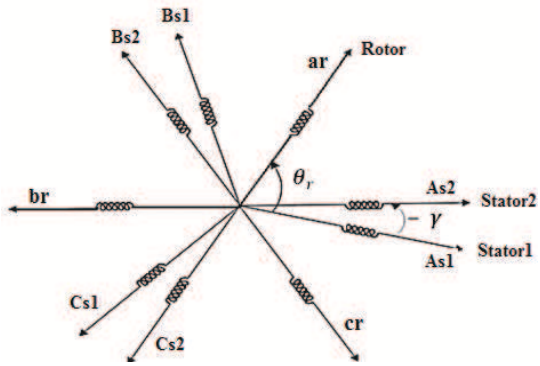

Figure 1: DSIM schema.

Park model of the double stator induction machines, with P pairs of poles, is defined by the following equations system (1).

$$[h]\begin{cases} V_{sd1} &= r_{s1}i_{sd1} + \dfrac{d\phi_{sd1}}{dt} - \omega_s\phi_{sq1}, \\ V_{sq1} &= r_{s1}i_{sq1} + \dfrac{d\phi_{sq1}}{dt} - \omega_s\phi_{sd1}, \\ V_{sd2} &= r_{s2}i_{sd2} + \dfrac{d\phi_{sd2}}{dt} - \omega_s\phi_{sq2}, \\ V_{sq2} &= r_{s2}i_{sq2} + \dfrac{d\phi_{sq2}}{dt} - \omega_s\phi_{sd2}, \\ 0 &= r_r r_{rd} + \dfrac{d\phi_{rd}}{dt} - (\omega_s - \omega_r)\phi_{rq}, \\ 0 &= r_r r_{rq} + \dfrac{d\phi_{rq}}{dt} - (\omega_s - \omega_r)\phi_{rq}. \end{cases} \tag{1}$$

The electromagnetic torque and speed are given by the following expressions (2):

$$\begin{cases} T_{em} = p\dfrac{L_m}{L_m + L_r}[\phi_{rd}(i_{sq1} + i_{sq2}) - \phi_{rq}(i_{sd1} + i_{sd2})], \\ J\dfrac{d\Omega}{dt} = C_{em} - C_r - K_f\Omega. \end{cases} \tag{2}$$

3 Matrix Converter Fundamentals

Recently there has been considerable interest in the potential benefits of matrix converter technology, especially for applications where size, weight, and long-term reliability are important factors [8]. For a three-phase to three-phase implementation, the matrix converter circuit consists of nine bidirectional switches so that any input line can be connected to any output line for any given length of time. The matrix converter used in the present work consists of two identical three-phase matrix converters. The schematic diagram of the converter is shown in Figure 2.

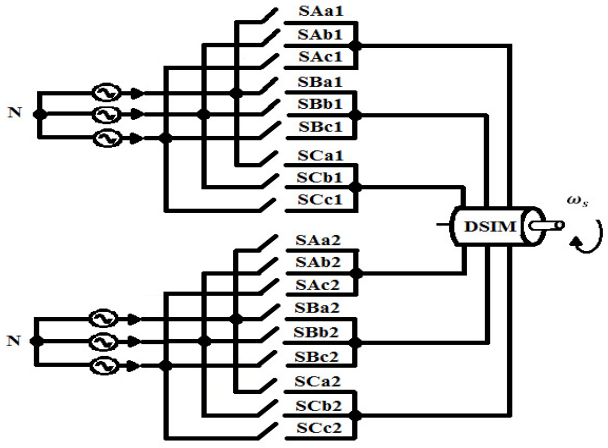

Figure 2: Schematic diagram of matrix converter-DSIM.

Each matrix is driven by three phase voltages (V_{Ak}, V_{Bk}, V_{Ck}) where a power is phase-shifted by 30° to each other, the double star induction motor load is connected to the

output. The switching function of a switch SI_{j_k} is defined as (3):

$$SI_{j_k} = \begin{cases} 1 & swicths \quad SIj_k \quad closed \\ 0 & swicths \quad SIj_k \quad closed \end{cases} \begin{matrix} I = \{A, B, C\}, j = \{a, b, c\}, \\ , k = \{1, 2\}. \end{matrix} \quad (3)$$

The mathematical expressions that represent the basic operation of the MC are obtained applying Kirchhoff's voltage and current laws to the switch array (4,5) [5, 6].

$$\begin{bmatrix} v_{ak}(t) \\ v_{bk}(t) \\ v_{ck}(t) \end{bmatrix} = \begin{bmatrix} SAak(t) & SBak(t) & SCak(t) \\ SAbk(t) & SBbk(t) & SCbk(t) \\ SAck(t) & SBck(t) & SCck(t) \end{bmatrix} \times \begin{bmatrix} V(t)_{Ak} \\ V(t)_{Bk} \\ V(t)_{Ck} \end{bmatrix}, \quad (4)$$

$$\begin{bmatrix} i_{Ak}(t) \\ i_{Bk}(t) \\ i_{Ck}(t) \end{bmatrix} = \begin{bmatrix} SAak(t) & SAbk(t) & SAck(t) \\ SBak(t) & SBbk(t) & SBck(t) \\ SCak(t) & SCbk(t) & SCck(t) \end{bmatrix} \times \begin{bmatrix} i(t)_{ak} \\ i(t)_{bk} \\ i(t)_{ck} \end{bmatrix}. \quad (5)$$

where v_{ak}, v_{bk} and v_{ck} $(k = 1, 2)$ are the output phase voltages, and i_{Ak}, i_{Bk} and i_{Ck} represent the input currents to the matrix. The output voltage is directly constructed switching between the input voltages and the input currents are obtained in the same way from the output ones. For these equations to be valid, the next expression (6) has to be taken into consideration:

$$\mathbf{S}_{Aj_k} + \mathbf{S}_{Bj_k} + \mathbf{S}_{Cj_k} = 1, j = \{a, b, c\}, \ (k = 1, 2). \quad (6)$$

What this expression says is that, at any time, one, and only one switch must be closed in an output branch. If two switches were closed simultaneously, a short circuit would be generated between two input phases. On the other hand, if all the switches in an output branch were open, the load current would be suddenly interrupted and, due to the inductive nature of the load, an over voltage problem would be produced in the converter.

4 Space Vector Approach

4.1 Modulation of MC

The Space Vector Modulation for MC is based on the instantaneous space vector representation of input currents and output voltages. SVM uses six sectors of the space, namely 1 to 6. The valid switching states (27) are shown in Table 1 [9, 10].

The first 18 switching states of Table 1 represent the active vectors and determine the output voltage vector v_o and input current vector which are presented in Figure 3.

The magnitude of these vectors depends upon the instantaneous values of the input current and output voltage. In these states any two output phases are connected to the same input phase. The remaining six switching states represent the zero vectors and each output phase is connected to a different input phase. Both the magnitude and the phase of the resultant rotating vectors are variable in these states.

4.2 Direct space vector modulation algorithm

In principle, the SVM algorithm is based on the selection of four active configurations which are applied for suitable time widths within each cycle period Tp. A zero configuration is then applied to complete Tp. At any cycle period, the output voltage vector

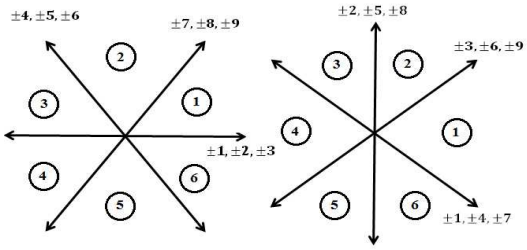

Figure 3: Output voltage and input current space vector hexagons.

States	Switches on	$\lvert \overline{v_o} \rvert$	$\angle \overline{v_o}$	$\lvert \overline{i_i} \rvert$	$\angle \overline{i_i}$
ABB +1	$S_{Aa}\ S_{Bb}\ S_{Bc}$	$+2/3V_{AB}$	0	$+2/\sqrt{3}i_a$	$-\pi/6$
BAA −1	$S_{Ba}\ S_{Ab}\ S_{Ac}$	$-2/3V_{AB}$	0	$-2/\sqrt{3}i_a$	$-\pi/6$
BCC +2	$S_{Ba}\ S_{Cb}\ S_{Cc}$	$+2/3V_{BC}$	0	$+2/\sqrt{3}i_a$	$\pi/2$
CBB −2	$S_{Ca}\ S_{Bb}\ S_{Bc}$	$-2/3V_{BC}$	0	$-2/\sqrt{3}i_a$	$\pi/2$
CAA +3	$S_{Ca}\ S_{Ab}\ S_{Ac}$	$+2/3V_{CA}$	0	$+2/\sqrt{3}i_a$	$7\pi/6$
ACC −3	$S_{Aa}\ S_{Cb}\ S_{Cc}$	$-2/3V_{CA}$	0	$-2/\sqrt{3}i_a$	$7\pi/6$
BAB +4	$S_{Ba}\ S_{Ab}\ S_{Bc}$	$+2/3V_{AB}$	$2\pi/3$	$+2/\sqrt{3}i_b$	$-\pi/6$
ABA −4	$S_{Aa}\ S_{Bb}\ S_{Ac}$	$-2/3V_{AB}$	$2\pi/3$	$-2/\sqrt{3}i_b$	$-\pi/6$
CBC +5	$S_{Ca}\ S_{Bb}\ S_{Cc}$	$+2/3V_{BC}$	$2\pi/3$	$+2/\sqrt{3}i_b$	$\pi/2$
BCB −5	$S_{Ba}\ S_{Cb}\ S_{Bc}$	$-2/3V_{BC}$	$2\pi/3$	$-2/\sqrt{3}i_b$	$\pi/2$
ACA +6	$S_{Aa}\ S_{Cb}\ S_{Ac}$	$+2/3V_{CA}$	$2\pi/3$	$+2/\sqrt{3}i_b$	$7\pi/6$
CAC −6	$S_{Ca}\ S_{Ab}\ S_{Cc}$	$-2/3V_{CA}$	$2\pi/3$	$-2/\sqrt{3}i_b$	$7\pi/6$
BBA +7	$S_{Ba}\ S_{Bb}\ S_{Ac}$	$+2/3V_{AB}$	$4\pi/3$	$+2/\sqrt{3}i_c$	$-\pi/6$
AAB −7	$S_{Aa}\ S_{Ab}\ S_{Bc}$	$-2/3V_{AB}$	$4\pi/3$	$-2/\sqrt{3}i_c$	$-\pi/6$
CCB +8	$S_{Ca}\ S_{Cb}\ S_{Bc}$	$+2/3V_{BC}$	$4\pi/3$	$+2/\sqrt{3}i_c$	$\pi/2$
BBC −8	$S_{Ba}\ S_{Bb}\ S_{Cc}$	$-2/3V_{BC}$	$4\pi/3$	$-2/\sqrt{3}i_c$	$\pi/2$
AAC +9	$S_{Aa}\ S_{Ab}\ S_{Cc}$	$+2/3V_{CA}$	$4\pi/3$	$+2/\sqrt{3}i_c$	$7\pi/6$
CCA −9	$S_{Ca}\ S_{Cb}\ S_{Ac}$	$-2/3V_{CA}$	$4\pi/3$	$-2/\sqrt{3}i_c$	$7\pi/6$
AAA 0_1	$S_{Aa}\ S_{Ab}\ S_{Ac}$	0	−	0	−
BBB 0_2	$S_{Ba}\ S_{Bb}\ S_{Bc}$	0	−	0	−
CCC 0_3	$S_{Ca}\ S_{Cb}\ S_{Cc}$	0	−	0	−

Table 1: Switching states and vectors used in DSVM.

v_o and the input current displacement angle φ_i are known as reference quantities. The input voltage vector is known from measured source voltage, the control of φ_i can be achieved controlling the phase angle β_i of the input current vector (Figure 4).

The modulation algorithm is explained using Figure 5 [9] representing the vectors, and i_i lie in sector 1. The reference voltage vector v_o is resolved into two components $v_o^{'}$ and $v_o^{''}$ along the two adjacent vectors. The $v_o^{'}$ component is synthesized using their two voltage vectors.

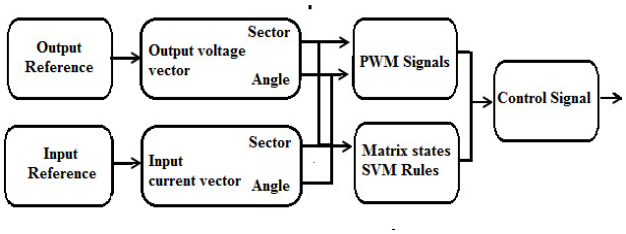

Figure 4: Modulation schema.

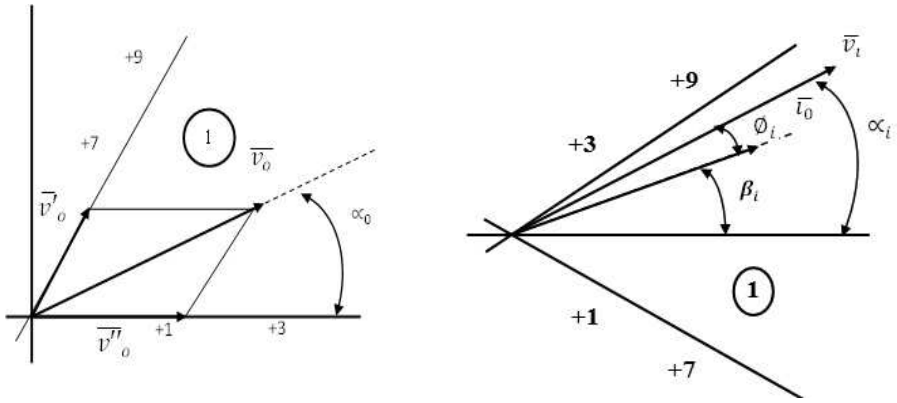

Figure 5: Modulation of the output voltage vectors and input current vectors.

The six switching states of $v_o^{'}$ are $\pm 7, \pm 8, \pm 9$. Among the six possible switching states $(\pm 7, \pm 8, \pm 9)$, the one that allows the modulation of the input current must be selected i.e. ± 7 and ± 9. Here the switching state ± 8 of $v_o^{'}$ does not allow the modulation of the input current vector because the reference input current vector has the switching states of $\pm 3, \pm 6, \pm 9$ and $\pm 1, \pm 4, \pm 7$.

Therefore, the switching state ± 8 is eliminated. From the remaining four switching states $(\pm 7, \pm 9)$, we assumed to apply the positive switching states $+7$ and $+9$. Similarly, the switching states required to synthesize the $v_o^{''}$ component can be selected as $+1$ and $+3$. Here ± 2 is eliminated. The reference current vector i_i is resolved into two components $i_i^{'}$ and $i_i^{''}$ along the two adjacent vectors.

The $i_i^{'}$ component is synthesized using their two current vectors. The six switching states of $i_i^{'}$ are $\pm 3, \pm 6, \pm 9$. Among the six possible switching states $(\pm 3, \pm 6, \pm 9)$, the one that allows the modulation of the output voltage must be selected ± 3 and ± 6. Here

the switching state ± 6 of $i_i^{'}$ does not allow the modulation of the output voltage vector because the reference output voltage vector has the switching states of $\pm 7, \pm 8, \pm 9$ and $\pm 1, \pm 2, \pm 3$. Therefore, the switching state 6 is eliminated. From the remaining four switching states $(\pm 3, \pm 9)$, we assumed to apply the positive switching states as $+3$ and $+9$. Similarly, the switching states required to synthesize the $i_i^{''}$ component can be selected as $+1$ and $+7$. Here ± 4 is eliminated.

Using the same procedure, it is possible to determine the four switches configurations correspondent to any possible combination of output voltage and input current sectors, which are quoted in Table 2 [10].

K_i \ K_v	1				2				3				4				5				6			
1	9	-7	-3	1	-6	4	9	-7	3	-1	-6	4	-9	7	3	-1	6	-4	-9	7	-3	1	6	-4
2	-8	9	2	-3	5	-6	-8	9	-2	3	5	-6	8	-9	-2	3	-5	6	8	-9	2	-3	-5	6
3	7	-8	-1	2	-4	5	7	-8	1	-2	-4	5	-7	8	1	-2	4	-5	-7	8	-1	2	4	-5
4	-9	7	3	-1	6	-4	-9	7	-3	1	6	-4	9	-7	-3	1	-6	4	9	-7	3	-1	-6	4
5	8	-9	-2	3	-5	6	8	-9	2	-3	-5	6	-8	9	2	-3	5	-6	-8	9	-2	3	5	-6
6	-7	8	1	-2	4	-5	-7	8	-1	2	4	-5	7	-8	-1	2	-4	5	7	-8	1	-2	-4	5
Duty	δ^{I}	δ^{II}	δ^{III}	δ^{IV}	δ^{I}	δ^{II}	δ^{III}	δ^{IV}	δ^{I}	δ^{II}	δ^{III}	δ^{IV}	δ^{I}	δ^{II}	δ^{III}	δ^{IV}	δ^{I}	δ^{II}	δ^{III}	δ^{IV}	δ^{I}	δ^{II}	δ^{III}	δ^{IV}

Table 2: Selection of active switching states for each combination of sector for output voltage K_V and input current K_I.

The required modulation duty cycles for switching states δ^I, δ^{II}, δ^{III} and δ^{IV} in the last row of Table 2 are given below:

$$\begin{aligned}
\delta^I &= \frac{2}{\sqrt{3}} \frac{V_O}{V_I} \frac{\cos(\widetilde{\alpha} - \frac{\pi}{3}) \cos(\widetilde{\alpha} - \frac{\pi}{3})}{\cos(\varphi_i)}, \\
\delta^{II} &= \frac{2}{\sqrt{3}} \frac{V_O}{V_I} \frac{\cos(\widetilde{\alpha} - \frac{\pi}{3}) \cos(\widetilde{\alpha} + \frac{\pi}{3})}{\cos(\varphi_i)}, \\
\delta^{III} &= \frac{2}{\sqrt{3}} \frac{V_O}{V_I} \frac{\cos(\widetilde{\alpha} + \frac{\pi}{3}) \cos(\widetilde{\alpha} - \frac{\pi}{3})}{\cos(\varphi_i)}, \\
\delta^{IV} &= \frac{2}{\sqrt{3}} \frac{V_O}{V_I} \frac{\cos(\widetilde{\alpha} + \frac{\pi}{3}) \cos(\widetilde{\alpha} + \frac{\pi}{3})}{\cos(\varphi_i)}.
\end{aligned} \tag{7}$$

Equations (7) have a general validity. For any combination of the output voltage sector K_v and the input current sector K_i (Table 2) provides the four switches configurations to be used within the cycle period Tp and equations (7) give the correspondent on-time ratios. In equations (7) the following angle limits apply:

$$-\frac{\pi}{6} < \widetilde{\alpha} < \frac{\pi}{6} \quad , \quad -\frac{\pi}{6} < \widetilde{\beta} < \frac{\pi}{6}.$$

For the feasibility of the control algorithm, the sum of the four on-time ratios must be lower than or equal to unity:

$$\delta^I + \delta^{II} + \delta^{III} + \delta^{IV} < 1. \tag{8}$$

4.3 Asymmetric switching strategies

Switching strategies deal with the switching configuration sequence, that is, the order in which the active and zero vectors are applied along the commutation period. The three zero configurations produce two degrees of freedom in order to complete the zero state switching time. In this paper one switching technique is simulated and analyzed: The Asymmetrical SVM (ASVM). The ASVM uses only one of the three zero configurations in the middle of the sequence so that minimum switch commutations are achieved between one switching state and the next one. Using this technique the switching commutations are up to 8 for each commutation period. In this way switching losses are minimized [5,6].

For example, considering both output voltage and input current reference vectors located in sector 1 within their respective hexagons, it can be seen that these are the only possible double-sided sequences that can be generated for ASVM techniques:

ACC-AAC-AAA-AAB-ABB | ABB-AAB-AAA-AAC-ACC

The zero configurations are obtained from Table 3 for ASVM:

i_{iref}	v_{oref} (1,2,3,4,5 or 6)
1 or 4	AAA
2 or 5	BBB
3 or 6	CCC

Table 3: Zero configuration for ASVM.

5 Simulation Results

5.1 Performance of the association matrix converter induction motor double star:

It directly feeds the induction machine double star by matrix converters. The simulation departs for startup vacuum after the steady state was established; we apply a torque load to the machine. The simulation results shown in Figure 6 represent the following quantities:

- The electromagntique torque.
- The speed of DSIM.
- Flux (ϕ_{rd} ,ϕ_{rq} and ϕ_r).

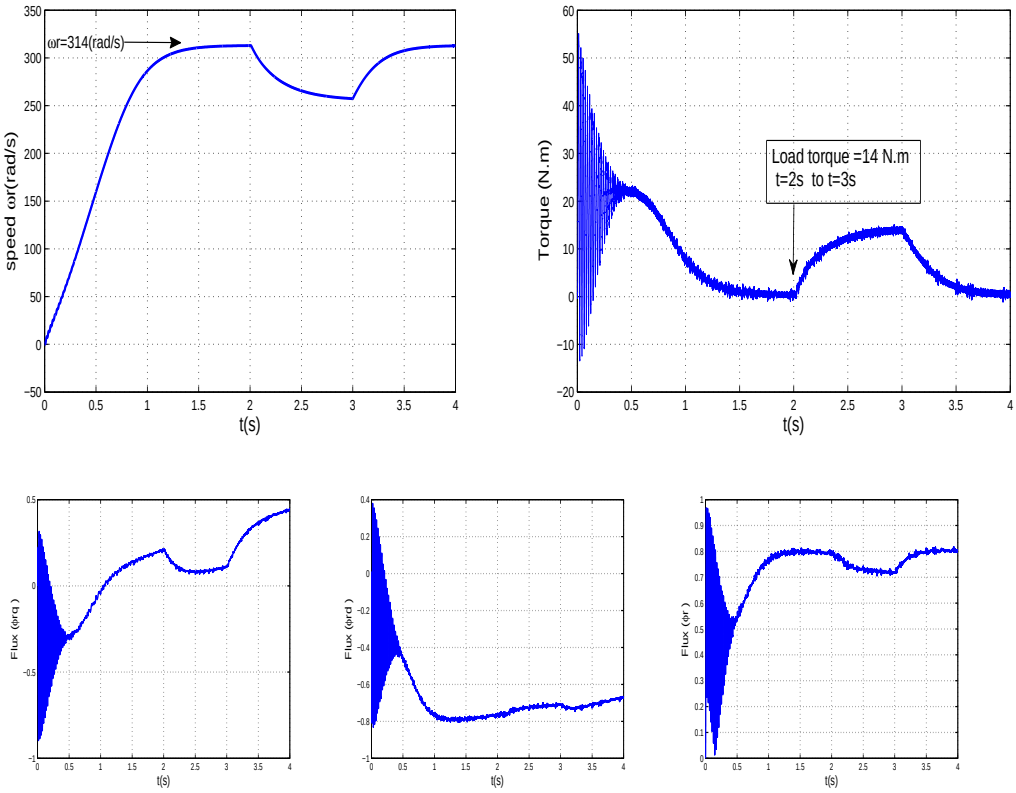

Figure 6: Performance of the association matrix converter double star induction machine controlled by Asymmetrical SVM

6 Conclusion

In this paper we have used the asymmetric strategy of space vector modulation to control directly the matrix converters, which feed a double-star induction machine. We can say that the matrix converter operates in the four quadrants. The performances obtained show that the proposed control strategy is distinguished by comparison with indirect converters (AC-DC-AC) by the reversibility of the converter. We can confirm that the benefits of using this type of converter are numerous; we include among other things, increasing the power, reduction of oscillations of the switching frequency of power switches and improved forms of output quantities.

Appendix

Double star induction machine parameters:

Pn=4.2KW, p=1, Ls1=0.011H, Ls2=0.011H, Lr=0.006H, Lm=0.3672H,

J=0.0625kG.m2, Kf=0.001 N.m.s/rad, Rs1=1.86Ω, Rs2=1.86Ω, Rr=2.12Ω.

switching frequency fs= 1/Ts = 10KHz.

References

[1] Hamidia, A., Larabi, A., Tlemcani, A. and Boucherit, M.S. AIDTC Techniques for Induction Motors. *Nonlinear Dynamics and Systems Theory* **3** (2) (2013) 135–145.

[2] Oudjebour, Z., Berkouk, E.M. and Mahmoudi, M.O. Modelling, Control and Feedback Control of the Multilevel Flying Capacitors Rectifier. Application to Double Star Induction Machine. In: *IEEE International, Energy Conference and Exhibition (EnergyCon)*, 2010, 507–512.

[3] Beriber, D., Berkouk, E.M., Talha, A. and Mahmoudi, M.O. Study and Control of Two Two - Level PWM Rectifiers - Clamping Bridge - Two Three - Level NPC VSI Cascade. Application to Double Stator Induction Machine. In: *IEEE 35th Annual, Power Electronics Specialists Conference* **5** (2004) 3894–3899.

[4] Casadei, D., Serra, G., Tani, A., Zarri, L. Matrix converter modulation strategies: a new general approach based on space-vector representation of the switch state. *IEEE Transactions on Industrial Electronics* **49** (2) (2002) 370–381.

[5] Vadillo, J., Echeverria, J.M., Fontan, L., Martinez-Iturralde, M. and Elosegui, I. Modelling and Simulation of a Direct Space Vector Modulated Matrix Converter using different Switching Strategies. *International Symposium on Power Electronics, Electrical Drives, Automation and Motion* (2008) 944–949.

[6] Vadillo, J., Echeverria, J.M., Galarza, A. and Fontan, L. Modelling and simulation of space vector modulation techniques for Matrix Converters: Analysis of different switching strategies. *International Electrical Machines and Systems* (2008) 1299–1304.

[7] Tlemcani, A., Sebaa, K. and Henini, N. Indirect Adaptive Fuzzy Control of Multivariable Nonlinear Systems Class with Unknown Parameters. *Nonlinear Dynamics and Systems Theory* **14** (2) (2014) 162–174.

[8] Azib, A., Tazerart, F., Metidji, B., Taib, N., Ziane, D.J. and Rekioua, T. Matrix Converter Control Algorithm Dedicated to Feed the Double Star Induction Machine. *International Journal of Research and Reviews in Computing Engineering.* **1** (2011) 1–6.

[9] Jayamala, V. and Kalaiarasi, B. Performance Evaluation of Matrix converter using Direct Space Vector Modulation Technique. In: *International Conference on Control, Automation, Communication and Energy Conservation* (4-6 June 2009) 1–6.

[10] Hong-Hee Lee, Nguyen, H.M. and Eui-Heon Jung. The development of direct space vector modulation method for matrix converter. *Korea Science and Engineering Foundation (KOSEF)*, 1–7.

[11] Bentouati, S., Tlemcani, A., Boucherit, M.S. and Barazane, L. A DTC Neurofuzzy Speed Regulation Concept for a Permanent Magnet Synchronous Machine. *Nonlinear Dynamics and Systems Theory* **13** (4) (2013) 344–358.

Nonlinear Dynamics and Systems Theory, **15** (4) (2015) 370–382

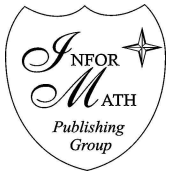

Existence Results for a Fractional Integro-Differential Equation with Nonlocal Boundary Conditions and Fractional Impulsive Conditions

Vidushi Gupta and Jaydev Dabas *

Department of Applied Science and Engineering, IIT Roorkee, Saharanpur Campus, Saharanpur–247001, India.

Received: September 13, 2014; Revised: October 31, 2015

Abstract: In this paper, we have established the existence and uniqueness of solution for a class of impulsive fractional integro-differential equations with nonlocal boundary conditions. The existence results are proved by applying the theory of fractional calculus and fixed point theorems. At last an application is given to verify our results.

Keywords: *fractional derivatives and integrals; differential equations with impulses; boundary value problems with impulses; equations with impulses; nonlocal and multi-point boundary value problems.*

Mathematics Subject Classification (2010): 26A33, 34A37, 34B37, 34K45, 34B10.

1 Introduction

Fractional differential equations are the corner stone for description of memory and hereditary properties of many materials and processes. Its useful applications include mathematical modeling in many engineering and science disciplines like physics, chemistry, biophysics, biology etc. Its non local behavior is the vital characteristic that makes it vary from its rival in classical calculus. For more details one can see the papers [1, 6, 8, 10, 13, 15, 22, 24, 25] and the references therein.

Integro-differential equations occur in probability theory, nonlinear viscoelastic bodies, acoustic scattering theory and bio-logical population models and systems with substantially distributed parameters. All these problems end up with boundary value problems of integro-differential equations. For details see the paper [21].

* Corresponding author: mailto:jay.dabas@gmail.com

© 2015 InforMath Publishing Group/1562-8353 (print)/1813-7385 (online)/http://e-ndst.kiev.ua

In recent years, the theory of impulsive differential equations for integer order comes in various applications of mathematical modeling of phenomena and practical situations. For instance, the impulsive differential equations captured from real world problems describe the dynamics of processes in which sudden, discontinuous jumps occur. For more details one can see the papers [2, 3, 6, 7, 12, 19, 20, 23, 26] and references therein.

C. Bai [4] has investigated the existence of solutions of multi-point boundary value problem of nonlinear impulsive fractional differential equations at resonance. Further in his subsequent study in [5] the author has extended the results for the boundary value problem of nonlinear impulsive differential equations at resonance. The author obtained the result of existence by using the coincidence degree theory due to Mawhin.

In [20] L. Yang et al. have proved the existence and uniqueness of solution for the following nonlocal boundary value problem of impulsive fractional differential equations:

$$\begin{cases} {}^cD^q u(t) = F(t, u(t), u'(t)),\ q \in (1,2],\ t \in [0,1], \\ \Delta u(t_k) = I_k(u(t_k^-)),\ \Delta(u'(t_k)) = J_k(u(t_k^-)),\ k = 1, 2...., p, \\ \alpha u(0) + \beta u'(0) = g_1(u),\ \alpha u(1) + \beta u'(1) = g_2(u),\ \alpha > 0,\ \beta \geq 0, \end{cases} \tag{1}$$

by means of a fixed point theorem due to ORegan, the authors established the sufficient conditions for the existence of at least one solution of the problem. In [7] J. Cao et al. have established the existence and uniqueness results for the impulsive fractional differential inclusions with a fractional order multi-point boundary condition and with fractional order impulses and proved the results by using the multi-valued analysis of topological fixed point theory.

In [11] X. Fu et al. concerned with the fractional separated boundary value problem of the following fractional differential equations with fractional impulsive conditions:

$$\begin{cases} {}^cD^\alpha x(t) = F(t, x(t),\ t \in J = [0,T],\ t \neq t_k,\ \alpha \in (1,2), \\ \Delta x(t_k) = I_k(x(t_k^-)),\ \Delta({}^cD^\gamma x(t_k)) = {I_k}^*(x(t_k^-)),\ k = 1, 2...., m, \\ a_1 x(0) + b_1({}^cD^\gamma x(0)) = c_1,\ a_2 x(T) + b_2({}^cD^\gamma x(T)) = c_2,\ \gamma \in (0,1), \end{cases} \tag{2}$$

where $a_i, b_i, c_i, \in \mathbb{R},\ i = 1, 2$, with $a_i \neq 0$ and $a_2 T^\gamma \Gamma(2-\gamma) \neq -b_2$. By using the Schaefer fixed point theorem, Banach fixed point theorem, and nonlinear alternative of Leray Schauder type, the authors obtained the existence results.

In [14] N. Kosmatov considered the following two impulsive problems:

$$\begin{cases} {}^cD^\delta x(t) = F(t, x(t)),\ t \in (0,1] \backslash \{t_1, t_2, ..., t_m\}, \\ {}^cD^\gamma x(t_k^+)) - {}^c D^\gamma x(t_k^-)) = J_k(x(t_k)),\ k = 1, 2...., m, \\ x(0) = x_0,\ x'(0) = x_1, \end{cases} \tag{3}$$

where ${}^cD^\delta$ is the Caputo fractional derivative of order $\delta \in (1,2)$ with the lower limit zero, $0 < \gamma < 1$, and

$$\begin{cases} {}^LD^\delta x(t) = F(t, x(t),\ t \in (0,1] \backslash \{t_1, t_2, ..., t_m\}, \\ {}^LD^\gamma x(t_k^+)) - {}^L D^\gamma x(t_k^-)) = J_k(x(t_k)),\ k = 1, 2...., m, \\ I^{1-\alpha} x(0) = x_0, \end{cases} \tag{4}$$

where ${}^LD^\delta$ is the Riemann-Liouville fractional derivative of order $\delta \in (0,1)$ with lower limit zero and $0 < \gamma < \delta$.

Motivated by the works [4,5,7,11,14,20] we investigate the existence and uniqueness solutions for the following impulsive fractional integro-differential equation with nonlocal boundary conditions:

$$\begin{cases} {}^cD^\alpha u(t) = f(t, u(t), \int_0^t K(t,s)u(s)ds),\ t \in [0,T],\ t \neq t_k,\ \alpha \in (1,2), \\ \Delta u(t_k) = I_k(u(t_k^-)), \\ \Delta({}^cD^q u(t_k)) = J_k(u(t_k^-)),\ q \in (0,1),\ k = 1,2,\ldots,m, \\ u(0) = a_1 - g(u), \quad u(T) = a_2 - h(u),\ a_1, a_2 \in \mathbb{R}, \end{cases} \tag{5}$$

where ${}^cD^\alpha$ is the Caputo's derivative, functions $f : [0,T] \times X \times X \to X$ for $K : [0,T] \times [0,T] \to [0,\infty)$ and $g, h \in X \to X$ are continuous. The impulsive conditions for $0 = t_0 < t_1 < \cdots < t_m < t_{m+1} = T$, $I_k, J_k \in C(X,X)$, are bounded functions. We have $\Delta u(t_k) = u(t_k^+) - u(t_k^-)$ and $\Delta({}^cD^q u(t_k)) = ({}^cD^q u(t_k^+)) - ({}^cD^q u(t_k^-)), u(t_k^+) = \lim_{h\to 0} u(t_k + h)$ and $u(t_k^-) = \lim_{h\to 0} u(t_k - h)$ represent the right and left-hand limits of $u(t)$ at $t = t_k$ respectively with $u(t_i^-) = u(t_i)$, where $K \in C(D, \mathbb{R}^+)$, the set of all positive functions which are continuous on $D = \{(t,s) \in \mathbb{R}^2 : 0 \le s \le t < T\}$ and $K^* = \sup_{t\in[0,T]} \int_0^t K(t,s)ds < \infty$.

In all the above cited papers except [4,5,7,11,14,20] the authors established the existence and uniqueness results of the fractional order boundary value problems by applying the standard fixed point theorems with the integer order impulsive conditions. In this paper, we show the existence and uniqueness solutions for the fractional integro differential equation with fractional impulsive conditions and nonlocal boundary conditions. The boundary value problems like (5) arise in many applications such as electromagnetic waves in dielectric media, the mathematical modeling of various phenomena of transport theory, the transfer of neutrons through thin plates and membranes in nuclear reactors, in the propagation of radiation through the atmosphere of planets and stars, and in several other transport problems.

In Section 2, we present some notations and preliminary results about fractional calculus and differential equations to be used in the following sections. In Section 3, we discuss existence and uniqueness results for solutions of the system (5) by using the Banach and Schauder fixed point theorems.

2 Preliminaries

Let $(X, \|\cdot\|_X)$ be a complex Banach space of functions with the norm $\|y\|_X = \sup_{t\in[0,T]}\{|y(t)| : y \in X\}$. To treat the impulsive conditions, define the following space

$$PC_t = PC([0,t] : X),\ 0 \le t \le T,$$

be a Banach space of all such functions $y : [0,T] \to X$, which are continuous everywhere except for a finite number of points t_i, $i = 1,2,\ldots,m$, at which $y(t_i^+)$ and $y(t_i^-)$ exist with $y(t_i^-) = y(t_i)$ and are endowed with the norm

$$\|y\|_{PC_t} = \sup_{t\in[0,T]} \{\|y(t)\|_X, y \in PC_t\},$$

and

$$PC_t^1 = PC^1([0,t] : X),\ 0 \le t \le T,$$

be a Banach space of all such functions $y : [0,T] \to X$, which are continuously differentiable everywhere except for a finite number of points t_i, $i = 1,\ldots,m$, at

which $y'(t_i^+)$ and $y'(t_i^-)$ exist with $y'(t_i^-) = y'(t_i)$ and are endowed with the norm $\|y\|_{PC_t^1} = \sup_{t\in[0,T]}\{\|y(t)\|_{PC_t}, \|y'(t)\|_{PC_t}, y \in PC_t\}$. All other notations in the paper have their usual meanings.

Definition 2.1 [15] The Riemann-Liouville fractional integral operator for order $\alpha > 0$, of a function $f : \mathbb{R}^+ \to \mathbb{R}$ and $f \in L^1(\mathbb{R}^+, X)$ is defined by

$$J_t^0 f(t) = f(t),\ J_t^\alpha f(t) = \frac{1}{\Gamma(\alpha)}\int_0^t (t-s)^{\alpha-1} f(s)ds,\ t > 0, \tag{6}$$

where $\Gamma(\cdot)$ is the Euler gamma function.

Definition 2.2 [15] The Riemann Liouville fractional derivative of order α with lower limit zero for a function $f : [0,\infty) \to \mathbb{R}$ can be written as

$${}^L D_t^\alpha f(t) = \frac{1}{\Gamma(n-\alpha)}\frac{d^n}{dt^n}\int_0^t \frac{f(s)}{(t-s)^{\alpha+1-n}}ds,\ t > 0,\ n-1 < \alpha < n. \tag{7}$$

Definition 2.3 [15] The Caputo's derivative of order α for a function $f : [0,\infty) \to \mathbb{R}$ can be written as

$${}^c D_t^\alpha f(t) = {}^L\ D_t^\alpha\Big[f(t) - \sum_{k=0}^{n-1}\frac{t^k}{k!}f^{(k)}(0)\Big],\ t > 0,\ n-1 < \alpha < n. \tag{8}$$

Remark 2.1 [15] If $f(t) \in C^n[0,\infty)$, for order $n-1 < \alpha < n$ then

$${}^c D_t^\alpha f(t) = \frac{1}{\Gamma(n-\alpha)}\int_0^t \frac{f^{(n)}(s)}{(t-s)^{\alpha+1-n}}ds = I_t^{n-\alpha} f^{(n)}(t),\ t > 0. \tag{9}$$

The Caputo's derivative of constant is equal to zero.

The following results are needed to prove the existence results of the paper, relevant references are cited.

Theorem 2.1 *[18] If U is a closed, bounded, convex subset of a Banach space X and the mapping $A : U \to U$ is completely continuous, then A has a fixed point in U.*

Lemma 2.1 *[1] Let $\alpha > 0$, then the differential equation*

$${}^c D^\alpha h(t) = 0 \tag{10}$$

has solutions $h(t) = c_0 + c_1 t + c_2 t^2 + \cdots + c_{n-1}t^{n-1},\ c_i \in \mathbb{R},\ i = 0, 1, \ldots, n-1,\ n = [\alpha]+1$.

Lemma 2.2 *[1] Let $\alpha > 0$, then*
$I^\alpha D^\alpha h(t) = h(t) + c_0 + c_1 t + c_2 t^2 + \cdots + c_{n-1}t^{n-1},\ c_i \in \mathbb{R},\ i = 0, 1, \ldots, n-1,\ n = [\alpha]+1$.

To investigate the nonlinear impulsive fractional integro differential equation (5), we first consider the associated linear system and obtain its solution.

Lemma 2.3 *Let $\alpha < (1,2)$, $q < (0,1)$ and $\sigma \in [0,T] \to \mathbb{R}$ be continuous. A function $u(t) \in PC_t^1$ is a solution of the following fractional integral equation:*

$$u(t) = \begin{cases} \int_0^t \frac{(t-s)^{\alpha-1}}{\Gamma(\alpha)}\sigma(s)ds + a_1 - g(u) - \frac{t}{T}\Big[a_1 - a_2 + h(u) - g(u) \\ + \int_0^T \frac{(T-s)^{\alpha-1}}{\Gamma(\alpha)}\sigma(s)ds + \sum_{i=1}^m I_i(u(t_i^-)) \\ + \sum_{i=1}^m (T-t_i)\left(\frac{\Gamma(2-q)}{{t_i}^{1-q}} J_i(u(t_i^-))\right)\Big], & t \in [0,t_1), \\ ..... \\ \int_0^t \frac{(t-s)^{\alpha-1}}{\Gamma(\alpha)}\sigma(s)ds + \sum_{i=1}^k I_i(u(t_i^-)) + a_1 - g(u) - \frac{t}{T}\Big[a_1 - a_2 \\ + h(u) - g(u) + \int_0^T \frac{(T-s)^{\alpha-1}}{\Gamma(\alpha)}\sigma(s)ds + \sum_{i=1}^m I_i(u(t_i^-)) \\ + \sum_{i=1}^m (T-t_i)\left(\frac{\Gamma(2-q)}{{t_i}^{1-q}} J_i(u(t_i^-))\right)\Big] \\ + \sum_{i=1}^k (t-t_i)\left(\frac{\Gamma(2-q)}{{t_i}^{1-q}} J_i(u(t_i^-))\right), & t \in (t_k, t_{k+1}], \end{cases} \tag{11}$$

iff $u(t)$ is a solution of the following BVP

$$\begin{cases} {}^cD^\alpha u(t) = \sigma(t),\ \alpha \in (1,2), \\ \Delta u(t_k) = I_k(u(t_k^-)), \Delta({}^cD^q u(t_k)) = J_k(u(t_k^-)),\ q \in (0,1), \\ u(0) = a_1 - g(u), \quad u(T) = a_2 - h(u). \end{cases} \tag{12}$$

Proof. Let for $t \in [0,t_1)$, $u(t)$ be the solution of (12), we have

$$u(t) = \int_0^t \frac{(t-s)^{\alpha-1}}{\Gamma(\alpha)}\sigma(s)ds - c_0 - c_1 t, \tag{13}$$

using the condition $u(0) = a_1 - g(u)$ we compute $c_0 = -(a_1 - g(u))$, then we have

$$u(t) = \int_0^t \frac{(t-s)^{\alpha-1}}{\Gamma(\alpha)}\sigma(s)ds + a_1 - g(u) - c_1 t. \tag{14}$$

If $t \in (t_1, t_2]$, we may write the solution as

$$u(t) = \int_0^t \frac{(t-s)^{\alpha-1}}{\Gamma(\alpha)}\sigma(s)ds - c_2 - c_3 t, \tag{15}$$

on applying first impulsive condition $\Delta u(t_1) = I_1(u(t_1^-))$, we get

$$-c_2 = I_1(u(t_1^-)) + c_3 t_1 + a_1 - g(u) - c_1 t_1. \tag{16}$$

Using the value of c_2 in (15), we obtain

$$u(t) = \int_0^t \frac{(t-s)^{\alpha-1}}{\Gamma(\alpha)}\sigma(s)ds + I_1(u(t_1^-)) + a_1 - g(u) - c_1 t_1 + c_3(t_1 - t).$$

From (17) and (14), we get

$$D^q u(t) = \frac{1}{\Gamma(\alpha-q)}\int_0^t (t-s)^{\alpha-q-1}\sigma(s)ds - c_3\frac{t^{1-q}}{\Gamma(2-q)}, \tag{17}$$

$$D^q u(t) = \frac{1}{\Gamma(\alpha-q)}\int_0^t (t-s)^{\alpha-q-1}\sigma(s)ds - c_1\frac{t^{1-q}}{\Gamma(2-q)}. \tag{18}$$

Using the second impulsive condition $\Delta(D^q u(t_1)) = J_1(u(t_1^-))$, we have

$$c_3 = -\frac{\Gamma(2-q)}{{t_1}^{1-q}} J_1(u(t_1^-)) + c_1. \tag{19}$$

Put c_3 in (17), we get

$$\begin{aligned} u(t) &= \int_0^t \frac{(t-s)^{\alpha-1}}{\Gamma(\alpha)}\sigma(s)ds + I_1(u(t_1^-)) \\ &\quad + a_1 - g(u) + (t-t_1)\frac{\Gamma(2-q)}{{t_1}^{1-q}} J_1(u(t_1^-)) - c_1 t. \end{aligned} \tag{20}$$

For $t \in (t_2, t_3]$, we have

$$u(t) = \int_0^t \frac{(t-s)^{\alpha-1}}{\Gamma(\alpha)}\sigma(s)ds - c_4 - c_5 t. \tag{21}$$

Applying the similar pattern we obtain the following form of the solution

$$\begin{aligned} u(t) &= \int_0^t \frac{(t-s)^{\alpha-1}}{\Gamma(\alpha)}\sigma(s)ds + I_1(u(t_1^-)) + I_2(u(t_2^-)) + a_1 - g(u) \\ &\quad + \frac{\Gamma(2-q)}{{t_1}^{1-q}} J_1(u(t_1^-))(t-t_1) + \frac{\Gamma(2-q)}{{t_2}^{1-q}} J_2(u(t_2^-))(t-t_2) - c_1 t. \end{aligned} \tag{22}$$

For generality, when $t \in (t_k, t_{k+1}]$, we may write the solution in the following form

$$\begin{aligned} u(t) &= \int_0^t \frac{(t-s)^{\alpha-1}}{\Gamma(\alpha)}\sigma(s)ds + \sum_{i=1}^{k} I_i(u(t_i^-)) + a_1 - g(u) - c_1 t \\ &\quad + \sum_{i=1}^{k}(t-t_i)\left(\frac{\Gamma(2-q)}{{t_i}^{1-q}} J_i(u(t_i^-))\right). \end{aligned} \tag{23}$$

On using the second boundary condition, $u(T) = a_2 - h(u)$, we compute the following value of the constant c_1:

$$\begin{aligned} c_1 &= \frac{1}{T}\Big[a_1 - a_2 + h(u) - g(u) + \int_0^T \frac{(T-s)^{\alpha-1}}{\Gamma(\alpha)}\sigma(s)ds \\ &\quad + \sum_{i=1}^{m} I_i(u(t_i^-)) + \sum_{i=1}^{m}(T-t_i)\left(\frac{\Gamma(2-q)}{{t_i}^{1-q}} J_i(u(t_i^-))\right)\Big], \end{aligned} \tag{24}$$

by summarizing the above computation, we get the required result. Conversely, assume that u satisfies the impulsive fractional integral equation (11), then by direct computation, it can be seen that the solution given by (11) satisfies (12). This completes the proof of the lemma.

3 Existence and Uniqueness Results

The following result is based on Lemma 2.3.

Definition 3.1 The function $u : [0,T] \to X$ such that $u \in PC_t^1([0,T] : X)$ is said to be the solution of the system (5) if it satisfies the following integral equation

$$u(t) = \begin{cases} \int_0^t \frac{(t-s)^{\alpha-1}}{\Gamma(\alpha)} f(s,u(s), \int_0^s K(s,\tau)u(\tau)d\tau)ds \\ +a_1 - g(u) - \frac{t}{T}\Big[a_1 - a_2 + h(u) - g(u) \\ + \int_0^T \frac{(T-s)^{\alpha-1}}{\Gamma(\alpha)} f(s,u(s), \int_0^s K(s,\tau)u(\tau)d\tau)ds \\ + \sum_{i=1}^m I_i(u(t_i^-)) + \sum_{i=1}^m (T-t_i)\left(\frac{\Gamma(2-q)}{t_i^{1-q}} J_i(u(t_i^-))\right)\Big], & t \in [0,t_1), \\ ..... \\ \int_0^t \frac{(t-s)^{\alpha-1}}{\Gamma(\alpha)} f(s,u(s), \int_0^s K(s,\tau)u(\tau)d\tau)ds + \sum_{i=1}^k I_i(u(t_i^-)) \\ +a_1 - g(u) - \frac{t}{T}\Big[a_1 - a_2 + h(u) - g(u) \\ + \int_0^T \frac{(T-s)^{\alpha-1}}{\Gamma(\alpha)} f(s,u(s), \int_0^s K(s,\tau)u(\tau)d\tau)ds \\ + \sum_{i=1}^m I_i(u(t_i^-)) + \sum_{i=1}^m (T-t_i)\left(\frac{\Gamma(2-q)}{t_i^{1-q}} J_i(u(t_i^-))\right)\Big] \\ + \sum_{i=1}^k (t-t_i)\left(\frac{\Gamma(2-q)}{t_i^{1-q}} J_i(u(t_i^-))\right), & t \in (t_k, t_{k+1}]. \end{cases} \tag{25}$$

Our first result is based on Banach fixed point theorem.

Theorem 3.1 *Let the functions f, g, h, I_k and J_k satisfy the Lipchitz condition with positive constants L_1, L_2, L_3, L_4, L_5 and L_6, such that*

$$\begin{aligned} &\|f(t,u,v) - f(t,x,y)\|_X \le L_1\|u-x\|_X + L_2\|v-y\|_X, \\ &\|g(u) - g(x)\|_X \le L_4\|u-x\|_X, \ \ \|h(u) - h(x)\|_X \le L_6\|u-x\|_X, \\ &\|I_k(x) - I_k(y)\|_X \le L_3\|x-y\|_X, \ \ \|J_k(x) - J_k(y)\|_X \le L_5\|x-y\|_X, \end{aligned}$$

$t \in [0,T]$, $\forall\ x, y, u, v \in X$. *If the following inequality holds*

$$\Delta = \Big[\frac{(L_1 + L_2K^*)}{\Gamma(\alpha+1)} 2T^\alpha + 2mL_3 + 2L_4 + L_6 + 2mT^q\Gamma(2-q)L_5\Big] < 1,$$

then the system (5) has a unique solution.

Proof. We transform the system (5) into a fixed point problem. Consider an operator $N : PC_t^1 \to PC_t^1$, defined by

$$(Nu)t = \begin{cases} \int_0^t \frac{(t-s)^{\alpha-1}}{\Gamma(\alpha)} f(s,u(s), \int_0^s K(s,\tau)u(\tau)d\tau)ds \\ +a_1 - g(u) - \frac{t}{T}\Big[a_1 - a_2 + h(u) - g(u) \\ + \int_0^T \frac{(T-s)^{\alpha-1}}{\Gamma(\alpha)} f(s,u(s), \int_0^s K(s,\tau)u(\tau)d\tau)ds \\ + \sum_{i=1}^m I_i(u(t_i^-)) + \sum_{i=1}^m (T-t_i)\left(\frac{\Gamma(2-q)}{t_i^{1-q}} J_i(u(t_i^-))\right)\Big], & t \in [0,t_1), \\ \dots \\ \int_0^t \frac{(t-s)^{\alpha-1}}{\Gamma(\alpha)} f(s,u(s), \int_0^s K(s,\tau)u(\tau)d\tau)ds + \sum_{i=1}^k I_i(u(t_i^-)) \\ +a_1 - g(u) - \frac{t}{T}\Big[a_1 - a_2 + h(u) - g(u) \\ + \int_0^T \frac{(T-s)^{\alpha-1}}{\Gamma(\alpha)} f(s,u(s), \int_0^s K(s,\tau)u(\tau)d\tau)ds \\ + \sum_{i=1}^m I_i(u(t_i^-)) + \sum_{i=1}^m (T-t_i)\left(\frac{\Gamma(2-q)}{t_i^{1-q}} J_i(u(t_i^-))\right)\Big] \\ + \sum_{i=1}^k (t-t_i)\left(\frac{\Gamma(2-q)}{t_i^{1-q}} J_i(u(t_i^-))\right), & t \in (t_k, t_{k+1}]. \end{cases} \tag{26}$$

To show that N has fixed point consider $u_1, u_2 \in PC_t^1$. For $t \in [0, t_1)$, we have the following estimate

$$\begin{aligned}
&\|N(u_1) - N(u_2)\|_X \leq \\
&\int_0^t \frac{(t-s)^{\alpha-1}}{\Gamma(\alpha)} \|f(s, u_1(s), \int_0^s K(s,\tau)u_1(\tau)d\tau) - f(s, u_2(s), \int_0^s K(s,\tau)u_2(\tau)d\tau)\|_X ds \\
&+\|g(u_1) - g(u_2)\|_X + \frac{|t|}{T}\Big[\|h(u_1) - h(u_2)\|_X + \|g(u_1) - g(u_2)\|_X \\
&+ \int_0^T \frac{(T-s)^{\alpha-1}}{\Gamma(\alpha)} \|f(s, u_1(s), \int_0^s K(s,\tau)u_1(\tau)d\tau) \\
&-f(s, u_2(s), \int_0^s K(s,\tau)u_2(\tau)d\tau)\|_X ds + \sum_{i=1}^m \|I_i(u_1(t_i^-)) - I_i(u_2(t_i^-))\|_X \\
&+\sum_{i=1}^m |(T-t_i)| \frac{\Gamma(2-q)}{|t_i|^{1-q}} \|J_i(u_1(t_i^-)) - J_i(u_2(t_i^-))\|_X\Big],
\end{aligned}$$

On simplifying, we obtain

$$\begin{aligned}
&\|N(u_1) - N(u_2)\|_{PC_t^1} \\
&\leq \Big[\frac{(L_1 + L_2K^*)}{\Gamma(\alpha+1)} 2T^\alpha + 2L_4 + L_6 + mL_3 + mT^q\Gamma(2-q)L_5\Big]\|u_1 - u_2\|_{PC_t^1}.
\end{aligned}$$

For $t \in (t_k, t_{k+1}]$, we have

$$\begin{aligned}
&\|N(u_1) - N(u_2)\|_X \\
&\leq \int_0^t \frac{(t-s)^{\alpha-1}}{\Gamma(\alpha)} \|f(s, u_1(s), \int_0^s K(s,\tau)u_1(\tau)d\tau) \\
&-f(s, u_2(s), \int_0^s K(s,\tau)u_2(\tau)d\tau)\|_X ds \\
&+\sum_{i=1}^k \|I_i(u_1(t_i^-)) - I_i(u_2(t_i^-))\|_X + \|g(u_1) - g(u_2)\|_X + \frac{|t|}{T}\Big[\|h(u_1) - h(u_2)\|_X \\
&+\|g(u_1) - g(u_2)\|_X + \int_0^T \frac{(T-s)^{\alpha-1}}{\Gamma(\alpha)} \|f(s, u_1(s), \int_0^s K(s,\tau)u_1(\tau)d\tau) \\
&-f(s, u_2(s), \int_0^s K(s,\tau)u_2(\tau)d\tau)\|_X ds + \sum_{i=1}^m \|I_i(u_1(t_i^-)) - I_i(u_2(t_i^-))\|_X \\
&+\sum_{i=1}^m |(T-t_i)| \frac{\Gamma(2-q)}{|t_i|^{1-q}} \|J_i(u_1(t_i^-)) - J_i(u_2(t_i^-))\|_X\Big] \\
&+\sum_{i=1}^k |(t-t_i)| \frac{\Gamma(2-q)}{|t_i|^{1-q}} \|J_i(u_1(t_i^-)) - J_i(u_2(t_i^-))\|_X,
\end{aligned}$$

Hence we estimate as

$$\begin{aligned}
&\|N(u_1) - N(u_2)\|_{PC_t^1} \\
&\leq \Big[\frac{(L_1 + L_2K^*)}{\Gamma(\alpha+1)} 2T^\alpha + 2mL_3 + 2L_4 + L_6 + 2mT^q\Gamma(2-q)L_5\Big]\|u_1 - u_2\|_{PC_t^1} \\
&\leq \Delta\|u_1 - u_2\|_{PC_t^1}.
\end{aligned}$$

Since $\Delta < 1$, it follows that the operator N is a contraction mapping and has a fixed point $u \in PC_t^1$, hence the system (5) has a unique solution on the interval $[0, T]$. This completes the proof of the theorem.

Our second result is based on Schauder fixed point theorem.

Theorem 3.2 *Let the functions f, g, h, I_k, J_k be continuous and there exist positive constants M_1, M_2, M_3, M_4 and M_5 such that $\|f(t,u,v)\|_X \leq M_1$, $\|g(u)\|_X \leq M_2$, $\|h(u)\|_X \leq M_3$, $\|I_k(y)\|_X \leq M_4$, $\|J_k(y)\|_X \leq M_5$, $\forall u, v, y \in X$. Then the system (5) has at least one solution on $[0, T]$.*

Proof. Consider an operator $N : PC_t^1 \to PC_t^1$ defined as in (26) in Theorem 3.1. First, we shall show that N is continuous, let us consider a sequence $u_n \to u$ in PC_t^1 in the interval $(t_k, t_{k+1}]$, $(k = 1, \ldots, m)$ we have

$$
\begin{aligned}
&\|N(u_n) - N(u)\|_X \\
&\leq \int_0^t \frac{(t-s)^{\alpha-1}}{\Gamma(\alpha)} \Big(\|f(s, u_n(s), \int_0^s K(s,\tau) u_n(\tau) d\tau) \\
&- f(s, u(s), \int_0^s K(s,\tau) u(\tau) d\tau) \|_X \Big) ds \\
&+ \sum_{i=1}^{k} \|I_i(u_n(t_i^-)) - I_i(u(t_i^-))\|_X + \|g(u_n) - g(u)\|_X - \frac{|t|}{T} \Big[\|h(u_n) - h(u)\|_X \\
&+ \|g(u_n) - g(u)\|_X + \int_0^T \frac{(T-s)^{\alpha-1}}{\Gamma(\alpha)} \Big(\|f(s, u_n(s), \int_0^s K(s,\tau) u_n(\tau) d\tau) \\
&- f(s, u(s), \int_0^s K(s,\tau) u(\tau) d\tau) \|_X \Big) ds + \sum_{i=1}^{m} \|I_i(u_n(t_i^-)) - I_i(u(t_i^-))\|_X \\
&+ \sum_{i=1}^{m} |(T - t_i)| \left(\frac{\Gamma(2-q)}{|t_i|^{1-q}} \|J_i(u_n(t_i^-)) - J_i(u(t_i^-))\|_X \right) \Big] \\
&+ \sum_{i=1}^{k} |(t - t_i)| \left(\frac{\Gamma(2-q)}{|t_i|^{1-q}} \|J_i(u_n(t_i^-)) - J_i(u(t_i^-))\|_X \right).
\end{aligned}
$$

Since the functions f, g, h, I_k, J_k are continuous, $\|N(u_n) - N(u)\|_{PC_t^1} \to 0$, as $n \to \infty$ which implies that the mapping N is continuous on PC_t^1.

Now, consider the space $\mathcal{B}_r = \{u \in PC_t^1 : \|u\|_{PC_t^1} \leq r\}$. It is obvious that $\mathcal{B}_r$ is closed, bounded and convex subset of PC_t^1. Let $u \in \mathcal{B}_r$, then for $t \in (t_k, t_{k+1}]$, we have

$$
\begin{aligned}
&\|Nu(t)\|_X \\
&\leq \int_0^t \frac{(t-s)^{\alpha-1}}{\Gamma(\alpha)} \|f(s, u(s), \int_0^s K(s,\tau) u(\tau) d\tau)\|_X ds \\
&+ \sum_{i=1}^{k} \|I_i(u(t_i^-))\|_X + a_1 + \|g(u)\|_X + \frac{|t|}{T} \Big[a_1 + a_2 + \|h(u)\|_X + \|g(u)\|_X \\
&+ \sum_{i=1}^{m} \|I_i(u(t_i^-))\|_X + \int_0^T \frac{(T-s)^{\alpha-1}}{\Gamma(\alpha)} \|f(s, u(s), \int_0^s K(s,\tau) u(\tau) d\tau)\|_X ds \quad (27)
\end{aligned}
$$

$$+\sum_{i=1}^{m}|(T-t_i)|\left(\frac{\Gamma(2-q)}{|t_i|^{1-q}}\|J_i(u(t_i^-))\|_X\right)\Big]$$
$$+\sum_{i=1}^{k}|(t-t_i)|\left(\frac{\Gamma(2-q)}{|t_i|^{1-q}}\|J_i(u(t_i^-))\|_X\right), \tag{28}$$

it can be estimated as

$$\|Nu(t)\|_{PC_t^1}\leq 2M_1\frac{T^\alpha}{\Gamma(\alpha+1)}+2mM_4+2a_1+2M_2+a_2+M_3+2mT^q\Gamma(2-q)M_5.$$

Its proves that N maps bounded set into bounded set in $\mathcal{B}_r$ for all subintervals $(t_k,t_{k+1}],\ (k=1,\dots,m)$.

Finally, we shall show that N maps bounded sets into equi-continuous sets in $\mathcal{B}_r$. Let $l_1,l_2\in(t_k,t_{k+1}]$ with $l_1<l_2,\ 1\leq k\leq m$, we have

$$\begin{aligned}
&\|(Nu)(l_2)-(Nu)(l_1)\|_X\\
&\leq\|\int_0^{l_2}\frac{(l_2-s)^{\alpha-1}}{\Gamma(\alpha)}f(s,u(s),\int_0^s K(s,\tau)u(\tau)d\tau)ds\\
&-\int_0^{l_1}\frac{(l_1-s)^{\alpha-1}}{\Gamma(\alpha)}f(s,u(s),\int_0^s K(s,\tau)u(\tau)d\tau)ds\|_X\\
&+\frac{|(l_2-l_1)|}{T}\Big[\int_0^T\frac{(T-s)^{\alpha-1}}{\Gamma(\alpha)}\|f(s,u(s),\int_0^s K(s,\tau)u(\tau)d\tau)\|_X ds\Big]\\
&+\sum_{i=1}^{k}|(l_2-l_1)|\left(\frac{\Gamma(2-q)}{|t_i|^{1-q}}\|J_i(u(t_i^-))\|_X\right).
\end{aligned}$$

it can be estimated as

$$\begin{aligned}
&\|(Nu)(l_2)-(Nu)(l_1)\|_{PC_t^1}\\
&\leq\frac{M_1}{\Gamma(\alpha+1)}\Big((l_2-l_1)^\alpha+\|-(l_2-l_1)^\alpha+(l_2-l_k)^\alpha-(l_1-l_k)^\alpha\|\Big)\\
&+\frac{(l_2-l_1)}{T}\Big[M_1\frac{T^\alpha}{\Gamma(\alpha+1)}\Big]+m(l_2-l_1)\left(\frac{\Gamma(2-q)}{T^{1-q}}M_5\right),
\end{aligned}$$

which is independent of u. Thus, N is equicontinuous. Thus all the assumptions of Sachuder's fixed point theorem are satisfied. Hence, the system (5) has at least one solution on $[0,T]$.

4 Example

Consider the following fractional order impulsive integro- differential equation with non-local conditions:

$$\begin{cases}
{}^cD^{3/2}u(t)=\frac{e^t|u(t)|}{(9+e^t)(1+|u(t)|)}+\int_0^t\frac{e^{-(s-t)}}{10}|u(s)|ds,\ t\in[0,1],\ t\neq(1/3),\\
\Delta u(1/3)=\frac{|u(1/3)|}{17+|u(1/3)|},\ \Delta({}^cD^{1/2}u(1/3))=\frac{|u(1/3)|}{19+|u(1/3)|},\\
u(0)=-\int_0^1\frac{|u(s)|}{23+|u(s)|}ds,\quad u(T)=-\int_0^1\frac{|u(s)|}{25+|u(s)|}ds.
\end{cases} \tag{29}$$

Here $f(t,u,\int_0^t K(t,s)u(s)ds) = \frac{e^t|u(t)|}{(9+e^t)(1+|u(t)|)} + \int_0^t \frac{e^{-(s-t)}}{10}|u(s)|ds$. Let $x,y \in X$ and $t \in [0,1]$ then we have

$$\begin{aligned}
&|f(t,x,\int_0^t K(t,s)x(s)ds) - f(t,y,\int_0^t K(t,s)y(s)ds)| \\
&= |\frac{e^{-t}}{(9+e^t)}\Big[\frac{|x(t)|}{1+|x(t)|} - \frac{|y(t)|}{1+|y(t)|}\Big]| + |\int_0^t K(t,s)[x(s)-y(s)]ds| \\
&= |\frac{e^{-t}}{(9+e^t)}[\frac{|x(t)(1+|y(t)|) - |y(t)|(1+|x(t)|)|}{(1+|x(t)|)(1+|y(t)|)}]| \\
&+|\int_0^t \frac{e^{-(s-t)}}{10}(x(s)-y(s))ds| = |\frac{e^{-t}}{(9+e^t)}[\frac{|x(t)|-|y(t)|}{(1+|x(t)|)(1+|y(t)|)}]| \\
&+|\int_0^t \frac{e^{-(s-t)}}{10}(x(s)-y(s))ds|.
\end{aligned}$$

By taking sup norm we estimate it as follows

$$||f(t,x,\int_0^t K(t,s)x(s)ds) - f(t,y,\int_0^t K(t,s)y(s)ds)||_X \leq \frac{1}{10}\|x-y\|_X.$$

In similar way we can verify the following estimates

$$\|g(x)-g(y)\|_X \leq \frac{1}{23}\|x-y\|_X,\ \|h(x)-h(y)\|_X \leq \frac{1}{25}\|x-y\|_X,\ \forall\, x,y \in X,$$
$$\|I_k(x)-I_k(y)\|_X \leq \frac{1}{17}\|x-y\|_X,\ \|J_k(x)-J_k(y)\|_X \leq \frac{1}{19}\|x-y\|_X,\ \forall\, x,y \in X.$$

The rest of the parameters used in Theorem 3.1 are computed as $q = \frac{1}{2},\ \alpha = \frac{3}{2},\ (L_1 + L_2K^*) = \frac{1}{10},\ L_3 = \frac{1}{17},\ L_4 = \frac{1}{23},\ L_5 = \frac{1}{19},\ L_6 = \frac{1}{25}$, and the inequality

$\Big[\frac{(L_1+L_2K^*)}{\Gamma(\alpha+1)}2T^\alpha + 2mL_3 + 2L_4 + L_6 + 2mT^q\Gamma(2-q)L_5\Big] = 0.48834 < 1.$

Thus, all the conditions of Theorem 3.1 are satisfied. Hence, the impulsive fractional boundary value problem (5) has a unique solution on $[0,1]$.

5 Conclusion

At the foundation of this paper, one can consider the fractional integro-differential equation of order $\alpha \in (1,2)$ with nonlocal boundary conditions and fractional impulsive conditions. For the solution of the system (5) we follow the concept from the recent contributions on impulsive fractional differential equations by M. Feckan et al. [12, 16, 19]. The existence and uniqueness of solutions for the system (5) are treated with the help of Banachs and Schauders fixed point theorems.

References

[1] Agarwal, R.P., Benchohra, M. and Hamani, S. A survey on existence results for boundary value problems of nonlinear fractional differential equations and inclusions. *Acta Applicandae Mathematicae* **109** (2010) 973–1033.

[2] Ahmad, B. and Nieto, J.J. Existence results for nonlinear boundary value problems of fractional integrodifferential equations with integral boundary conditions. *Boundary Value Problems*, Article ID 708576 (2009) 1–11.

[3] Ahmad, B., and Sivasundaram, S. Existence of solutions for impulsive integral boundary value problems of fractional order. *Nonlinear Analysis, Hybrid Systems* **4** (2010) 134–141.

[4] Bai, C. Solvability of multi-point boundary value problem of nonlinear impulsive fractional differential equation at resonance. *Electronic Journal of Qualitative Theory of Differential Equations* **89** (2011) 1–19.

[5] Bai, C. Existence result for boundary value problem of nonlinear impulsive fractional differential equation at resonance. *Journal of Applied Mathematics and Computing* **39** (2012) 421–443.

[6] Chuhan, A., Dabas, J. and Kumar, M. Integral boundary value problem for impulsive fractional functional differential equations with infinte delay. *Electronic Journal of Differential Equations* **229** (2012) 1–13.

[7] Cao, J. and Chen, H. Some results on impulsive boundary value problem for fractional differential inclusions. *Electronic Journal of Qualitative Theory of Differential Equations* **11** (2011) 1–24.

[8] Dabas, J., Chauhan, A. and Kumar, M. Existence of the mild solutions for impulsive fractional equations with infinite delay. *International Journal of Differential Equations* (2011), Art. ID 793023.

[9] Dabas, J. and Gautam, G. R. Impulsive neutral fractional integro-differential equations with state dependent delays and integral condition. *Electronic Journal of Differential Equations* **273** (2013) 1–13.

[10] Deimling, K. Nonlinear Functional Analysis. Springer-Verlag Berlin Heidelberg New York Tokyo, New York, 1980.

[11] Fu, X. and Liu, X. Existence results for fractional differential equations with separated boundary conditions and fractional impulsive conditions. *Abstract and Applied Analysis*, Article ID 785078 (2013) 1–9.

[12] Feckan, M., Zhou, Y. and Wang, J. On the concept and existence of solution for impulsive fractional differential equations. *Communications in Nonlinear Science and Numerical Simulation* **17** (2012) 3050–3060.

[13] Kilbas, A.A., Srivastava, H.M. and Trujillo, J.J. Theory and Applications of Fractional Differential Equations. Elsevier Science B.V, Amsterdam, 2006.

[14] Kosmatov, N. Initial value problems of fractional order with fractional impulsive conditions. *Results in Mathematics* **63** (2013) 1289–1310.

[15] Podlubny, I. Fractional Differential Equations. Acadmic press, New York, 1993.

[16] Feckan, M., Zhou, Y. and Wang, J. Response to "Comments on the concept of existence of solution of existence of solution for impulsive fractional differential equations". *Commun Nonlinear Sci Numer Simulat* **19** (2014) 4213–4215.

[17] Wang, J., Ibrahim, A.G. and Feckan, M. Nonlocal impulsive fractional differential inclusions with fractional sectorial operators on Banach spaces. *Appl. Math. Comput.* **257** (2015) 103–118.

[18] Atmania, R. and Mazouzi, S. Existence of local and global solutions to some impulsive fractional differential equation. *Electronic Journal of Differential Equations* **136** (2009) 1–9.

[19] Wang, J., Zhou, Y. and Feckan, M. On recent developments in the theory of boundary value problems for impulsive fractional differential equations. *Computers and Mathematics with Applications* **64** (2012).

[20] Yang, L. and Chen, H. Nonlocal boundary value problem for impulsive differential equations of fractional order. *Advances in Difference Equations*, Article ID 404917 (2011) 1–16.

[21] Dabas, J. Existence and uniqueness of solutions to quasilinear integro-differential equations by the method of lines. *Nonlinear Dynamics and Systems Theory* **11** (4) (2011) 397–410.

[22] Becker, L.C., Burton, T.A., Purnaras, I.K. An inversion of a fractional differential equation and fixed points. *Nonlinear Dynamics and Systems Theory* **15** (3) (2015) 242–271.

[23] Shukla, A., Sukavanam, N., Pandey, D.N. Approximate controllability of semilinear stochastic control system with nonlocal conditions. *Nonlinear Dynamics and Systems Theory* **15** (3) (2015) 321–333.

[24] Benchohra, M., Graef, J. R., Mostefai, F.Z. Weak solutions for boundary value problems with nonlinear fractional differential inclusions. *Nonlinear Dynamics and Systems Theory* **11** (3) (2011) 227–237.

[25] Yu, J.M., Luo, Y.W., Zhou, S.B. and Lin, X.R. Existence and uniqueness for nonlinear multi-variables fractional differential equations. *Nonlinear Dynamics and Systems Theory* **11** (2) (2011) 213–221.

[26] Bahuguna, D., Shukla, R.K. and Saxena, S. Functional differential equations with nonlocal conditions in Banach spaces. *Nonlinear Dynamics and Systems Theory* **10** (4) (2010) 317–323.

Nonlinear Dynamics and Systems Theory, **15** (4) (2015) 383–399

Passive Kinematic Synchronization of Dissimilar and Uncoupled Rotating Systems

I. Handžić *, H. Muratagić, and K.B. Reed

University of South Florida,
Department of Mechanical Engineering,
Tampa, FL, USA

Received: April 3, 2015; October 31, 2015

Abstract: Passive kinematic synchronization enables two dynamic physical systems to generate the same motion without any physical interaction or mediating control laws. In this paper, we demonstrate a generalized kinematic matching technique to model and passively synchronize two physically dissimilar and uncoupled rotating systems. The method is demonstrated by matching the motion of systems with different masses and mass distributions. Specifically, we matched the nonlinear motion between three single-link pendulums and the motions of two double-link pendulums. Despite the highly nonlinear dynamics of a double-link pendulum, temporal and spectral analysis results show that the two different and kinematically-matched systems generate nearly identical motion. The method is generalizable and can be used to describe and match the kinematics of any dissimilar open-ended rotating system chain such as rotors, discs, cams, or pendulum type systems. This method has implications for the modeling of physical rotating system dynamics, the study of swinging limbs in humans, animals, and robots, and in limb prosthesis design. We also present a step-by-step method to create a dissimilar but synchronized, rotating system, that is, passively matched to an original system. Further, we present a step-by-step method to kinematically synchronize two already available dissimilar rotating systems.

Keywords: *passive synchronization; nonlinear systems; uncoupled systems; pendulum; kinematic matching; physical rotating systems.*

Mathematics Subject Classification (2010): 93C10, 70K99.

* Corresponding author: mailto:ihandzic@mail.usf.edu

© 2015 InforMath Publishing Group/1562-8353 (print)/1813-7385 (online)/http://e-ndst.kiev.ua

1 Introduction

Kinematic synchronization of systems is the matching of motion between two moving systems. The synchronization of any two rotating systems can be as simple as physically placing a joining spring or damper between the systems or may require sophisticatedly controlled actuators that augment natural system dynamics. Here, we focus on *dissimilar* rotating systems *without* any physical coupling. Our passive kinematic matching technique allows two independent systems to generate the same motion without any physical system coupling or actuator control law. To validate this method, this passive synchronization technique is applied to two open-ended rotating kinematic chains: single- and double- link pendulums with different masses at different mass locations along links. Even though double-link pendulums are highly nonlinear systems that are sensitive to changes in initial conditions and system parameters, our passive matching technique enables the same generated motion on dissimilar double-link pendulums.

The practical application of such a passive matching technique is the flexibility in mechanical design as one is able to describe the same kinematics with a variety of parameters (i.e., masses and mass distributions). In essence, one is able to decouple the mass and the first moment and second moment of inertia so systems with dissimilar masses and mass distributions will have the same motion. For example, the motion of a double-link pendulum modeled as two links with one mass per link can only be described by one unique combination of masses and mass locations along the links. However, having two masses per link allows the kinematics to be described with an infinite number of distinct systems with distinct masses and mass distribution that all have the same resulting motion. In fact, the minimum number of masses per rotating link to describe any arbitrary rotational kinematics is two masses, yet many models only include one mass. Using only one mass per link inherently couples the moments of inertia so that any change in the location of the mass necessarily affects both the first and second moments of inertia.

The modeling method to derive our synchronization technique can be used to simplify complicated rotational kinematics problems by simplifying the dynamics model of the system by assuming a finite distribution of point masses along swinging members. For example, the rotation of a fan blade can be represented with two masses distributed as specified using this method instead of finding detailed masses, mass distributions, or moments of inertias of the continuous system. This type of modeling can also be applied to human or robotic limbs and in prosthesis design. It is stressed that this point-mass modeling technique is not novel, however is used to develop our novel passive synchronization method that matches the rotational kinematics of two dissimilar and uncoupled rotational systems.

The only requirements for our passive kinematic synchronization of dissimilar systems are: identical degrees of freedom, initial conditions, and torques applied to the systems. These same requirements are also needed to cause two identical systems to have the same motion.

In the proceeding sections we will derive the essential and general model for an open-ended multi-degree of freedom rotational system, define the kinematic matching coefficients needed for system synchronization, and outline the step-by-step instructions on how to passively match the kinematics of newly created or already available systems.

We further form two examples providing proof and application of this system representation and unique passive matching method of dissimilar systems by

mathematically and experimentally analyzing three dissimilar one-degree-of-freedom systems and also two dissimilar two-degree-of-freedom systems.

2 Background

2.1 Coupled synchronization

In 1657, in the quest to improve nautical navigation, Dutch mathematician Christiaan Huygenes invented the first pendulum clock [2]. Pendulum clocks were astounding mechanisms of their day. An interesting aspect is that they tend to synchronize and operate in phase or anti-phase when hung on the same wall with another pendulum clock. He deduced that the clocks were coupled by their common supporting structures which transferred small movements between clocks. This clock can be considered the first observation of a *synchronized coupled* oscillator.

The kinematic synchronization of two or more coupled mechanical systems such as Huygen's clock has been extensively studied since the time of Huygen himself. More recent such studies include the synchronization of coupled nonlinear oscillators [3], analysis of coupled multi-pendulum systems [5], and synchronization of double pendulums under the effects of external forces [18]. Osipov et al. [24] published a thorough review on synchronization in oscillatory networks, which mainly discusses different aspects of synchronization in chains and lattices of interconnected oscillatory elements.

As part of the rise of faster computing power came the ability to actively synchronize coupled mechanical systems with linear, nonlinear, passivity-based, or active control laws. There are hundreds of publications which demonstrate such control laws, some of these publications are on controlled motion synchronization for gyroscopes [23], inverted pendulum systems [22], and chaotic systems [19].

2.2 Uncoupled synchronization

Passive kinematic synchronization of physically uncoupled systems has been studied significantly less and the authors were only able to find two examples of uncoupled passive synchronization, both of which are rooted in sports science.

A golfer's technique as well as familiar equipment play an essential role in a golfer's performance. It is for this reason that all golf clubs in a set are matched (synchronized) statically and dynamically, so when swung, each club behaves and feels the same to the golfer [1]. Statically a golf club is matched by simply balancing it on a fulcrum, however dynamically matching the golf club can be achieved by matching the moment of inertia for each club in the set about the swinging axis [4]. Jorgensen presents a golf club dynamic synchronization technique by modeling the swing arm and golf club and matching overall moments of inertia about the wrist axis [17]. In these examples the kinematics of each uncoupled system (golf club) is synchronized given the same input torque (the golfer's swing). While this technique of golf club matching is practical in its specific application, it lacks generalization and flexibility to apply to other rotating systems to be synchronized.

Although very little can be found in the field of passive synchronization of uncoupled systems, a generalized passive synchronization method for physically uncoupled rotating systems has practical implications for locomotion robotics, lower limb gait analysis, and prosthetics. For instance, an individual's walk can largely be modeled as two inverted

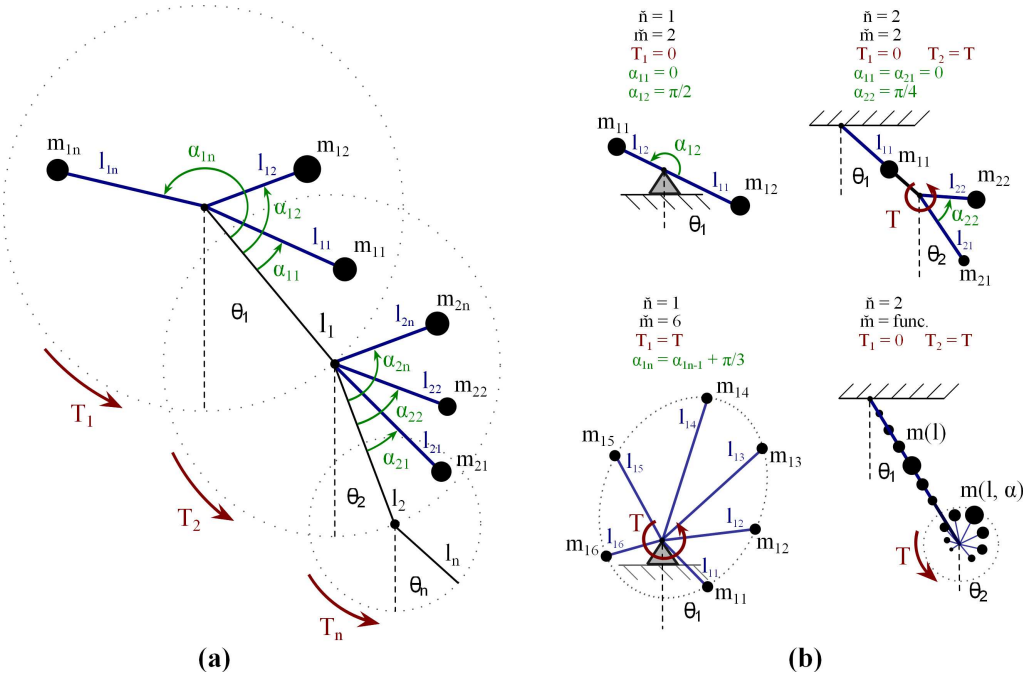

Figure 1: (a) General Rotating System Model. (b) The general rotating systems model can be adjusted to represent various configurations for rotating systems. These configurations can represent a sea-saw/rotor, double pendulum, cam, or a continuous mass distribution along rotating members.

pendulums (left and right step) rotating about the stance foot and progressing down a decline with gravity as the only source of energy [20]. Such models are called passive dynamic walkers (PDW) and have been shown to predict certain aspects of human gait dynamics [7, 13, 14]. Honeycutt et. al [16] used a brute force search through a numerical PDW model to show that asymmetric limbs can have symmetric kinematics, and moving a prosthetic knee joint lower while lowering the prosthetic mass can result in a spatially symmetric gait. Gregg [10, 11] examined symmetry from the other point of view by finding symmetric PDW parameters that yielded asymmetric kinematics. A leg synchronization technique for PDWs, general walking robots, and individuals can be helpful to design and implement devices and methods which either even out gait asymmetries [8], or intentionally exaggerate gait asymmetries for rehabilitation [12, 25]. These gait asymmetries can also arise from the asymmetric size and weight of a prosthetic limb [15].

3 Passive Kinematic Synchronization Technique Derivation

This section outlines the equations used to derive the kinematics of a two-dimensional general rotating system essential for our passive synchronization method. Subsequently we will use this generalized model to draw out a method to synchronize two or more dissimilar rotating systems with the same degrees of freedom, initial conditions, and torque input.

3.1 General rotating system model description

We begin by deriving the equation of motion for a general rotating system with $\check{n}$ *degrees of freedom* and $\check{m}$ *masses per degree of freedom*. Variable notation m symbolizes each individual mass whereas $\check{m}$ symbolizes the *total number* of masses per rotating member (or link). This generalized model is shown in Figure 1a, and can be described using Lagrangian mechanics where the Lagrangian is defined as the difference of kinetic and potential energy. Note that this following formulation of the generalized equation of motion is not novel, however it is used in the subsequently described kinematic matching technique

$$L(\theta, \dot{\theta}, t) = K(\theta, \dot{\theta}, t) - U(\theta, t). \tag{1}$$

To find the equation of motion, the Euler-Lagrange expression is applied:

$$\frac{d}{dt}\left(\frac{\partial L(\theta, \dot{\theta}, t)}{\partial \dot{\theta}_{1,2\ldots\check{n}}}\right) = \frac{\partial L(\theta, \dot{\theta}, t)}{\partial \theta_{1,2\ldots\check{n}}}. \tag{2}$$

Equation (2) produces $\check{n}$ equations for $\check{n}$ degrees of freedom of the system. After differentiating and collecting coefficients, the equations of motion of this general dynamic system are a set of $\check{n}$ number of first order nonlinear ordinary differential equations shown in matrix coefficient form in equation (3)

$$[M]\,\ddot{\Theta} \;+\; [N]\,\dot{\Theta}^2 \;+\; [G] \;=\; [T], \tag{3}$$

where the coefficient matrices [M], [N], and [G] are given in equations (4), (7), and (8), respectively. [M] is the inertia matrix coefficient, [N] is the velocity matrix coefficient, and [G] is the position/gravity coefficient matrix. [T] can represent any applied or non-conservative torque functions applied to the system such as actuator torque, joint friction torque, or air resistance experienced by a swinging member,

$$[M]^{\check{n},\check{n}}_{\text{sym}} = \begin{bmatrix} \mathbf{M}_{1,1} & \mathbf{M}_{1,2}\,cos(\theta_1-\theta_2) & \cdots & \mathbf{M}_{1,j}\,cos(\theta_1-\theta_j) \\ \mathbf{M}_{1,2}\,cos(\theta_1-\theta_2) & \mathbf{M}_{2,2} & & \vdots \\ \vdots & & \ddots & \mathbf{M}_{i-1,j}\,cos(\theta_{i-1}-\theta_j) \\ \mathbf{M}_{1,j}\,cos(\theta_1-\theta_j) & \cdots & & \mathbf{M}_{i,i} \end{bmatrix}. \tag{4}$$

Here, each of the coefficients on the diagonal are given by

$$\mathbf{M}_{i,i} = \sum_{p=1}^{\check{m}} l_{i,p}^2 m_{i,p} + l_i^2 \sum_{q=i+1}^{\check{n}} \sum_{p=1}^{\check{m}} m_{q,p} \tag{5}$$

and the remaining non-diagonal coefficients are given by

$$\mathbf{M}_{i,j} = l_i \left[\sum_{p=1}^{\check{m}} l_{j,p} m_{j,p} + \begin{cases} l_j \sum_{q=j+1}^{\check{n}} \sum_{p=1}^{\check{m}} m_{q,p} & j < \check{n} \\ 0 & j \geq \check{n} \end{cases} \right]. \tag{6}$$

The subscripts i and j represent the matrix entry indexes for matrix row and matrix column, respectively,

$$[N]^{\check{n},\check{n}} = \begin{bmatrix} 0 & M_{1,2}\sin(\theta_1-\theta_2) & \cdots & M_{1,j}\sin(\theta_1-\theta_j) \\ -M_{1,2}\sin(\theta_1-\theta_2) & 0 & & \vdots \\ \vdots & & \ddots & M_{i-1,j}\sin(\theta_{i-1}-\theta_j) \\ -M_{1,j}\sin(\theta_1-\theta_j) & \cdots & & 0 \end{bmatrix}, \tag{7}$$

$$[G]^{\check{n}} = \begin{bmatrix} \sum_{\mathbf{p=1}}^{\check{m}} \mathbf{l_{1,p}m_{1,p}sin}(\alpha_{\mathbf{1,p}}+\theta_{\mathbf{1}}) + (\mathbf{l_1}\sum_{\mathbf{q=2}}^{\check{n}}\sum_{\mathbf{p=1}}^{\check{m}}\mathbf{m_{q,p}})\ sin(\theta_1) \\ \vdots \\ \sum_{\mathbf{p=1}}^{\check{m}} \mathbf{l_{i,p}m_{i,p}\,sin}(\alpha_{\mathbf{i,p}}+\theta_{\mathbf{i}}) + (\mathbf{l_i}\sum_{\mathbf{q=i+1}}^{\check{n}}\sum_{\mathbf{p=1}}^{\check{m}}\mathbf{m_{q,p}})\ sin(\theta_i) \\ \vdots \\ \sum_{\mathbf{p=1}}^{\check{m}} \mathbf{l_{\check{n},p}m_{\check{n},p}sin}(\theta_{\mathbf{\check{n},p}}+\theta_{\mathbf{\check{n}}}) \end{bmatrix} g. \tag{8}$$

These are the coefficient matrices for the equations of motion of a general rotating system model with $\check{n}$ degrees of freedom and $\check{m}$ masses per degree of freedom. The [M] matrix is a symmetric matrix, while the [N] matrix is a negatively mirrored matrix with a zero diagonal. Note that the coefficients [equations (5) and (6)] are all unique matrix components in the $[N]$ matrix that all appear in the $[M]$ matrix. Also note that the last row of $[G]$ ($i = \check{n}$) is different since there are no masses from links further down the kinematic chain sequence. Masses (m) and mass distributions (l) are shown in Figure 1a.

Equation (3) can model any degree of rotating system or rotating system links. Degrees of freedom (links), mass, and mass distribution within each link can be easily modified to create models for such systems as shown in Figure 1b. These modified models can represent rotors, pendulums, cams, or rotating kinematic systems and open kinematic chains.

3.2 Passive kinematic synchronization using kinematically matched coefficients

Now that we have defined the general point-mass model for a rotational open-ended swinging system, we are able to utilize to create synchronized motion between two dissimilar systems.

Given the same torque input and initial conditions, two or more systems with the same degrees of freedom will exactly match in dynamics if all four coefficient matrices, $[M]$, $[N]$, $[G]$, and $[T]$ in equation (3) are matched between the systems. Since only the computed end values of these coefficients determine the dynamic behavior of the rotating systems, the masses and mass distribution do not have to match between them. This allows for two

or more systems with dissimilar mass and mass distribution parameters to kinematically behave identically, that is, have identical dynamic coefficients $[M]$, $[N]$, $[G]$ and $[T]$. For instance, assuming identical torque input and initial conditions, a swinging single link pendulum with two masses can be designed to swing identically to another single link pendulum with two or more masses, where the masses are distributed differently along the pendulum link. This concept allows for the first and second moments of inertia to be decoupled and greater design flexibility is obtained. Given that each link has two or more masses distributed along the link ($\check{m} \geq 2$), there are infinite combinations of kinetmatically matched systems, that is, there is an infinite number of ways the masses can be distributed such that the four coefficient matrices in equation (3) match another system.

When the coefficient matrices are generalized for systems with $\check{n}$ degrees of freedom with $\check{m}$ masses per link (equations 4, 7 and 8), a pattern of repeating matrix entries emerges. It is seen that for the coefficient matrices to match between two rotating systems and cause synchronized dynamics, only unique parts of the coefficient matrices need to be matched between systems. We will call each unique term that appears in the coefficient matrices a *kinematically matched coefficient* (KMC). The KMCs are represented in equations (5), (6) and (8) and are written in **bold and highlighted** font. The total number of KMCs that have to be matched between kinematically synchronized systems is given in Table 1. For example, to synchronize the dynamics of a pair of one degree of freedom rotating systems, two KMCs need to be matched, while for a pair of three degree of freedom systems to be synchronized, nine KMCs need to be matched.

In the following section, we will review step-by-step instructions on how to apply the passive kinematic synchronization technique for dissimilar and rotating systems, while in Sections 4 and 5 we present two examples of this matching technique for one and two degree-of-freedom systems with experimental validation.

4 Example 1: Passive Single Link Pendulum

In this section, we utilize the method derived in Section 3 and experimentally demonstrate its validity. We start with creating two matched variations of a traditional passive ($[T] = 0$) single mass ($\check{m}$=1) single link ($\check{n}$=1) pendulum that is shown in Figure 2a. Our created variations of the single link pendulum have two masses per link ($\check{m}$=2) (Figure 2b).

Although more masses could be utilized to match the motion of this single link pendulum, two masses are sufficient to describe any number of masses and mass

Table 1: Number of Kinematically Matched Coefficients For Synchronized Uncoupled Motion between Two or More Systems.

DOF ($\check{n}$)	**Number of KMCs**
1	2
2	5
3	9
$\vdots$	$\vdots$
$\check{n}$	$KMC_{\check{n}-1} + (\check{n}+1)$

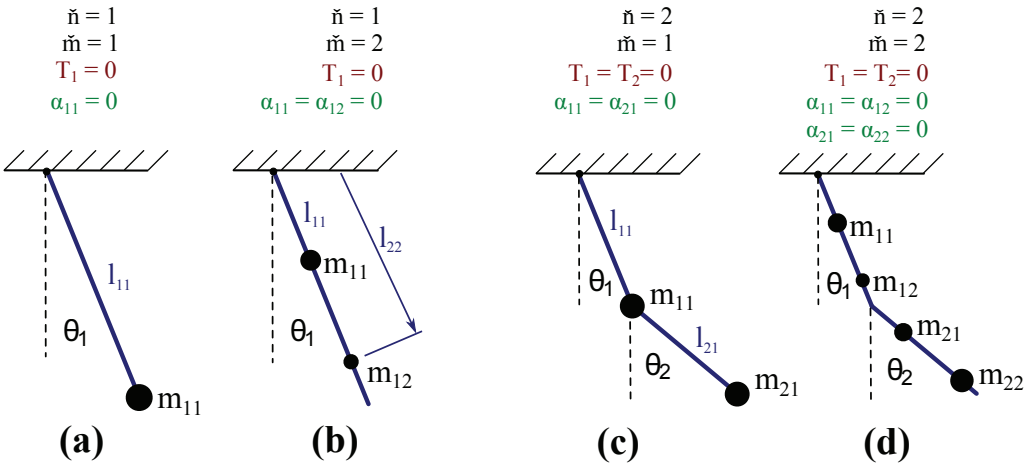

Figure 2: Single link and double (2-link) pendulum representation model. (a), (b), and (d) were used experimentally.

distributions. The parameters of all three dissimilar single link pendulums are shown in Table 2. Since a single link pendulum is one degree of freedom, only two KMCs had to be matched between systems ($M_{1,1}$=33,600 g-cm^2 and G_1=1,260 g-cm).

4.1 Experiment description

The three dissimilar single link pendulum systems were constructed from rigid foam board that was light (1.125g per link) relative to the entire pendulum. Mass and mass distributions were calculated using KMCs in equation 4, 7, and 8. Lead weights were used as pendulum masses and attached to the link at appropriate positions. The mass values listed in Table 2 were rounded to whole grams for the experimental pendulums. To ensure precise link dimensions, each pendulum was cut with a 60W laser cutter (Universal Systems VLS4.60).

The links were attached to a short and rigid 0.375in (0.9525cm) aluminum rod using

Table 2: Single Pendulum (ň=1) System Synchronization Coefficient Equations and System Experimental Parameters.

	Coefficient Index	**Coefficient Value**	**System 1 (m̌=1)**	**System 2 (m̌=2)**	**System 3 (m̌=2)**
KMCs	$\mathbf{M}_{1,1}$	33,600 g-cm^2	$m_{11}l_{11}^2$	$m_{11}l_{11}^2 + m_{12}l_{12}^2$	
	$\mathbf{G}_1$	1,260 g-cm	$m_{11}l_{11}$	$m_{11}l_{11} + m_{12}l_{12}$	
Masses (g)			m_{11}=47.3	m_{11}=35.0 m_{12}=21.0	m_{11}=49.0 m_{12}=31.8
Lengths (cm)			l_{11}=26.7	l_{11}=15.0 l_{12}=35.0	l_{11}=5.0 l_{12}=31.9

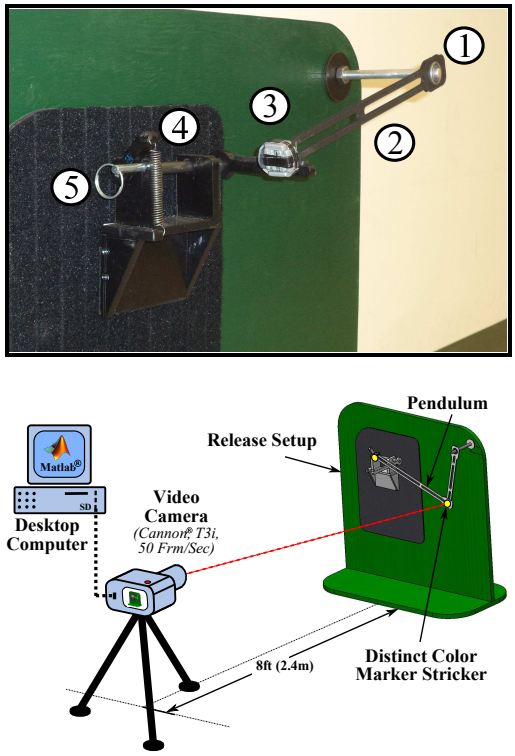

Figure 3: Release mechanism used for all pendulum measurements. (1) Ball Bearing (2) Rigid Foam Link (3) Lead Weights (4) Extension Spring (5) Release Pin.

a precision steel ball bearing to reduce friction. To minimize variability due to friction (negative torque), the exact same bearing was used for each system. Each pendulum system was dropped from the same initial position with an adjustable spring loaded release mechanism. This complete setup can be seen in Figure 3.

The pendulums were video recorded at 50 frames/second (50 Hertz) using a Cannon® T3i digital camera with a Cannon® EF 50mm f/1.8 II lens. Link angular position was interpreted with Matlab®, which was used to load video frames and identify each link's distinct color while in motion.

4.2 Results

Five videos of each pendulum were recorded (15 total). The recorded angular position was averaged and filtered using a low pass 2^{nd} order Butterworth filter at 6 Hz. This angular position data is presented in Figure 4 and compared with ideal predicted model behavior. Modeled systems have the same masses and mass distribution as measured physical systems. As predicted, all three ideal modeled systems have the same temporal kinematics and exactly overlap in Figure 4. Spectral analysis shows the same frequency peak between all measured physical systems, while all three modeled systems peaked 0.06 Hz below the measured system peaks.

While the recorded physical systems were affected by non-conservative forces, such as air resistance and friction, all three dissimilar pendulums matched kinematically. Their

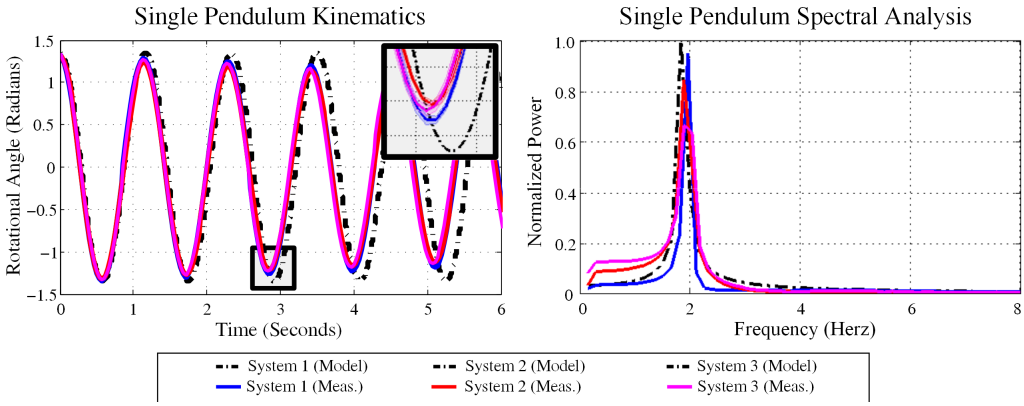

Figure 4: Temporal and spectral motion of three kinematically synchronized single link pendulums (ň=1) with dissimilar masses and mass distributions. The motion of the dissimilar modeled systems (dashed line) is matched exactly and overlaps while the measured motion of the three physical system is matched as well. The discrepancy of the modeled and physical system is due to non-conservative forces.

slight difference in amplitude can be explained by the variable mass and mass distribution in the pendulums that leads to variable weight and centripetal forces on the bearing, which in turn increases rotational friction. Similarly, the effect of the friction torque is affected by the inertia of the system. Although the kinematics are matched, the kinetics in these dissimilar systems does not match; the different masses will generate different forces. Despite these small effects, all three physically dissimilar pendulums had a frequency of 0.88 ± 0.04 Hz.

When comparing the collected and model data, the effects of damping become distinct. As a result, the amplitude and period decrease over time for the actual systems as shown in Figure 4. As previously explained, the model derivation did not include a damping coefficient, thus its effects on motion were not predicted. Despite this difference, the model and all three physically dissimilar pendulums have very similar motion.

5 Example 2: Passive Double (Two-Link) Pendulum

We further investigate our kinematic matching technique by passively synchronizing two passive ($[T] = 0$) dissimilar two degree-of-freedom (ň=2) systems with two masses per link (m̌=2). This double pendulum model is depicted in Figure 2c and 2d and KMCs are shown in Table 3. Either step-by-step kinematic synchronization matching technique could have been used to generate identical motion of these systems. That is, the second system may have been newly created or already available and subsequently matched by adding an additional mass.

Traditionally the double pendulum is modeled in Figure 2c, however this model is impractical from a design perspective considering that the pivot point between the upper and lower link is exactly where the mass is placed and the link is massless. Hence, for our comparison, we add design flexibility and utilize two masses per link.

Table 3: Double Pendulum (ň=2) Synchronization Coefficient Equations and Experimental System Parameters.

	Coefficient Index	Coefficient Value	System 1 (m̌=2)	System 2 (m̌=2)
KMCs	$\mathbf{M}_{1,1}$	28,175 g-cm^2	$l_{11}^2 m_{11} + l_{12}^2 m_{12} + l_1^2(m_{21} + m_{22})$	
	$\mathbf{M}_{1,2}$	23,800 g-cm^2	$l_1(l_{21} m_{21} + l_{22} m_{22})$	
	$\mathbf{M}_{2,2}$	32,900 g-cm^2	$l_{21}^2 m_{21} + l_{22}^2 m_{22}$	
	$\mathbf{G}_1$	1,715 g-cm	$l_{11} m_{11} + l_{12} m_{12} + l_1(m_{21} + m_{22})$	
	$\mathbf{G}_2$	1,190 g-cm	$l_{21} m_{21} + l_{22} m_{22}$	
Masses (g)			m_{11}= 5.0	m_{11}=52.6
			m_{12}=35.0	m_{12}=29.1
			m_{21}=14.0	m_{21}=23.0
			m_{22}=35.0	m_{22}=28.0
Lengths (cm)			l_1=20.0	l_1=20.0
			l_{11}=7.0	l_{11}=5.0
			l_{12}=14.0	l_{12}=15.0
			l_{21}=10.0	l_{21}=12.4
			l_{22}=30.0	l_{22}=32.4

5.1 Experiment description

Two double pendulums were created using the same fabrication technique and material as the single pendulum experiment in Section 4. An additional small ball bearing was placed at the pivot point between the upper and lower link with a 0.25in (6.25mm) wooden pin. Both small bearing and pin had a combined weight less than 2 grams.

The links were attached to the same aluminum rod, ball bearing, and were released with the same release mechanism shown in Figure 3. Specific colors were placed on each link to track their angular positions. Due to greater acceleration of links, the double pendulum nonlinear motion was again recorded at 50 frames/second with the same camera.

5.2 Results

As before, each pendulum's angular kinematics were recorded five times (10 total), averaged, and filtered with a 2$^{\text{nd}}$ order Butterworth filter at 6 Hz. The results of these angular positions are illustrated in Figure 5 and compared with the ideal predicted systems.

The motion for both link 1 (upper link) and link 2 (lower link) was in agreement with model conditions through around 4 seconds, but were in good agreement between experimental measurements throughout the whole trial, which was 12 seconds. This movement of the two dissimilar systems can be seen in Figure 6 and in the accompanying video. All collected data deviated less for link 1 than link 2, which can be explained by the more chaotic movement of the lower link and also because of more variability due to friction in the additional middle pivot. In summary, we have demonstrated two dissimilar chaotic systems that have the same motion by kinematically matching the two systems.

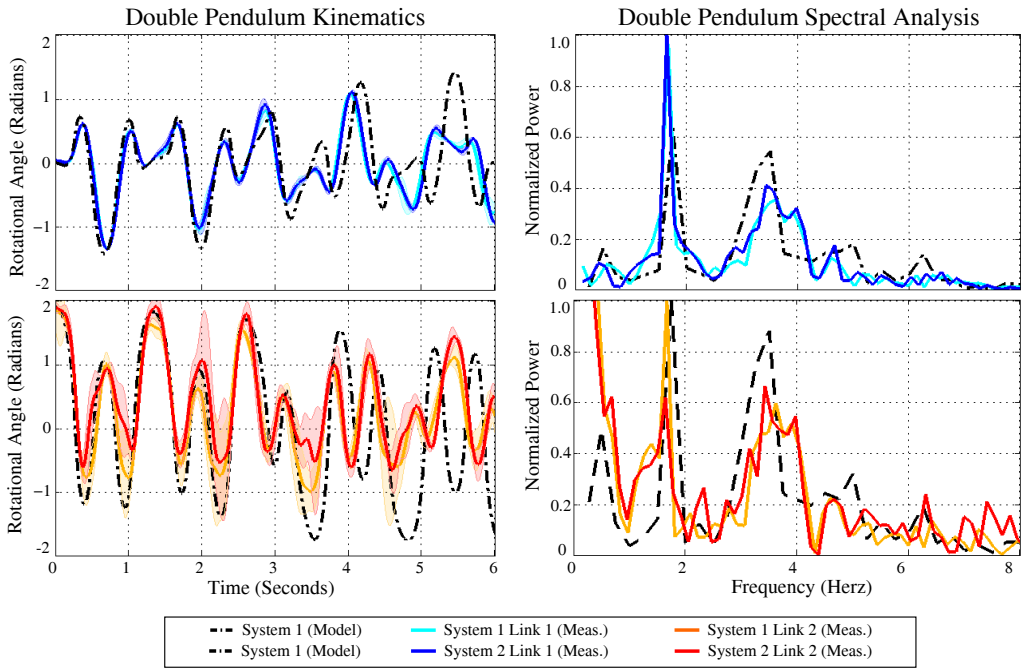

Figure 5: Double pendulum ($\check{n}$=2) model and experimental rotational link position and spectral analysis.

6 Practical Application

The preceding sections presented the derivation and validation of the kinematic synchronization technique. In this section we present a step-by-step tutorial for passive synchronization of two dissimilar and rotating systems and some possible applications of this method.

6.1 Creating a rotating system that is synchronized to an existing system

When one complete rotating system is available and another rotating system is to be created to precisely match the rotational kinematics of the available systems, the following steps can be applied to accomplish this.

Step 1: Determine the degrees of freedom for the original and available system (A) ($\check{n}^A$). For example, a swinging arm as a whole may be represented as a single degree of freedom rotating system, while a swinging leg may be represented as a double degree of freedom system as it bends at the knee. This is the number of degrees of freedom the newly created and synchronized rotation system will have ($\check{n}^A = \check{n}^B$).

Step 2: Measure and represent the mass distribution of this system as lumped point masses along each link. Make sure that each link in a system has the same number of masses ($\check{m}$) as any other link in that system, even though some may be set to zero. For example, for a three degree of freedom system, link one, two, and three each has five point mass representations along each link. However, link one and

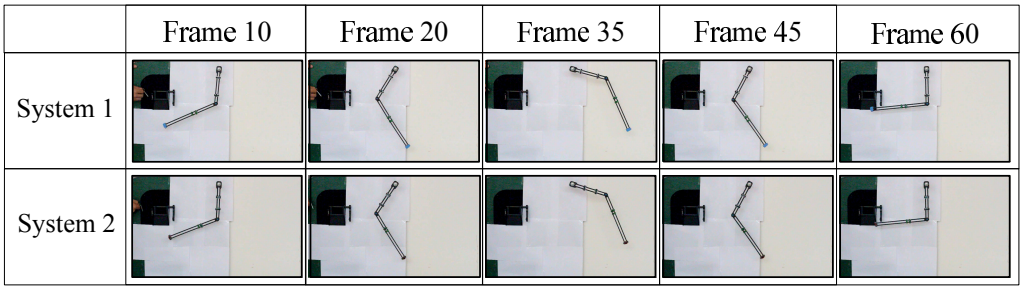

Figure 6: Temporal and spectral motion of two kinematically synchronized double link pendulums (ň=2) with dissimilar masses and mass distributions. The motion both dissimilar modeled systems is exactly the same, while of both dissimilar physically measured systems are also synchronized. The discrepancy of the modeled and physical system is due to non-conservative forces.

two could be represented as five masses along each link, but link three may be represented as four non-zero masses and one mass set to zero.

Step 3: Calculate the total numerical values of KMCs of the available system (A) using equations 4, 7, and 8. For example:
$M_{1,1}^{A}$ = 30,000 g-cm^2
G_1^A = 1000 g-cm
(see Table 2 and Table 3 for other KMC examples)

Step 4: Model a newly created rotational system (B) with the same degrees of freedom ($\check{n}^A = \check{n}^B$) and represent the mass distribution of each link with the same number of masses per link. The number of masses per link must be equal to or greater than two masses ($\check{m}^B \geq 2$). As before in Step 2, some masses on links may be set to zero.

Step 5: Set the numerical KMCs of the available system (A) equal to the symbolic KMCs of the newly created system (B). For example:
$M_{1,1}$ = 30,000 g-cm^2 = $m_{11}^B l_{11}^{2B} + m_{12}^B l_{12}^{2B}$
G_1 = 1,000 g-cm = $m_{11}^B l_{11}^B + m_{12}^B l_{12}^B$
etc.

Step 6: Input approximate values for the masses, mass locations, and link lengths of the newly created system (B). Leave as many unknown parameter variables as variables as there are KMCs. That is, the number of variables to be found should equal the number of KMCs. For example:
$M_{1,1}$ = 30,000 g-cm^2 = $(35g)l_{11}^{2B} + m_{12}^{2B}(31.9cm)$
G_1 = 1,000 g-cm = $(35g)l_{11}^B + m_{12}^B(31.9cm)$
etc.

Step 7: Solve for the unknown system parameter for the newly created system (B).

6.2 Synchronizing two existing rotating systems

Two already available, dissimilar, and rotating systems with equal degrees of freedom can be passively synchronized in their independent rotational motion by augmenting one of the systems to match the other. The following succession of steps describes how to

passively synchronize two such independent, dissimilar, and uncoupled systems.

Step 1: Verify that the first system (A), the reference system, and second system (B) are of equal degrees of freedom ($\check{n}^A = \check{n}^B$). For example, the kinematics of a one degree of freedom rotational system such as a rotating blade may only be matched to the motion of another one degree of freedom rotational system.

Step 2: Measure and represent the mass distribution of this system as lumped point masses along each link. Make sure that each link in a system has the same number of masses ($\check{m}$) as any other link in that system, even though some may be set to zero. For example, for a three degree of freedom system, link one, two, and three each has five point mass representation along each link. However, link one and two could be represented as five masses along each link, but link three may be represented as four masses with one mass set to zero.

Step 3: Calculate the total numerical values of KMCs of the available system (A) using equations 4, 7, and 8. For example:
$M^A_{1,1}$ = 30,000 g-cm^2
G^A_1 = 1,000 g-cm
etc.

Step 4: For the second system (B), add one additional mass for each link. This additional mass per link and its location on the link are to be determined subsequently.

Step 5: Using equations 4, 7, and 8, find the KMC equations for the second system (B) ($M^B_{1,1}$, G^B_1, etc.), and input the known (measured) lumped point masses and their locations.

Step 6: Set the numerical KMC values for the first system (A) equal to the KMC equations found for the second system (B) For example:
$M_{1,1}$ = 30,000 g-cm^2 $= m^B_{11} l^{2B}_{11} + m^B_{12} l^{2B}_{12}$
G_1 = 1,000 g-cm $= m^B_{11} l^B_{11} + m^B_{12} l^B_{12}$
etc.

Step 7: Solve for the added and unknown point masses and their locations (from Step 4) for each link of the second system (B). There should be as many unknown parameters (added masses, mass locations, and link lengths) as there are KMCs.

6.3 Kinematic system simplification technique

We have shown that given the same degrees of freedom and torque input, two dissimilar rotating systems can be motion matched. A minimum of two masses per degree of freedom are required to mimic the motion of a matching system. In essence, this kinematic matching technique can be used to simplify a complicated rotating system. For example, a rotating fan blade, gear, or cam of arbitrary shape can be modeled as one link with two masses, while an open ended chain with any number of links can be modeled as two masses per link. This can greatly simplify computation resulting in the same kinematics.

6.4 Gait pattern manipulation

In humans [7, 13, 14], animals [6], and some insects [21], the limbs can be modeled as swinging pendulums that swing in accordance to their masses and mass distribution. It is possible to manipulate limb movements by simply changing mass and mass distributions such as adding mass to a specific location of the limb. For example, a gait asymmetry (walking limp) can be created in an individual by attaching an extra weight to one leg [14], while in contrast a symmetric gait can be restored from an asymmetric walking pattern by adding weight to a specific location [8]. With the presented kinematic matching technique, we can match two swinging limbs, such as human legs, so they move symmetrically, but out 180° out of phase. While walking kinematics are the most obvious application, other parts of the body can be synchronized such as swinging arms during walking or moving fingers while playing an instrument or typing on a keyboard. This technique can also be used for the kinematic behavior prediction of swinging robotic limbs [6, 9].

6.5 Prosthetics

Wearing a prosthesis that does not have the exact size and weight of the missing limb can create gait asymmetries [15]. Prosthetics research commonly tries to mimic the lost limb in regards to size, weight, and length; however this design constraint can often times seem unrealistic and overconstraining. Using a numerical passive dynamic walker model, Sushko et. al [26] showed that this design constraint can be alleviated by changing left and right limb mass and mass distribution parameters to obtain symmetric gait with asymmetric limb parameters. As previously stated the presented kinematic matching technique can analytically match two limbs with symmetric limb mass and mass distribution parameters. That is, we can apply this technique to match the healthy limb with the other limb with a prosthetic by adding masses to one or both limbs, yielding a symmetric gait.

7 Conclusions and Future Work

We derived a general equation of motion for two-dimensional $\check{n}$ degree-of-freedom $\check{m}$ masses per degree of freedom open ended rotating systems. Further we developed a passive kinematic matching technique that is applicable to such systems. In order to match the same rotating kinematics, only two masses per degree of freedom are necessary. The motion analysis of three matched one-degree-of-freedom unactuated single link pendulums with dissimilar masses and mass distribution showed that these dissimilar systems were kinematically identical, although unmodeled nonconservative forces created slight deviations between ideal model predictions and actual measurements. While chaotic in motion, the same results were shown in the motion analysis of two two-degree-of-freedom unactuated double link pendulums with synchronous motion lasting for about 4 seconds before nonconservative forces caused deviation. Measured kinematics of the two dissimilar experimental double pendulums matched for more than 12 seconds.

It is possible to alter the mass distribution of a rotating system by moving masses along system links in order to kinematically match it to another system. It is also possible to add or remove masses at key locations along a rotating link. These methods could be utilized to synchronize the kinematics of two swinging legs while walking. However, although dissimilar kinematically synchronized systems move identically, the

kinetics can vary. This was seen in our first example between three dissimilar single link pendulums. While system kinematics matched, pendulum bearing reaction forces varied, yielding dissimilar damping forces. Unless mass and mass distribution parameters are exactly matched, the internal forces throughout the system will not match. Future work includes the analysis and possible synchronization of inter-system kinetics. The authors hypothesis is that either the kinematics or kinetics can be matched, but not both simultaneously in dissimilar systems.

It is also presumed that similar passive synchronization techniques can also be derived in all three dimensions; further derivations are needed.

Acknowledgments

This material is based upon work supported by the National Science Foundation under Grant Number IIS-1319802.

References

[1] Budney, D. R. and Bellow, D. G. On the swing mechancis of a matched set of golf clubs. *Research Quarterly for Exercise and Sport* **53** (3) (1982) 185–192.

[2] Bunnett, M., Schatz, M. F., Rockwood, H. and Wiesenfeld, K. Huygens's clocks. *Proceedings: Mathematical, Physical and Engineering Sciences* **458** (March 2002), 563–579.

[3] Dilao, R. Antiphase and in-phase synchronization of nonlinear oscillators: The huygenss clocks system. *Chaos* **19** (2) (June 2009) 023118.

[4] Everett, J. L. Dynamical matched set of golf clubs. US Patent. 4, 415, 156, Oct.17, October 1972.

[5] Frandkov, A. L. and Andrievsky, B. Synchronization and phase relations in the motion of two-pendulum system. *International Journal of Non-Linear Mechanics* **42** (March 2007) 895–901.

[6] Fukuda, T., Hasegawa, Y., Sekiyama, K. and Aoyama, T. *Multi-Locomotion Robotic Systems*, vol. 81. Springer, 2012.

[7] Geyer, H., Seyfarth, A. and Blickhan, R. Compliant leg behavior explains basic dynamics of walking and running. *Proceedings of the Royal Scociety* **273** (August 2006) 2861–2867.

[8] Gibson-Horn, C. Balance-based torso-weighting in a patient with ataxia and multiple sclerosis: A case report. *Journal of Neurologic Physical Therapy* **32** (3) (2008) 139–146.

[9] Gluck, T., Eder, A. and Kugi, A. Swing-up control of a triple pendulum on a cart with experimental validation. *Automatica* **49** (2013) 801–808.

[10] Gregg, R., Dhaher, Y., Degani, A. and Lynch, K. On the mechanics of functional asymmetry in bipedal walking. *IEEE Transactions on Biomedical Engineering* **59** (5) (2012) 1310–1318.

[11] Gregg, R. D., Degani, A., Dhahe, Y. and Lynch, K. M. The basic mechanics of bipedal walking lead to asymmetric behavior. In: *Proc. IEEE Int. Conf. Rehabilitation Robotics* (2011) 816–821.

[12] Handžić, I., Barno, E., Vasudevan, E. V. and Reed, K. B. Design and pilot study of a gait enhancing mobile shoe. *J. of Behavioral Robotics* **2** (4) (2011) 193–201.

[13] Handžić, I. and Reed, K. B. Validation of a passive dynamic walker model for human gait analysis. In: *Proc. IEEE Eng. Med. Biol. Soc.* (2013) 6945–6948.

[14] Handžić, I. and Reed, K. B. Comparison of the passive dynamics of walking on ground, tied-belt and split-belt treadmills, and via the gait enhancing mobile shoe (GEMS). In: *Proc. IEEE Int. Conf. Rehabilitation Robotics* (June 2013).

[15] Hekmatfard, M., Farahmand, F. and Ebrahimi, I. Effects of prosthetic mass distribution on the spatiotemporal characteristics and knee kinematics of transfemoral amputee locomotion. *Gait* **37** (2013) 78–81.

[16] Honeycutt, C., Sushko, J. and Reed, K. B. Asymmetric passive dynamic walker. In *Proc. IEEE Int. Conf. Rehabilitation Robotics* (June 2011) 852–857.

[17] Jorgensen, T. P. Matched set of golf clubs. US Patent. 4, 415, 156, Nov.15, November 1983.

[18] Khan, A. and Tripathi, P. Synchronization, anti-synchronization and hybrid-synchronization of a double pendulum under the effect of external forces. *International Journal Of Computational Engineering Research* **3** (1) (2013) 166–176.

[19] Khan, A. and Tripathi, P. Synchronization between a fractional order chaotic system and an integer order chaotic system. *Nonlinear Dynamics and Systems Theory* **13** (2013) 425–436.

[20] Kuo, A. D. The six determinants of gait and the inverted pendulum analogy: A dynamic walking perspective. *Human Movement Science* **26** (July 2007) 617–656.

[21] Mongeau, J.-M., McRae, B., Jusufi, A., Birkmeyer, P., Hoover, A. M., Fearing, R. and Full, R. J. Rapid inversion: Running animals and robots swing like a pendulum under ledges. *Plos One* **7** (6) (June 2012) 0038003.

[22] Nair, S. and Leonard, N. E. Stable synchronization of mechanical system networks. *Journal of Control Optimization* **47** (2) (2008) 661–683.

[23] Olusola, O., Vincent, A. and Njah, B. I. Global stability and synchronization criteria of linearly coupled gyroscope. *Nonlinear Dynamics and Systems Theory* **13** (2013) 258–269.

[24] Osipov, G. V., Kurths, J. and Zhou, C. *Synchronization in Oscillatory Networks*. Springer, 2007.

[25] Reisman, D., McLean, H., Keller, J., Danks, K. and Bastian, A. Repeated split-belt treadmill training improves poststroke step length asymmetry. *Neurorehabilitation* **27** (5) (Feb 2013) 460-8.

[26] Sushko, J., Honeycutt, C. and Reed, K. B. Prosthesis design based on an asymmetric passive dynamic walker. In: *Proc. IEEE Conf. Biorob* (June 2012) 1116–1121.

Nonlinear Dynamics and Systems Theory, **15** (4) (2015) 400–408

A New Approach To Synchronize Different Dimensional Chaotic Maps Using Two Scaling Matrices

Adel Ouannas [1*] and M. Mossa Al-Sawalha [2]

[1] *Department of Mathematics and Computer Science, Constantine University, Algeria.*
[2] *Mathematics Department, Faculty of Science, University of Hail, Kingdom of Saudi Arabia.*

Received: December 1, 2014; Revised: October 28, 2015

Abstract: In this paper, a new type of synchronization, called $\Theta-\Phi$ synchronization, is introduced for different chaotic discrete-time systems using two scaling matrices. The proposed synchronization approach allows us to study synchronization between two different dimensional discrete-time chaotic systems in different dimensions. By using Lyapunov stability theory and stability property of linear discrete-time systems, some control schemes are proposed and new synchronization results are derived. To verify the effectiveness of our approach, numerical example and simulations are given.

Keywords: *synchronization; chaotic maps; hyperchaotic maps; different dimensions; scaling matrices.*

Mathematics Subject Classification (2010): 74H55, 74H60, 74H65, 93C55.

1 Introduction

Over the last two decades, many scholars have proposed various control schemes in chaos synchronization [1–6], but the most of works have concentrated on continuous-time rather than discrete-time chaotic systems. Recently, synchronization of chaotic and hyperchaotic maps has attracted a great deal of interest of applied scientists and engineers due to it's potential applications in cryptology and secure communication [7–10]. Different methods have been developed to study the synchronization in discrete-time chaotic dynamical systems [11–13].

* Corresponding author: mailto:ouannas_adel@yahoo.fr

© 2015 InforMath Publishing Group/1562-8353 (print)/1813-7385 (online)/http://e-ndst.kiev.ua

Until now, a variety of approaches have been proposed for the synchronization of discrete chaotic such as synchronization and anti-synchronization [14,15], adaptive function projective synchronization [16,17], full-state hybrid projective synchronization [18], Lag synchronization [19], impulsive synchronization [20], function cascade synchronization [21], generalized synchronization [22, 23] and Q-S synchronization [24]. Among all types of synchronization, matrix projective synchronization (MPS) is effective approach for achieving the synchronization of chaotic and hyperchaotic discrete-time systems [25, 26]. In (MPS), the drive chaotic system and the response chaotic system are synchronized up to scaling constant matrix.

In this paper, we generalize the (MPS) type to a new type of synchronization using two scaling constants matrices ($\Theta-\Phi$ synchronization). The aim of this work is to present constructive schemes to synchronize n-dimensional drive system and m-dimensional response system in m-D and n-D, respectively. The derived results are based on Lyapunov stability theory, stability property of linear discrete-time systems and nonlinear control laws. To verify the validity and the feasibility of the new synchronization results, the proposed control schemes are applied to 2D Lorenz discrete time system and 3D discrete-time Rössler system in different dimensions.

This paper is organized as follows. In Section 2, the problem of $\Theta-\Phi$ synchronization is formulated. In section 3, the $\Theta-\Phi$ synchronization is studied in m-D. The n-dimensional $\Theta-\Phi$ synchronization is investigated in Section 4. In Section 5, numerical simulations are given to illustrate the effectiveness of the main results. Finally, conclusions are drawn in Section 6.

2 $\Theta-\Phi$ Synchronization in Discrete-Time Systems

The drive and the response chaotic systems are in the following forms

$$X(k+1) = AX(k) + f(X(k)), \tag{1}$$

$$Y(k+1) = BY(k) + g(Y(k)) + U, \tag{2}$$

where $X(k) \in \mathbf{R}^n$, $Y(k) \in \mathbf{R}^m$ are state vectors of the drive system and the response system, respectively, $A \in \mathbf{R}^{n\times n}$, $B \in \mathbf{R}^{m\times im}$ are linear parts of the drive system and the response system, respectively, $f : \mathbf{R}^{\ n} \to \mathbf{R}^n$, $g : \mathbf{R}^m \to \mathbf{R}^m$ are nonlinear parts of the drive system and the response system, respectively, and $U \in \mathbf{R}^m$ is a vector controller.

Definition 2.1 The drive system (1) and the response system (2) are said to be synchronized in dimension d, with respect to scaling matrices Θ and Φ, respectively, if there exists a controller $U = (u_i)_{1\leq i\leq m} \in \mathbf{R}^m$ and given matrices $\Theta = (\Theta)_{d\times m}$ and $\Phi = (\Phi)_{d\times n}$ such that the synchronization error

$$e(k) = \Theta Y(k) - \Phi X(k) \tag{3}$$

satisfies the condition $\lim_{k\longrightarrow+\infty} \|e(k)\| = 0$.

3 $\Theta-\Phi$ Synchronization in m-D

In this case, we assume that the synchronization dimension $d = m$. The error system between the drive system (1) and the response system (2) can be derived as

$$\begin{aligned} e(k+1) &= \Theta Y(k+1) - \Phi X(k+1) \\ &= \Theta BY(k) + \Theta g(Y(k)) + \Theta U - \Phi AX(k) - \Phi f(X(k)), \end{aligned} \tag{4}$$

where $\Theta = (\Theta_{ij}) \in \mathbf{R}^{m\times m}$ and $\Phi = (\Phi_{ij}) \in \mathbf{R}^{n\times m}$ are the scaling matrices.

Theorem 3.1 *The drive system (1) and the response system (2) are globally synchronized, with respect to scaling matrices Θ and Φ, if the following conditions are satisfied:*
(i) $U = -\Theta^{-1} \times [(L_1 - B)\, e(k) + \Theta BY(k) + \Theta g(Y(k)) - \Phi AX(k) - \Phi f(X(k))]$, where Θ^{-1} is the inverse of the matrix Θ.
(ii) $(B - L_1)^T (B - L_1) - I$ is a negative definite matrix, where $L_1 \in \boldsymbol{R}^{m\times m}$ is a control matrix.

Proof. Then, the error system (4) can be described as

$$\begin{aligned} e(k+1) &= (B - L_1)\, e(k) + \Theta U + (L_1 - B)\, e(k) + \Theta BY(k) \\ &\quad + \Theta g(Y(k)) - \Phi AX(k) - \Phi f(X(k)), \end{aligned} \tag{5}$$

where $L_1 \in \mathbf{R}^{\,m\times m}$ is a control matrix. By substituting (i) into equation (5), the error system can be written as

$$e(k+1) = (B - L_1)\, e(k). \tag{6}$$

Construct the candidate Lyapunov function in the form $V(e(k)) = e^T(k)e(k)$, we obtain

$$\begin{aligned} \Delta V(e(k)) &= e^T(k+1)e(k+1) - e^T(k)e(k) \\ &= e^T(k)(B - L_1)^T(B - L_1)e(k) - e^T(k)e(k) \\ &= e^T(k)\left[(B - L_1)^T(B - L_1) - I\right], \end{aligned}$$

and by using (ii) we get $\Delta V(e(k)) < 0$. Thus, from the Lyapunov stability theory, it is immediate that $\lim_{k\to\infty} e_i(k) = 0,\ \ i = 1, 2, ..., n$. That is the zero solution of the error system (6) is globally asymptotically stable and therefore, the systems (1) and (6) are globally $\Theta - \Phi$ synchronized in m-D.

4 $\Theta - \Phi$ Synchronization in n-D

Now, the synchronization dimension $d = n$. The error system between the drive system (1) and the response system (2) can be derived as

$$\begin{aligned} e(k+1) &= (A - L_2)\, e(k) + \Theta U + (L_2 - A)\, e(k) \\ &\quad + \Theta BY(k) + \Theta g(Y(k)) - \Phi AX(k) - \Phi f(X(k)), \end{aligned} \tag{7}$$

where $\Theta = (\Theta_{ij}) \in \mathbf{R}^{n\times m}$ and $\Phi = (\Phi_{ij}) \in \mathbf{R}^{n\times n}$ are the scaling matrices. In this case, we assume that $m > n$ and we take the controller components v_i, where $i > n$, as

$$u_i = 0, \quad i = n+1, n+2, ..., m. \tag{8}$$

Then, the error system (7) can be written as

$$e(k+1) = (A - L_2)\, e(k) + \hat{\Theta}\hat{U} + R, \tag{9}$$

where $\hat{\Theta} = (\Theta_{ij})_{m\times m}$, $\hat{U} = (u_i)_{1\le i\le n}$,

$$R = (L_2 - A)\, e(k) + \Theta BY(k) + \Theta g(Y(k)) - \Phi AX(k) - \Phi f(X(k)), \tag{10}$$

and $L_2 \in \mathbf{R}^{n\times n}$ is a control matrix.

Theorem 4.1 *The drive system (1) and the response system (2) are globally synchronized, with respect to the scaling matrices* Θ *and* Φ*, if the following conditions are satisfied:*

(i) $\hat{U} = -\hat{\Theta}^{-1} \times R$*, where* $\hat{\Theta}^{-1}$ *is the inverse of the matrix* $\hat{\Theta}$*.*

(ii) All the eigenvalues of $A - L_2$ *lie inside the unit disk.*

Proof. By substituting (i) into equation (9), the error system can be written as

$$e(k+1) = (A - L_2)\, e(k). \tag{11}$$

With respect to the asymptotic stability property of linear discrete-time systems, if all eigenvalues of $A - L_2$ are strictly inside the unit disk, it is immediate that all solutions of error system (11) go to zero as $k \to \infty$. Therefore, the systems (1) and (2) are globally $\Theta - \Phi$ synchronized in n-D.

5 Numerical Application and Simulations

In this section, a numerical example is given to illustrate the effectiveness of the theoretical results derived in the previous sections. Thus, we consider the 2D Lorenz discrete time system as the drive system and the controlled 3D discrete-time Rössler system as the response system. The Lorenz discrete time system is described by

$$\begin{aligned} x_1(k+1) &= (1+ab)\, x_1(k) - b x_1(k)\, x_2(k), \\ x_2(k+1) &= (1-b)\, x_2(k) + b x_1^2(k), \end{aligned} \tag{12}$$

which has a chaotic attractor, for example, when $(a,\ b) = (1.25,\ 0.75)$ [27].

The controlled discrete-time Rössler system can be described as:

$$\begin{aligned} y_1(k+1) &= \alpha y_1(k)\,(1 - y_1(k)) - \beta\,(y_3(k) + \gamma)\,(1 - 2y_2(k)) + u_1, \\ y_2(k+1) &= \delta y_2(k)\,(1 - y_2(k)) + \varsigma y_3(k) + u_2, \\ y_3(k+1) &= \eta\,((y_3(k) + \gamma)\,(1 - 2y_2(k)) - 1)\,(1 - \theta y_1(k)) + u_3, \end{aligned} \tag{13}$$

where $U = (u_1, u_2, u_3)^T$ is the vector controller. When $\alpha = 3.8$, $\beta = 0.05$, $\gamma = 0.35$, $\delta = 3.78$, $\varsigma = 0.2$, $\eta = 0.1$ and $\theta = 1.9$, the discrete-time Rössler system (i.e., the system map (18) with $u_1 = 0$, $u_2 = 0$ and $u_3 = 0$) has a hyperchaotic attractor [28].

The linear part A and the nonlinear part f of the Lorenz discrete time system are given by

$$A = \begin{pmatrix} 1+ab & 0 \\ 0 & 1-b \end{pmatrix},\ f = \begin{pmatrix} -b x_1(k)\, x_2(k) \\ b x_1^2(k) \end{pmatrix}.$$

The linear part B and the nonlinear part g of the discrete-time Rössler system are given by

$$\begin{aligned} B &= \begin{pmatrix} \alpha & 2\beta\gamma & -\beta \\ 0 & \delta & \varsigma \\ \eta\theta\,(1-\gamma) & -2\gamma\eta & \eta \end{pmatrix}, \\ g &= \begin{pmatrix} 2\beta y_3(k)\, y_2(k) - \alpha y_1^2(k) - \beta\gamma \\ -\delta y_2^2(k) \\ \eta\,(\gamma - 1) - \eta y_3(k)\,(\theta y_1(k) + 2y_2(k)) + 2\theta y_1(k)\, y_2(k)\,(\gamma + \eta y_3(k)) \end{pmatrix}. \end{aligned}$$

5.1 Synchronization of the Lorenz discrete time system and the discrete-time Rössler system in 3D

In this case, the scaling matrices are chosen as

$$\Theta = \begin{pmatrix} 2 & 0 & 0 \\ 0 & 1 & 0 \\ 0 & 0 & 3 \end{pmatrix}, \ \Phi = \begin{pmatrix} 1 & 2 \\ 2 & 3 \\ 1 & 1 \end{pmatrix},$$

so,

$$\Theta^{-1} = \begin{pmatrix} \frac{1}{2} & 0 & 0 \\ 0 & 1 & 0 \\ 0 & 0 & \frac{1}{3} \end{pmatrix}.$$

The control matrix L_1 is selected as

$$L_1 = \begin{pmatrix} \frac{3\alpha}{4} & 2\beta\gamma & -\beta \\ 0 & \frac{4\delta}{5} & \varsigma \\ \eta\theta\left(1-\gamma\right) & -2\gamma\eta & 0 \end{pmatrix}. \tag{14}$$

Using simple calculations, we can show that $(B-L_1)^T(B-L_1)-I$ is a negative definite matrix. According to our approach presented in Section 3, the vector controller $U=(u_1,u_2,u_3)^T$ can be obtained as

$$\begin{aligned} u_1 &= -\frac{\alpha}{8}e_1\left(k\right) - \alpha y_1\left(k\right) - 2\beta\gamma y_2\left(k\right) + \beta\gamma \\ &\quad +\beta y_3\left(k\right) - 2\beta y_3\left(k\right) y_2\left(k\right) + \alpha y_1^2\left(k\right) \\ &\quad +\frac{1}{2}\left(1+ab\right)x_1\left(k\right) - \frac{1}{2}bx_1\left(k\right)x_2\left(k\right), \\ u_2 &= -\frac{\delta}{5}e_2\left(k\right) - \delta y_2\left(k\right) - \varsigma y_3\left(k\right) + \delta y_2^2\left(k\right) \\ &\quad +3\left(1-b\right)x_2\left(k\right) + bx_1^2\left(k\right), \\ u_3 &= -\frac{\eta}{3}e_3\left(k\right) - \eta\theta\left(1-\gamma\right)y_1\left(k\right) + 2\gamma\eta y_2\left(k\right) - \eta y_3\left(k\right) \\ &\quad +\eta y_3\left(k\right)\left(\theta y_1\left(k\right) + 2y_2\left(k\right)\right) - 2\theta y_1\left(k\right)y_2\left(k\right)\left(\gamma+\eta y_3\left(k\right)\right) \\ &\quad +\frac{1}{3}\left(1+ab\right)x_1\left(k\right) - \frac{b}{3}x_1\left(k\right)x_2\left(k\right) + \frac{1}{3}\left(1-b\right)x_2\left(k\right) + \frac{b}{3}x_1^2\left(k\right) \\ &\quad -\eta\left(\gamma-1\right), \end{aligned} \tag{15}$$

where $e_1\left(k\right) = 2y_1\left(k\right) - x_1\left(k\right) - 2x_2\left(k\right)$, $e_2\left(k\right) = y_2\left(k\right) - 2x_1\left(k\right) - 3x_2\left(k\right)$ and $e_3\left(k\right) = 3y_3\left(k\right) - x_1\left(k\right) - x_2\left(k\right)$. Therefore, the systems (12) and (13) are globally synchronized in 3D, with respect to the scaling matrices Θ and Φ. In this case, the error system can be described as: $e_1\left(k+1\right) = \frac{\alpha}{4}e_1\left(k\right)$, $e_2\left(k+1\right) = \frac{\delta}{5}e_2\left(k\right)$ and $e_3\left(k+1\right) = \eta e_3\left(k\right)$. The time evolution of errors $e_1(k), e_2(k)$ and $e_3(k)$ between the maps (12) and (13) in 3D is shown in Figure 1.

5.2 Synchronization of the Lorenz discrete time system and the discrete-time Rössler system in 2D

In this case, the scaling matrices are chosen as

$$\Theta = \begin{pmatrix} 2 & 0 & 1 \\ 0 & 4 & 1 \end{pmatrix}, \ \Phi = \begin{pmatrix} 2 & 0 \\ 1 & 3 \end{pmatrix},$$

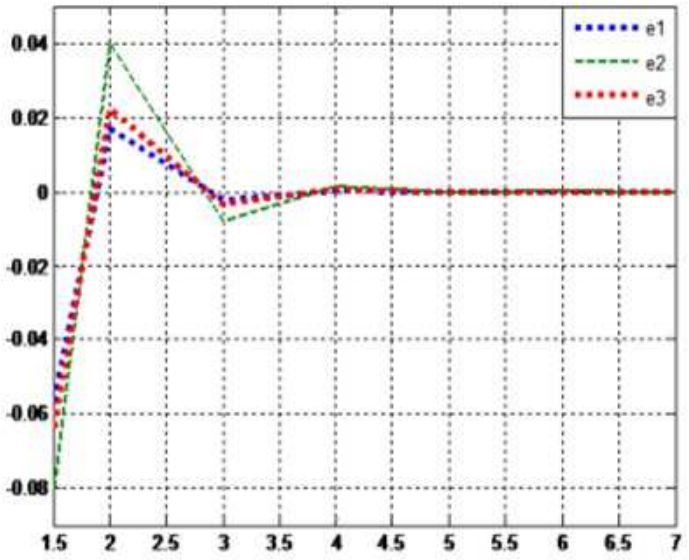

Figure 1: Time evolution of errors $e_1(k), e_2(k)$ and $e_3(k)$ between the maps (12) and (13) in 3D.

so,

$$\hat{\Theta} = \begin{pmatrix} 2 & 0 \\ 0 & 4 \end{pmatrix}, \ \hat{\Theta}^{-1} = \begin{pmatrix} \frac{1}{2} & 0 \\ 0 & \frac{1}{5} \end{pmatrix}.$$

The control matrix L_2 is selected as

$$L_1 = \begin{pmatrix} 1 & 0 \\ 0 & 1 \end{pmatrix}. \tag{16}$$

Simply, we can see that all eigenvalues of $A - L_2$ are strictly inside the unit disk. According to the control scheme proposed in Section 4, the vector controller $U = (u_1, u_2, u_3)^T$ can be designed as follows

$$\begin{aligned} u_1 \quad = \quad & \frac{1}{2}abe_1(k) - \frac{1}{2}\eta\left(\left(y_3(k)+\gamma\right)\left(1-2y_2(k)\right)-1\right)\left(1-\theta y_1(k)\right) \\ & -\alpha y_1(k)\left(1-y_1(k)\right)+\beta\left(y_3(k)+\gamma\right)\left(1-2y_2(k)\right) \\ & +\left(1+ab\right)x_1(k) - \frac{1}{2}bx_1(k)\,x_2(k), \end{aligned} \tag{17}$$

$$\begin{aligned} u_2 &= -\frac{1}{5}be_2(k) - \frac{1}{5}\eta\left(\left(y_3(k)+\gamma\right)\left(1-2y_2(k)\right)-1\right)\left(1-\theta y_1(k)\right) \\ &\quad -4\frac{1}{5}\delta y_2(k)\left(1-y_2(k)\right) - \frac{1}{5}\varsigma y_3(k) + \frac{1}{5}\left(1+ab\right)x_1(k) \\ &\quad -\frac{1}{5}bx_1(k)\,x_2(k) + \frac{1}{5}3\left(1-b\right)x_2(k) + \frac{1}{5}3bx_1^2(k), \\ u_3 &= 0, \end{aligned}$$

where $e_1(k) = 2y_1(k) + y_3(k) - 2x_1(k)$ and $e_2(k) = 4y_2(k) + y_3(k) - x_1(k) - 3x_2(k)$. Therefore, the systems (12) and (13) are globally synchronized in 2D, with respect to the scaling matrices Θ and Φ. In this case, the error system can be written as: $e_1(k+1) = abe_1(k)$ and $e_2(k+1) = -be_2(k)$. The time evolution of errors $e_1(k)$ and $e_2(k)$ between the maps (12) and (13) in 2D is shown in Figure 2.

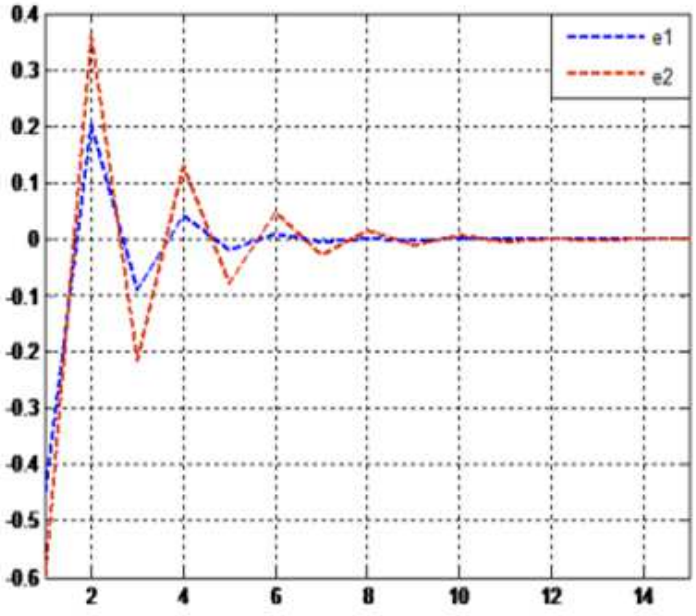

Figure 2: Time evolution of errors $e_1(k)$ and $e_2(k)$ between the maps (12) and (13) in 2D.

6 Conclusion

In this paper, the $\Theta - \Phi$ synchronization was proposed to synchronize n-dimensional drive system and m-dimensional response system. To derive new results, two control schemes were proposed using two constants scaling matrices Θ and Φ. The first scheme was presented when the synchronization dimension $d = m$, ($\Theta - \Phi$ synchronization in m-D) and the second one was constructed when the synchronization dimension $d = n$, ($\Theta - \Phi$ synchronization in n-D). Numerical example and simulation results were used to verify the effectiveness of the proposed schemes.

References

[1] Fu, S.H. and Pei, L.J. Synchronization of chaotic systems by the generalized hamiltonian systems approach. *Nonlinear Dynamics and Systems Theory* **10** (4) (2010) 387–396.

[2] Vincent, U. E. and Guo, R. Adaptive synchronization for oscillators in ϕ^6 potentials. *Nonlinear Dynamics and Systems Theory* **13** (1) (2013) 93–106.

[3] Olusola, O.I., Vincent, U.E., Njah, A.N. and Idowu, B.A. Global stability and synchronization criteria of linearly coupled gyroscope. *Nonlinear Dynamics and Systems Theory* **13** (3) (2013) 258–269.

[4] Khan, A. and Pal, R. Adaptive hybrid function projective synchronization of Chaotic Space-Tether System. *Nonlinear Dynamics and Systems Theory* **14** (1) (2014) 44–57.

[5] Ouannas, A. Chaos synchronization approach based on new criterion of stability. *Nonlinear Dynamics and Systems Theory* **14** (4) (2014) 395–401.

[6] Ojo, K.S., Njah, A.N., Ogunjo, S.T. and Olusola, O.I. Reduced order function projective combination synchronization of three Josephson functions using backstepping technique. *Nonlinear Dynamics and Systems Theory* **14** (2) (2014) 119–133.

[7] Aguilar–Bustos, A.Y., Cruz–Hernández, C., Lopez–Gutierrez, R.M. and Posadas–Castillo, C. Synchronization of different hyperchaotic maps for encryption. *Nonlinear Dynamics and Systems Theory* **8** (3) (2008) 221–236.

[8] Aguilar-Bustos, A. Y. y C. Cruz Hernandez. Synchronization of discrete-time hyperchaotic systems: An apllication in communications. *Chaos, Solitons and Fractals* **41** (3) (2009) 1301–1310.

[9] Inzunza-González, E. and Cruz-Hernández, C. Double hyperchaotic encryption for security in biometric systems. *Nonlinear Dynamics and Systems Theory* **13** (1) (2013) 55–68.

[10] Filali, R.L., Benrejeb, M. and Borne, P. On observer-based secure communication design using discrete-time hyperchaotic systems. *Communications in Nonlinear Science and Numerical Simulation* **19** (5) (2014) 1424–1432.

[11] Grassi, G. and Miller, D. A. Dead-beat full state hybrid projective synchronization for chaotic maps using a scalar synchronizing signal. *Chinese Physics B* **17** (4) (2012) 1824–1830.

[12] Ouannas, A. A new chaos synchronization criterion for discrete dynamical systems. *Applied Mathematical Sciences* **8** (41) (2014) 2025–2034.

[13] Ouannas, A. Some synchronization criteria for N-dimensional chaotic dynamical systems in discrete-time. *Journal of Advanced Research in Applied Mathematics* **6** (4) (2014) 1–9.

[14] Filali, R.L., Hammami, S., Benrejeb, M. and Borne, P. On synchronization, anti-synchronization and hybrid synchronization of 3D discrete generalized Hénon map. *Nonlinear Dynamics and Systems Theory* **12** (1) (2012) 81–95.

[15] Ouannas, A. A new synchronization scheme for general 3D quadratic chaotic systems in discrete-time. *Nonlinear Dynamics and Systems Theory* **15** (2) (2015) 163-170.

[16] Li, Y., Chen, Y., and Li, B. Adaptive control and function projective synchronization in 2D discrete-time chaotic systems. *Communications in Theoretical Physics* **51** (2) (2009) 270–278.

[17] Li, Y., Chen, Y., and Li, B. Adaptive function projective synchronization of discrete-time chaotic systems. *Chinese Physics Letters* **26** (4) (2009) 040504-5.

[18] Ouannas, A. On full-state hybrid projective synchronization of general discrete chaotic systems. *Journal of Nonlinear Dynamics* **2014** 1–6.

[19] Chai, Y., Lü, L., and Zhao, H.Y. Lag synchronization between discrete chaotic systems with diverse structure. *Applied Mathematics and Mechanics* **31** (6) (2010) 733-738.

[20] Yanbo, G., Xiaomei, Z., Guoping, L., and Yufan, Z. Impulsive synchronization of discrete-time chaotic systems under communication constraints. *Communications in Nonlinear Science and Numerical Simulation* **16** (3) (2011) 580–1588.

[21] Hong-Li An, Yong Chen. The function cascade synchronization scheme for discrete-time hyperchaotic systems. *Communications in Nonlinear Science and Numerical Simulation* **14** (2009) 1494–1501.

[22] Grassi, G. Generalized synchronization between different chaotic maps via dead-beat control. *Chinese Physics B* **21** (5) (2012) 050505.

[23] Ouannas, A., and Odibat, Z. Generalized synchronization of different dimensional chaotic dynamical systems in discrete time. *Nonlinear Dynamics* **81** (1) (2015) 765–771.

[24] Yan, Z.Y. Q-S synchronization in 3D Hénon-like map and generalized Hénon map via a scalar controller. *Physics Letters A* **342** (2005) 309–317.

[25] Ouannas, A., Mahmoud, E. E. Inverse matrix projective synchronization for discrete chaotic systems with different dimensions. *Journal of Computational Intelligence and Electronic Systems* **3** (3) (2014) 188–192.

[26] Feng, L. Matrix projective synchronization of chaotic systems and the application in secure communication. *Applied Mechanics and Materials* **644-650** (2014) 4216–4220.

[27] Yan, Z.Y. Q-S (complete or anticipated) synchronization backstepping scheme in a class of discrete-time chaotic (hyperchaotic) systems: A symbolic-numeric computation approach. *Chaos* **16** (2006) 013119-11.

[28] Itoh, M., Yang, T. and Chua, L.O. Conditions for impulsive synchronization of chaotic and hyperchaotic systems. *International Journal of Bifurcation and Chaos* **11** (2) (2001) 551.

Nonlinear Dynamics and Systems Theory, **15** (4) (2015) 409–417

A Simple Analytical Technique to Investigate Nonlinear Oscillations of an Elastic Two Degrees of Freedom Pendulum

Md. Abdur Razzak * and Md. Helal Uddin Molla

Dept of Mathematics, Rajshahi University of Engineering and Technology (RUET), Kazla, Rajshahi 6204, Bangladesh.

Received: September 6, 2014; Revised: October 28, 2015

Abstract: Based on the general Struble's technique, a simple analytical technique has been presented to investigate nonlinear oscillations of an elastic pendulum. The method is illustrated by swinging spring pendulum in the resonance cases (frequencies ratio is equal to 1 : 2). Solutions not only show a good coincidence with the corresponding numerical solution but also give better result than multiple scales (MS) method.

Keywords: *nonlinear oscillation; swinging spring pendulum; Struble's technique.*

Mathematics Subject Classification (2010): 34A34, 34C25.

1 Introduction

Struble's technique [1], Krylov-Bogoliubov-Mitropolskii (KBM) method [2, 3], multiple time-scales method [4] are usually applied to determine the approximation solutions of weakly nonlinear differential equations. Popov [5] extended the KBM method to a damped system. Bojadziev [6] studied second order nonlinear system with strong damping effect by the two time scales method and justified that the solution is similar to that obtained by Popov [5]. Sometimes, all classical perturbation techniques [1–3] are useless to solve some nonlinear differential equations. In this regard, Shamsul [7] presented a general Struble's techniques to determine approximate solution of n-th order weakly non-linear differential systems. It is easy to apply the general Struble's technique to solve nonlinear differential equations with various damping effect.

* Corresponding author: mailto:raz_math61@yahoo.com

© 2015 InforMath Publishing Group/1562-8353 (print)/1813-7385 (online)/http://e-ndst.kiev.ua

In this paper, we have partially used this method [7] to solve nonlinear oscillations of elastic pendulum, in which the internal resonance occurs. In particular, a swinging spring pendulum without or with damping force has been investigated. Earlier Gorelik and Witt [8] studied this nonlinear oscillator in the case without damping. Then Kane and Kahn [9] studied the character of resonant case. Some authors studied similar type of swinging spring by the method of averaging [4, 10–12]. Latter, Nayfeh and Mook [13] studied two-degree-of freedom system by multiple scales (MS) method. Zaripov and Petrov [14]; Awrejcewicz and Petrov [15] investigated a spring type swinging pendulum in the resonance case by using Poincare–Birkhoff normal form method. Recently, some authors [16–19] have studied nonlinear differential equations. The solution obtained by the presented method is not only a better result than that by MS method [13] but also shows a nice coincidence with the corresponding numerical solution.

2 The Method

Consider a nonlinear oscillator of two degree-of-freedoms with strong damping effect

$$\ddot{x} + 2k_1\dot{x} + \omega_1^2 x = \varepsilon f(x, \theta, \dot{x}, \dot{\theta}), \tag{1}$$

$$\ddot{\theta} + 2k_2\dot{\theta} + \omega_2^2 \theta = \varepsilon \Phi(x, \theta, \dot{x}, \dot{\theta}), \tag{2}$$

where over dot denotes the derivatives with respect to t, $\omega_1, \omega_2 \geq 0$, k_1, k_2, ν are constants, ε denotes small parameter, ω_1 and ω_2 are natural frequency, $f(x, \theta, \dot{x}, \dot{\theta})$ and $\Phi(x, \theta, \dot{x}, \dot{\theta})$ are nonlinear functions.

When $\varepsilon = 0$, equations (1)–(2) become a linear equation and there are two eigenvalues of that two equations, say $\lambda_1 = -k_1 + i\omega_1^*$, $\lambda_2 = -k_1 - i\omega_1^*$, where $\omega_1^* = \sqrt{\omega_1^2 - k_1^2}$ and $\mu_1 = -k_2 + i\omega_2^*$, $\mu_2 = -k_2 - i\omega_2^*$, where $\omega_2^* = \sqrt{\omega_2^2 - k_2^2}$, respectively.

On the other hand when $\varepsilon \neq 0$, the first approximation solution of equations (1)–(2) is chosen in the form [7]

$$x = a_1 e^{\lambda_1 t} + a_2 e^{\lambda_2 t} + \varepsilon u_1 \tag{3}$$

and

$$\theta = b_1 e^{\mu_1 t} + b_2 e^{\mu_2 t} + \varepsilon v_1. \tag{4}$$

Equations (1)–(2) can be rewritten in the following form:

$$(D - \lambda_1)(D - \lambda_2)x = \varepsilon f, \tag{5}$$

$$(D - \mu_1)(D - \mu_2)\theta = \varepsilon \Phi. \tag{6}$$

Substituting equations (3)–(4) into equations (5)–(6), we obtain the following results, respectively as

$$(D - \lambda_1)(D - \lambda_2)(a_1 e^{\lambda_1 t} + a_2 e^{\lambda_2 t} + \varepsilon\, u_1) = \varepsilon f$$

or

$$(D - \lambda_2)(\dot{a}_1\, e^{\lambda_1 t}) + (D - \lambda_1)(\dot{a}_2\, e^{\lambda_2 t}) + (D - \lambda_1)(D - \lambda_2)(\varepsilon u_1) = \varepsilon f; \tag{7}$$

$$(D - \mu_1)(D - \mu_2)(b_1 e^{\mu_1 t} + b_2 e^{\mu_2 t} + \varepsilon\, v_1) = \varepsilon \Phi$$

or

$$(D - \mu_2)(\dot{b}_1\, e^{\mu_1 t}) + (D - \mu_1)(\dot{b}_2\, e^{\mu_2 t}) + (D - \mu_1)(D - \mu_2)(\varepsilon v_1) = \varepsilon \Phi, \tag{8}$$

since $(D - \lambda_1)(a_1\, e^{\lambda_1 t}) = \dot{a}_1\, e^{\lambda_1 t}$, $(D - \lambda_2)(a_2\, e^{\lambda_2 t}) = \dot{a}_2\, e^{\lambda_2 t}$, $(D - \mu_1)(b_1\, e^{\mu_1 t}) = \dot{b}_1\, e^{\mu_1 t}$ and $(D - \mu_2)(b_2\, e^{\mu_2 t}) = \dot{b}_2\, e^{\mu_2 t}$.

Herein the nonlinear functions f and Φ can be expanded in a Taylor series as

$$f = \sum_{m_1=0,\, m_2=0}^{\infty,\,\infty} F_{m_1,m_2} e^{(m_1\lambda_1+m_2\lambda_2)t}, \quad \Phi = \sum_{r_1=0,\, r_2=0}^{\infty,\,\infty} \Phi_{r_1,r_2} e^{(r_1\mu_1+r_2\mu_2)t}$$

and the unknown functions u_1 and v_1 can be obtained in terms of the variables a_1, a_2 and t; b_1, b_2 and t under the condition that u_1 and v_1 exclude the terms $F_{m_1,m_2}e^{(m_1\lambda_1+m_2\lambda_2)t}$ of f and $\Phi_{r_1,r_2}e^{(r_1\mu_1+r_2\mu_2)t}$ of Φ where, $m_1 - m_2 = \pm 1$ and $r_1 - r_2 = \pm 1$. On the other hand, both $\dot{a}_1$ and $\dot{a}_2$ respectively, contain the terms $F_{m_1,m_2}e^{(m_1\lambda_1+m_2\lambda_2)t}$ where $m_1 - m_2 = 1$ and $m_1 - m_2 = -1$. This assumption takes u_1 free from secular terms, *i.e.*, $t\cos t$, $t\sin t$. Similarly, both $\dot{b}_1$ and $\dot{b}_2$ respectively contain the terms $\Phi_{r_1,r_2}e^{(r_1\mu_1+r_2\mu_2)t}$ where $r_1 - r_2 = 1$ and $r_1 - r_2 = -1$. This assumption makes v_1 free from secular terms.

Now, separating equation (7) into three parts for $\dot{a}_1$, $\dot{a}_2$ and u_1 we get

$$(D-\lambda_2)(\dot{a}_1\, e^{\lambda_1 t}) = \sum_{m_1=0,\, m_2=0}^{\infty,\,\infty} F_{m_1,m_2} e^{(m_1\lambda_1+m_2\lambda_2)t}, \quad m_1 - m_2 = 1, \tag{9}$$

$$(D-\lambda_1)(\dot{a}_2\, e^{\lambda_2 t}) = \sum_{m_1=0,\, m_2=0}^{\infty,\,\infty} F_{m_1,m_2} e^{(m_1\lambda_1+m_2\lambda_2)t}, \quad m_1 - m_2 = -1, \tag{10}$$

$$(D-\lambda_1)(D-\lambda_2)u_1 = \sum_{m_1=0,\, m_2=0}^{\infty,\,\infty} F_{m_1,m_2} e^{(m_1\lambda_1+m_2\lambda_2)t}, \quad m_1 - m_2 \neq \pm 1. \tag{11}$$

Similarly, separating equation (8) into three parts for $\dot{b}_1$, $\dot{b}_2$ and p_1 we get

$$(D-\mu_2)(\dot{b}_1\, e^{\mu_1 t}) = \sum_{r_1=0,\, r_2=0}^{\infty,\,\infty} \Phi_{r_1,r_2} e^{(r_1\mu_1+r_2\mu_2)t}, \quad r_1 - r_2 = 1, \tag{12}$$

$$(D-\mu_1)(\dot{b}_2\, e^{\mu_2 t}) = \sum_{r_1=0,\, r_2=0}^{\infty,\,\infty} \Phi_{r_1,r_2} e^{(r_1\mu_1+r_2\mu_2)t}, \quad r_1 - r_2 = -1, \tag{13}$$

$$(D-\mu_1)(D-\mu_2)v_1 = \sum_{r_1=0,\, r_2=0}^{\infty,\,\infty} \Phi_{r_1,r_2} e^{(r_1\mu_1+r_2\mu_2)t}, \quad r_1 - r_2 \neq \pm 1. \tag{14}$$

Under transformation $a_1 = \frac{a}{2}\, e^{i\varphi_1}$, $a_2 = \frac{a}{2}\, e^{-i\varphi_1}$, $b_1 = \frac{b}{2}\, e^{i\varphi_2}$, $b_2 = \frac{b}{2}\, e^{-i\varphi_2}$, equations (9)–(14) are transformed to amplitude and phase equations. On the other hand, this transformation keeps u_1 and v_1 in an amplitude and phase form. Therefore, the first approximate solution is clearly found.

3 Example

Consider a swinging spring pendulum with damping force whose governing equation [4] is given by

$$\ddot{x} + \delta_1\dot{x} + \frac{k}{m}x + g(1-\cos\theta) - (l+x)\dot{\theta}^2 = 0, \tag{15}$$

$$\ddot{\theta} + \delta_2\dot{\theta} + \frac{g}{l+x}\sin\theta + \frac{2}{l+x}\dot{x}\dot{\theta} = 0, \tag{16}$$

where l is a length of swinging spring, $\omega_1^2 = \frac{k}{m} \approx 4\omega_2^2 = \frac{4g}{l}$ and k is constant.

If $x \ll l$, then equations (15) and (16) become

$$\ddot{x} + 2k_1\dot{x} + \omega_1^2 x + \omega_2^2\,\theta^2\,l/2 - l\,\dot{\theta}^2 = 0, \tag{17}$$

$$\ddot{\theta} + 2k_2\dot{\theta} + \omega_2^2\theta - \omega_2^2\,x\,\theta/l + 2\,\dot{x}\,\dot{\theta}/l = 0. \tag{18}$$

Substituting $x = \varepsilon\,x$ and $\theta = \varepsilon\,\theta$ in equations (17)–(4) , we obtain

$$\ddot{x} + 2k_1\dot{x} + \omega_1^2\,x = -\varepsilon\omega_2^2\theta^2 l/2 + \varepsilon l\,\dot{\theta}^2, \tag{19}$$

$$\ddot{\theta} + 2k_2\dot{\theta} + \omega_2^2\theta = \varepsilon\omega_2^2 x\theta/l - 2\varepsilon\dot{x}\dot{\theta}/l, \tag{20}$$

where $\delta_1 = 2k_1$, $\delta_2 = 2k_2$.

Equations (19)–(20) can be written as

$$(D-\lambda_1)(D-\lambda_2)x = -\varepsilon(\omega_2^2\theta^2 l/2 - l\,\dot{\theta}^2), \tag{21}$$

$$(D-\mu_1)(D-\mu_2)\theta = \varepsilon\omega_2^2 x\theta/l - 2\varepsilon\dot{x}\dot{\theta}/l. \tag{22}$$

When $\varepsilon = 0$, equation (21) becomes a linear equation and there are two eigenvalues, say $\lambda_1 = -k_1 + i\omega_1^*$, $\lambda_2 = -k_1 - i\omega_1^*$, where $\omega_1^* = \sqrt{\omega_1^2 - k_1^2}$ and $x = a_1 e^{\lambda_1 t} + a_2 e^{\lambda_2 t} + \varepsilon u_1$; $\theta = b_1 e^{\mu_1 t} + b_2 e^{\mu_2 t} + \varepsilon p_1$; and

$$\begin{aligned} f = -(\omega_2^2\theta^2 l/2 - l\dot{\theta}^2) = {} & -l\omega_2^2 b_1^2 e^{2\mu_1 t}/2 - l\omega_2^2 b_2^2 e^{2\mu_2 t}/2 - 2lb_1 b_2\omega_2^2 e^{(\mu_1+\mu_2)t}/2 \\ & + lb_1^2\mu_1^2 e^{2\mu_1 t} + 2lb_1 b_2\mu_1\mu_2 e^{(\mu_1+\mu_2)t} + lb_2^2\mu_2^2 e^{2\mu_2 t} + \cdots \end{aligned}$$

Therefore, equation (21) becomes

$$\begin{aligned} & (D-\lambda_2)(\dot{a}_1 e^{\lambda_1 t}) + (D-\lambda_1)(\dot{a}_2 e^{\lambda_2 t}) + \varepsilon(D-\lambda_1)(D-\lambda_2)u_1 \\ & = -\varepsilon l\omega_2^2 b_1^2 e^{2\mu_1 t}/2 - \varepsilon l\omega_2^2 b_2^2 e^{2\mu_2 t}/2 - 2\varepsilon lb_1 b_2\omega_2^2 e^{(\mu_1+\mu_2)t}/2 \\ & + \varepsilon lb_1^2\mu_1^2 e^{2\mu_1 t} + 2\varepsilon lb_1 b_2\mu_1\mu_2 e^{(\mu_1+\mu_2)t} + \varepsilon lb_2^2\mu_2^2 e^{2\mu_2 t} + \cdots, \end{aligned} \tag{23}$$

It is mentioned that $\lambda_1 = -k_1 + i\omega_1^*$, $\lambda_2 = -k_1 - i\omega_1^*$, $\mu_1 = -k_2 + i\omega_2^*$, $\mu_2 = -k_2 - i\omega_2^*$ in the case of under-damped systems. For the resonance case, we have used $\omega_1^* \approx 2\omega_2^*$. Since $e^{\lambda_1 t}$ and $e^{2\mu_1 t}$ contain $e^{i\omega_1^* t}$, we equate the terms with $e^{\lambda_1 t}$ and $e^{2\mu_1 t}$ of equation (23). In a similar way, we equate the terms with $e^{\lambda_2 t}$ and $e^{2\mu_2 t}$ of equation (23). On the other hand, u_1 contains the term $e^{(\mu_1+\mu_2)t}$.

Now, separating equation (23) into three parts for $\dot{a}_1$, $\dot{a}_2$ and u_1 we get (see paper [7])

$$(D-\lambda_2)(\dot{a}_1 e^{\lambda_1 t}) = -\varepsilon l\omega_2^2 b_1^2 e^{2\mu_1 t}/2 + \varepsilon lb_1^2\mu_1^2 e^{2\mu_1 t}, \tag{24}$$

$$(D-\lambda_1)(\dot{a}_2 e^{\lambda_2 t}) = -\varepsilon l\omega_2^2 b_2^2 e^{2\mu_2 t}/2 + \varepsilon lb_2^2\mu_2^2 e^{2\mu_2 t}, \tag{25}$$

and

$$(D-\lambda_1)(D-\lambda_2)u_1 = -l\omega_2^2 b_1 b_2 e^{(\mu_1+\mu_2)t} + 2lb_1 b_2\mu_1\mu_2 e^{(\mu_1+\mu_2)t}. \tag{26}$$

From equation (24), we obtain

$$\dot{a}_1 e^{\lambda_1 t} = -\frac{\varepsilon l\omega_2^2 b_1^2 e^{2\mu_1 t}}{2(D-\lambda_2)} + \frac{\varepsilon lb_1^2\mu_1^2 e^{2\mu_1 t}}{(D-\lambda_2)} = \varepsilon lb_1^2\left(\mu_1^2 - \frac{\omega_2^2}{2}\right)e^{2\mu_1 t}/(2\mu_1 - \lambda_2). \tag{27}$$

Equation (27) can be written as

$$\dot{a}_1 = \varepsilon l b_1^2 \left(\mu_1^2 - \frac{\omega_2^2}{2}\right) e^{(2\mu_1-\lambda_1)t}/(2\mu_1 - \lambda_2). \tag{28}$$

Substituting $a_1 = \frac{a}{2}e^{i\varphi_1}$, $a_2 = \frac{a}{2}e^{-i\varphi_1}$, $b_1 = \frac{b}{2}e^{i\varphi_2}$, $b_2 = \frac{b}{2}e^{-i\varphi_2}$, $\lambda_1 = -k_1 + i\omega_1^*$, $\lambda_2 = -k_1 - i\omega_1^*$, and $\mu_1 = -k_2 + i\omega_2^*$, $\mu_2 = -k_2 - i\omega_2^*$ into equation (28), we obtain

$$\begin{aligned}(\dot{a} + ia\dot{\varphi}_1)/2 &= \frac{\varepsilon l b^2 (2(-k_2 + i\omega_2^*)^2 - \omega_2^2) e^{(2(-k_2+i\omega_2^*)-(-k_1+i\omega_1^*))t + 2i\varphi_2 - i\varphi_1}}{8(2(-k_2 + i\omega_2^*) - (-k_1 - i\omega_1^*))} \\ &= \frac{\varepsilon l b^2 e^{(k_1-2k_2)t}}{4((k_1-2k_2)^2 + (2\omega_2^* + \omega_1^*)^2)} \left[(4k_2^2 - 3\omega_2^2)(k_1 - 2k_2) - 4k_2\omega_2^*(2\omega_2^* + \omega_1^*)\right. \\ &\quad \left. - i(4k_2\omega_2^*(k_1 - 2k_2) + (4k_2^2 - 3\omega_2^2)(2\omega_2^* + \omega_1^*))\right] e^{i\gamma},\end{aligned} \tag{29}$$

where $\gamma = (2\omega_2^* - \omega_1^*)t + 2\varphi_2 - \varphi_1$.

Separating the real and imaginary parts from both sides of equation (29), we obtain

$$\begin{aligned}\dot{a} = \frac{\varepsilon l b^2 e^{(k_1-2k_2)t}}{4((k_1-2k_2)^2 + (2\omega_2^* + \omega_1^*)^2)} &[(4k_2^2 - 3\omega_2^2)(k_1 - 2k_2) - 4k_2\omega_2^*(2\omega_2^* + \omega_1^*)\cos\gamma \\ &+ (4k_2\omega_2^*(k_1 - 2k_2) + (4k_2^2 - 3\omega_2^2)(2\omega_2^* + \omega_1^*))\sin\gamma],\end{aligned} \tag{30}$$

$$\begin{aligned}\dot{\varphi}_1 = \frac{\varepsilon l b^2 e^{(k_1-2k_2)t}}{4a((k_1-2k_2)^2 + (2\omega_2^* + \omega_1^*)^2)} &[(4k_2^2 - 3\omega_2^2)(k_1 - 2k_2) - 4k_2\omega_2^*(2\omega_2^* + \omega_1^*)\sin\gamma \\ &- (4k_2\omega_2^*(k_1 - 2k_2) + (4k_2^2 - 3\omega_2^2)(2\omega_2^* + \omega_1^*))\cos\gamma].\end{aligned} \tag{31}$$

Similarly, equation (22) becomes

$$\begin{aligned}&(D-\mu_1)(\dot{b}_2 e^{\mu_2 t}) + (D-\mu_2)(\dot{b}_1 e^{\mu_1 t}) + \varepsilon(D-\mu_1)(D-\mu_2)v_1 \\ &= \varepsilon\omega_2^2(a_1 b_1 e^{(\lambda_1+\mu_1)t} + a_1 b_2 e^{(\lambda_1+\mu_2)t} + a_2 b_1 e^{(\lambda_2+\mu_1)t} \\ &+ a_2 b_2 e^{(\lambda_2+\mu_2)t})/l - 2\varepsilon(a_1 b_1 \lambda_1\mu_1 e^{(\lambda_1+\mu_1)t} + a_1 b_2 \lambda_1\mu_2 e^{(\lambda_1+\mu_2)t} \\ &+ a_2 b_1 \lambda_2\mu_1 e^{(\lambda_2+\mu_1)t} + a_2 b_2 \lambda_2\mu_2 e^{(\lambda_2+\mu_2)t})/l.\end{aligned} \tag{32}$$

Herein we have used $\dot{a}_1 = 0$, $\dot{b}_1 = 0$.

Applying the separation rule to equation (32), we obtain the following equations for $\dot{b}_1$, $\dot{b}_2$ and v_1

$$(D-\mu_2)(\dot{b}_1 e^{\mu_1 t}) = \varepsilon\omega_2^2 a_1 b_2 e^{(\lambda_1+\mu_2)t}/l - 2\varepsilon\, a_1 b_2 \lambda_1\mu_2 e^{(\lambda_1+\mu_2)t}/l, \tag{33}$$

$$(D-\mu_1)(\dot{b}_2 e^{\mu_2 t}) = \varepsilon\omega_2^2 a_2 b_1 e^{(\lambda_2+\mu_1)t}/l - 2\varepsilon\, a_2 b_1 \lambda_2\mu_1 e^{(\lambda_2+\mu_1)t}/l \tag{34}$$

and

$$\begin{aligned}(D-\mu_1)(D-\mu_2)v_1 = (\omega_2^2 a_1 b_1 e^{(\lambda_1+\mu_1)t} + \omega_2^2 a_2 b_2 e^{(\lambda_2+\mu_2)t})/l \\ - 2(a_1 b_1 \lambda_1\mu_1 e^{(\lambda_1+\mu_1)t} + 2a_2 b_2 \lambda_2\mu_2 e^{(\lambda_2+\mu_2)t})/l\end{aligned} \tag{35}$$

From equation (33), we obtain

$$\begin{aligned}\dot{b}_1 e^{\mu_1 t} &= \frac{\varepsilon\omega_2^2 a_1 b_2 e^{(\lambda_1+\mu_2)t}}{l(D-\mu_2)} - \frac{2\varepsilon\, a_1 b_2 \lambda_1\mu_2 e^{(\lambda_1+\mu_2)t}}{l(D-\mu_2)} \\ &= \frac{\varepsilon\omega_2^2 a_1 b_2 e^{(\lambda_1+\mu_2)t}}{l\lambda_1} - \frac{2\varepsilon\, a_1 b_2 \lambda_1\mu_2 e^{(\lambda_1+\mu_2)t}}{l\lambda_1}.\end{aligned} \tag{36}$$

From equation (36), we obtain

$$\dot{b}_1 = \frac{\varepsilon\omega_2^2 a_1 b_2 e^{(\lambda_1+\mu_2-\mu_1)t}}{l\lambda_1} - \frac{2\varepsilon\, a_1 b_2 \lambda_1 \mu_2 e^{(\lambda_1+\mu_2-\mu_1)t}}{l\lambda_1}. \tag{37}$$

Using a transformation $a_1 = \frac{a}{2}e^{i\varphi_1}$, $a_2 = \frac{a}{2}e^{-i\varphi_1}$, $b_1 = \frac{b}{2}e^{i\varphi_2}$, $b_2 = \frac{b}{2}e^{-i\varphi_2}$ for equation (37), we obtain

$$\dot{b} + ib\dot{\phi}_2 = \frac{\varepsilon a b e^{-k_1 t}}{2l\omega_1^2}\left[(2\omega_1^2 k_2 - \omega_2^2 k_1) + i(2\omega_1^2\omega_2^* - \omega_2^2\omega_1^*)\right] e^{-i\gamma}, \tag{38}$$

where $\gamma = (2\omega_2^* - \omega_1^*)t + 2\varphi_2 - \varphi_1$.

Separating the real and imaginary parts from both sides of equation (38), we obtain

$$\dot{b} = \frac{\varepsilon\, a\, b e^{-k_1 t}}{2l\omega_1^2}[(2\,\omega_1^2 k_2 - \omega_2^2 k_1)\cos\gamma + (2\,\omega_1^2\omega_2^* - \omega_2^2\omega_1^*)\sin\gamma], \tag{39}$$

$$\dot{\varphi}_2 = \frac{\varepsilon\, a\, e^{-k_1 t}}{2l\omega_1^2}[(2\,\omega_1^2\omega_2^* - \omega_2^2\omega_1^*)\cos\gamma - (2\,\omega_1^2 k_2 - \omega_2^2 k_1)\sin\gamma]. \tag{40}$$

Therefore, the first approximate solution of equations (15)–(16) becomes

$$x = \varepsilon a e^{-k_1 t}\cos(\omega_1 t + \varphi_1) + O(\varepsilon^2), \tag{41}$$

$$\theta = \varepsilon b e^{-k_2 t}\cos(\omega_2 t + \varphi_2) + O(\varepsilon^2). \tag{42}$$

If the damping force is absent i.e. $k = 0$, then equations (30)–(31) and (39)–(40) become

$$\dot{a} = -3\varepsilon l b^2\omega_2^2 \sin\psi/(4(2\omega_2 + \omega_1)), \tag{43}$$

$$\dot{\varphi}_1 = 3\varepsilon l b^2\omega_2^2 \cos\psi/(4a(2\omega_2 + \omega_1)), \tag{44}$$

and

$$\dot{b} = \frac{\varepsilon a b\omega_2(2\omega_1 - \omega_2)\sin\psi}{2l\omega_1}, \tag{45}$$

$$\dot{\varphi}_2 = \frac{\varepsilon a\omega_2(2\omega_1 - \omega_2)\cos\psi}{2l\omega_1}, \tag{46}$$

where $\psi = (2\omega_2 - \omega_1)t + 2\varphi_2 - \varphi_1$.

In this case (undamped), the first approximate solution of equations (15)–(16) is

$$x = \varepsilon a\cos(\omega_1 t + \varphi_1) + O(\varepsilon^2), \tag{47}$$

$$\theta = \varepsilon b\cos(\omega_2 t + \varphi_2) + O(\varepsilon^2). \tag{48}$$

4 Results and Discussion

Usually a nonlinear problem is solved by a perturbation method [5, 20–23]. In this paper, a simple analytical technique has been developed based on the general Struble's technique [7] to investigate nonlinear oscillations of an elastic pendulum. The technique is very easy and straightforward. Nonlinear oscillations of the swinging spring pendulum in the case of resonance $\omega_1 : \omega_2 = 1 : 2$ have been considered. The solutions have been obtained without and with damping effect and presented respectively in Figure 1 and Figure 3.

On the other hand, the corresponding perturbation solutions have been obtained by MS method and shown in Figure 2 and Figure 4. To compare our solution with existing perturbation solutions, we have provided the numerical solutions in all the figures.

From Figure 2 and Figure 4, we see that the solutions by MS method deviate from numerical solution after a certain time. On the other hand, our solutions (see Figures 1, 3) show a good coincidence with the numerical solutions.

Comparing all the results of swinging spring pendulum in the case of resonance $\omega_1 : \omega_2 = 1 : 2$, we observe that the general Struble's technique provides more correct solution than other perturbation solutions especially those obtained by the multiple time scale method [13].

5 Conclusion

Based on the general Struble's technique [7], a simple analytical technique has been presented to investigate nonlinear oscillations of an elastic pendulum in which damping effect is present. Nonlinear oscillations of the swinging spring pendulum with or without damping effect in the case of resonance are considered. Previously, some authors (see [9, 14–15]) investigated swinging spring pendulum without damping effect. On the other hand, some perturbation methods especially MS methods are not suitable to investigate nonlinear oscillations of elastic pendulum. In this paper, a simple perturbation method has been presented and has given better result than MS method. The method also provides a good result compared to the numerical solution (considered to exact).

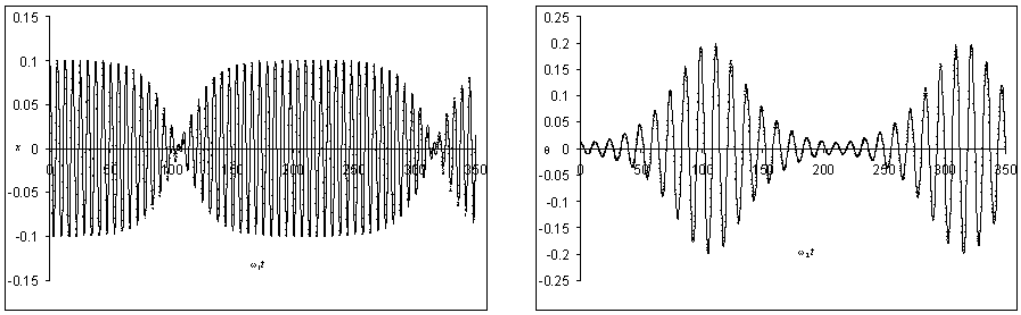

Fig 1: Solution of equations (15) and (16) obtained by the presented method has been presented (denoted by dots) when $k_1 = k_2 = 0, , \omega_2 = 0.5\,\omega_1, l = 1, \varepsilon = 0.1$ with initial conditions $[x(0) = 1,\ \dot{x}(0) = 0,\ \theta(0) = 0.1,\ \dot{\theta}(0) = 0]$. Corresponding numerical solution (obtained by fourth-order Runge-Kutta method) has been presented (represented by solid line) to be compared with the present solution.

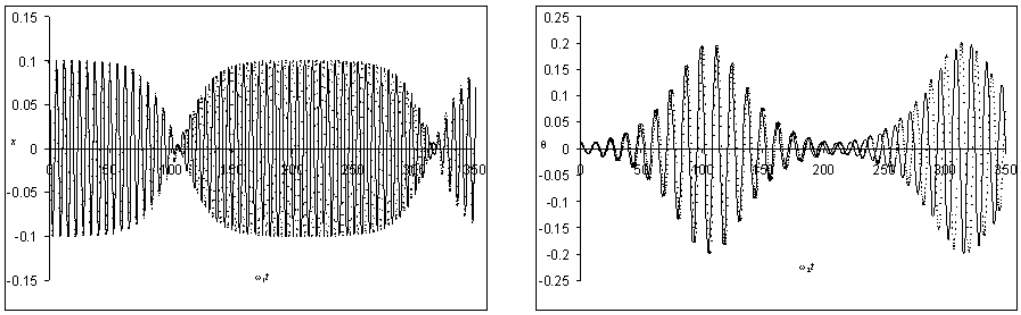

Fig 2: Solution of equations (15) and (16) obtained by MS method has been presented

(denoted by dots) when $k_1 = k_2 = 0, \omega_2 = 0.5\,\omega_1, l = 1, \varepsilon = 0.1$ with initial conditions $[x(0) = 1,\ \dot{x}(0) = 0,\ \theta(0) = 0.1,\ \dot{\theta}(0) = 0]$. Corresponding numerical solution (obtained by fourth-order Runge-Kutta method) has been presented (represented by solid line) to be compared with MS method solution.

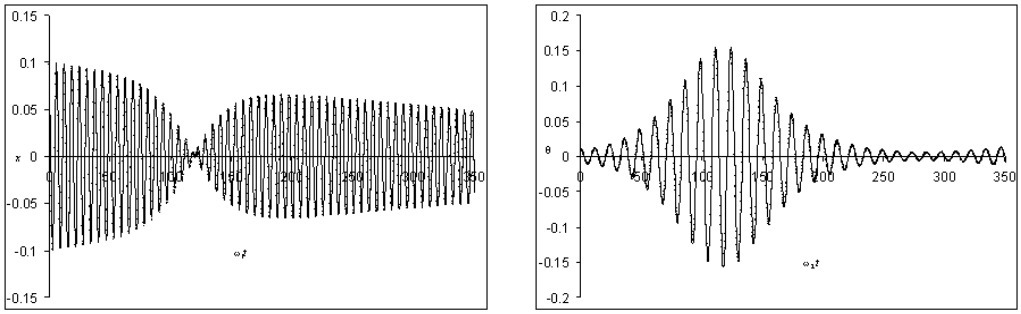

Fig 3: Solution of eqations (30) and (31) by the present method has been presented (denoted by dots) when $\omega_2 = 0.5\,\omega_1, l = 1, \varepsilon = 0.1, k_1 = \delta_1/2 = 0.002,\ k_2 = \delta_2/2 = 0.002$ and the initial conditions $[x(0) = 1,\ \dot{x}(0) = 0,\ \theta(0) = 0.1,\ \dot{\theta}(0) = 0]$. Corresponding numerical solution (obtained by fourth-order Runge-Kutta method) has been presented (represented by solid line) to be compared with the present solution.

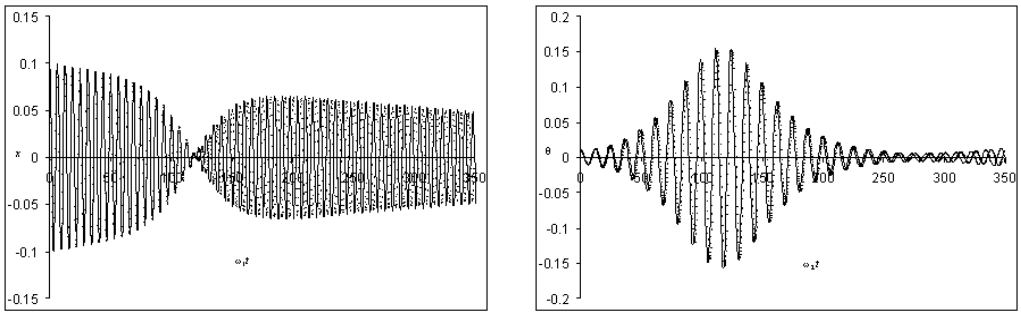

Fig 4: Solution of eqations (30) and (31) by MS method has been presented (denoted by dots) when $\omega_2 = 0.5\,\omega_1, l = 1, \varepsilon = 0.1, k_1 = \delta_1/2 = 0.002,\ k_2 = \delta_2/2 = 0.002$ and the initial conditions $[x(0) = 1,\ \dot{x}(0) = 0,\ \theta(0) = 0.1,\ \dot{\theta}(0) = 0]$. Corresponding numerical solution (obtained by fourth-order Runge-Kutta method) has been presented (represented by solid line) to be compared with MS method solution.

References

[1] Struble, R. A. The geometry of the orbits of artificial satellities. *Arch. Rational Mech. Anal.* **7** (1961) 87–104.

[2] Krylov, N. N. and Bogoliubov, N. N. *Introduction to Nonlinear Mechanics.* Princeton University Press, New Jersey, 1947.

[3] Bogoliubov, N. N. and Mitropolskii, Yu. A. *Asymptotic Methods in the Theory of Non-linear Oscillations.* Gordan and Breach, New York, 1961.

[4] Nayfeh, A. H. *Perturbation Methods.* John Wiley & Sons, New York, 1973.

[5] Popov, I. P. A generalization of the Bogoliubov asymptotic method in the theory of nonlinear oscillation. *Dokl. Akad. Nauk. SSSR* **111** (1956) 308–310.

[6] Bojadziev, G. N. Two variables expansion method applied to the study of damped nonlinear oscillations. *Nonlinear Vib. Probl.* **21** (1981) 11–18.

[7] Shamsul Alam, M., Azad, M. A. K., and Haque, M. A. A general Struble's technique for solving an n-th order weakly nonlinear differential system with damping. *Int. J. Nonlinear Mech.* **41** (2006) 905–918.

[8] Gorelik, G. and Witt, A. Swing of an elastic pendulum as an example of two parametrically bound linear vibration systems. *J. Tech. Phys. (USSR)* **3** (1933) 244–307.

[9] Kane, T. R. and Kahn, M. E. On a class of two-degree-of-freedom oscillations. *J. Appl. Mech.* **35** (1968) 547–552.

[10] Mettler, E. Stabilitatsfragen bei freien Schwingungen mechanischer Systeme. *Ingenieur-Archiv.* **28** (1959) 213–228.

[11] Sethna, P. R. Vibrations of dynamical systems with quadratic nonlinearities. *J. Appl. Mech.* **32** (1965) 576–582.

[12] Bogaevskii, V. N. and Povzner, A. Y. *Algebraic Methods in Non-linear Theory of Perturbation.* Nauka, Moscow, 1987.

[13] Nayfeh, A. H. and Mook, D. T. *Nonlinear Oscillations.* John Wiley & Sons, New York, 1979.

[14] Zaripov, M.N. and Petrov, A. G. Nonlinear oscillations of a swinging spring. *Doklady Physics* **49** (2004) 691–696.

[15] Awrejcewicz, J. and Petrov, A. G. Nonlinear oscillations of an elastic two-degrees-of-freedom pendulum. *Nonlinear Dyn.* **53** (2008) 19–30.

[16] Desale, B. S. and Dasre, N. R. Numerical solutions of system of non-linear ODEs by Euler modified method. *Nonlinear Dynamics and Systems Theory* **12** (3) (2012) 215–236.

[17] Tunc, C. Instability for nonlinear differential equations of fifth order subject to delay. *Nonlinear Dynamics and Systems Theory* **12** (2) (2012) 207–214.

[18] Denk, A. and Topal, S. Existence and uniqueness of a nontrivial solution for second order nonlinear m-point eigenvalue problems on time scales. *Nonlinear Dynamics and Systems Theory* **13** (4) (2013) 389–399.

[19] Korkmaz, E. and Tunc. C. On the convergence of solutions of some nonlinear differential equations of fourth order. *Nonlinear Dynamics and Systems Theory* **14** (4) (2014) 313–322.

[20] Bojadziev, G. N. Damped nonlinear oscillations modeled by a 3-dimensional differential system. *Acta Mech.* **48** (1983) 193–201.

[21] Osiniskii, Z. Longitudinal, torsional and bending vibrations of a uniform bar with nonlinear internal friction and relaxation. *Nonlinear Vib. Probl.* **4** (1962) 159–166.

[22] Mulholland, R. J. Nonlinear oscillations of third-order differential equation. *Int. J. Nonlinear Mech.* **6** (1971) 279–294.

[23] Murty, I. S. N., Deekshatulu, B. L., and Krisna, G. On asymptotic method of Krylov-Bogoliubov for over damped nonlinear systems. *J. Franklin Inst.* **288** (1969) 49–64.

Nonlinear Dynamics and Systems Theory, **15** (4) (2015) 418–427

Mathematical Analysis in a Model of Primary Succession

R.V. Ruzich *

Department of Applied Mathematics and Social Informatics, Khmelnitsky National University, Khmelnitsky, Ukraine

Received: October 29, 2014; Revised: June 24, 2015

Abstract: This paper is concerned with a long-term ecological primary succession. The model of open Eigen's hypercycle has been used for modeling of the process. The multi-dimension case is analyzed. It is shown that consideration of system's dynamics can be simplified by partial reduction to the cases of lower dimension. The dynamics of ecological system can be considered as a self-organizing process with quasi-discrete characteristic. The quasi-discrete dynamics is explained by bifurcation properties of the system, that produce step-by-step changing of system's structure.

Keywords: *biogeocoenose; primary succession; stability; evolution; bifurcation; self-organization.*

Mathematics Subject Classification (2010): 34A34, 34D20, 37F99, 92D99.

1 Introduction

Since the second half of the 20th century, illusion of happiness with regard to the development of a technocratic society disappears, while the number and severeness of the ecological crises increase. At this time researchers began to pay more attention to the study of ecological processes [2, 7, 17, 25, 26, 30].

The main object of the study is biogeocoenosis (as a collection of fauna and flora that exist in some area), and in particular a succession that takes place in it. In classical ecological theory there are two main types of succession: primary and secondary succession [26]. Note that a lot of works [5, 15, 19, 21, 28] are concerned with the mathematical modeling of the second type of ecological process. As to the first type, the works are mostly descriptive, of non-formalized character [12, 24, 27]. In this paper we examine the behavior of ecological systems during primary succession.

* Corresponding author: mailto:ninasus@gmail.com

© 2015 InforMath Publishing Group/1562-8353 (print)/1813-7385 (online)/http://e-ndst.kiev.ua

Ecological processes (including the succession) are complex and characterized by oscillating processes, processes of self-organization, abrupt change of the mode of a system, the effects of histereses and others. The experience of using linear models showed that they can not adequately describe the behavior of real systems, but only reflect some common trends. Often the stochastic models are used to describe succession processes [1, 12, 20, 22, 23]. The basic parameter that determines the dynamics of biogeocoenosis in such models is the probability of transition. It represents probability of some association to become dominant. Such approach can be useful for simulation of system dynamics, but does not reflect driving forces of the process.

Another tool that is used to describe the succession are differential equations, in particular of the Volltarian type [8, 29]. In such models competition between associations is considered as the basic driving force of ecological process. Note that quite a number of researchers adhere this point of view [16, 25, 26]. However, these models have several weaknesses: they do not reflect the interaction between biotic elements and inert components of the ecosystem; it is possible that associations do not compete, but reach the optimum number. These flaws can be corrected by using a special modification (called an "open hypercycle" [10]) of the famous Eigen hypercycle [14] for description of primary successions. This model is similar,but not equivalent to Lotka-Volterra models of the competition or is of the "predator-prey" type.

2 The Model

Let us consider the behavior of biological associations $x(t) = (x_1(t), ..., x_n(t))$ that is described by the model of open Eigen's hypercycle:

$$\frac{dx_i}{dt} = \left(F_i(t) - \frac{1}{S_0} \sum_{j=0}^{n} x_j F_j(t) \right) x_i, i = \overline{1,n}, \tag{1}$$

where S_0 is a capacity of environment (size of ecological niche), $S_0 > 0$.

Suppose that the coefficients of propagation and interaction between associations are defined by Allen's functions:

$$F_i(t) = a_{i-1} x_{i-1}(t) - x_i(t), i = \overline{1,n},$$

here $a_1 > 0, i = \overline{1,n-1}, x_0 = 1, a_0 = N$; N is a coefficient which determines the equilibrium size of the first association, when it develops alone; a_1 is a coefficient which describes a level of dependence of the $(i+1)$th association on the previous one, $i = \overline{1,n-1}$. Allen's functions reflect the nature of the relationship between associations where associations are included into a system at certain level of development of stagnant environment.

3 The Jacobi Matrix

The structure of a Jacobi matrix row of system (1) can be represented as

$$\underbrace{f_1 \dots f_1}_{m} \underbrace{f_2 \dots f_2}_{l} f_3 \underbrace{f_4 \dots f_4}_{d}, \tag{2}$$

where $f_1 = -x_i S_0^{-1} (a_{k-1} x_{k-1} - 2x_k + a_k x_{k+1})$,

$f_2 = a_{i-1}x_i - x_i S_0^{-1}\left(a_{i-2}x_{i-2} - 2x_{i-1} + a_{i-1}x_i\right)$,

$$f_3 = \begin{cases} a_{i-1}x_{i-1} - 2x_i - S_0^{-1}\sum_{j=1}^{n}\left(a_{j-1}x_{j-1}x_j - x_j^2\right) - \\ -x_i S_0^{-1}\left(a_{i-1}x_{i-1} - 2x_i + a_i x_{i+1}\right), k < n; \\ a_{i-1}x_{i-1} - 2x_i - S_0^{-1}\sum_{j=1}^{n}\left(a_{j-1}x_{j-1}x_j - x_j^2\right) - x_i S_0^{-1}\left(a_{i-1}x_{i-1} - 2x_i\right), \\ k = n; \end{cases}$$

$$f_4 = \begin{cases} -x_i S_0^{-1}\left(a_{k-1}x_{k-1} - 2x_k + a_k x_{k+1}\right), k < n; \\ -x_i S_0^{-1}\left(a_{k-1}x_{k-1} - 2x_k\right), k = n; \end{cases}$$

$m = \varphi(i-2)$, $l = \begin{cases} 1, i > 1; \\ 0, i = 1; \end{cases}$, $d = n - m - l - 1$, $\varphi(x) = \begin{cases} x, x \geq 10; \\ 0, x < 0; \end{cases}$, k, i are a number of column and a row of the Jacobi matrix respectively, $k = \overline{1,n}, i = \overline{1,n}$.

Theorem 3.1 *If the coordinate x_p of a stationary point is zero, then one of eigenvalues of the Jacobi matrix of the system (1) at this stationary point can be calculated as*

$$a_{p-1}x_{p-1} - S_0^{-1}\sum_{j=1}^{n}\left(a_{j-1}x_{j-1}x_j - x_j^2\right), \tag{3}$$

if x_{p-1} is not zero or $p = 1$. Otherwise the eigenvalue equals

$$-S_0^{-1}\sum_{j=1}^{n}\left(a_{j-1}x_{j-1}x_j - x_j^2\right). \tag{4}$$

Proof. If some coordinate x_p of the stationary point is zero, than row p of the Jacobi matrix can be written as (taking into account (2))

$$\underbrace{0\ldots0}_{p-1}a_{p-1}x_{p-1} - S_0^{-1}\sum_{j=1}^{n}\left(a_{j-1}x_{j-1}x_j - x_j^2\right)\underbrace{0\ldots0}_{n-p}.$$

Write the characteristic equation of this matrix

$$|J - \Lambda I| = 0,$$

here I is an identity matrix, Λ is a matrix of eigenvalues, J is the Jacobi matrix.

Expanding the determinant in algebraic complement to the row p, we find that the eigenvalues are computed as

$$\left[\begin{array}{l} \lambda = a_{p-1}x_{p-1} - S_0^{-1}\sum_{j=1}^{n}\left(a_{j-1}x_{j-1}x_j - x_j^2\right), \\ A_p = 0, \end{array}\right.$$

here A_p is determinant of minor on diagonal item of row p. Apparently if $x_{p-1} = 0$, then

$$\lambda = -S_0^{-1}\sum_{j=1}^{n}\left(a_{j-1}x_{j-1}x_j - x_j^2\right).$$

Thus, the theorem is proved. □

Considering the set of stationary points of the model of open Eigen's hypercycle one can see that there is a subset of points whose first coordinates are equal to the corresponding coordinates of stationary points of lower dimension model and all the other (the last) coordinates are zero. These stationary points are called the "points-descendants".

Theorem 3.2 *$n-1$ eigenvalues of the Jacobi matrix at the "points-descendants" of n-dimensional model of open Eigens hypercycle are the same as at the corresponding stationarity points of $(n-1)$-dimensional model, and the last one is calculated as*

$$a_{n-1}x_{n-1} - S_0^{-1}\sum_{j=1}^{n}\left(a_{j-1}x_{j-1}x_j - x_j^2\right). \tag{5}$$

Proof. According to Theorem 3.1 one eigenvalue of the Jacobi matrix of system (1) at the "point-descendant" equals

$$a_{n-1}x_{n-1} - S_0^{-1}\sum_{j=1}^{n}\left(a_{j-1}x_{j-1}x_j - x_j^2\right).$$

Consider the $(n-1)\times(n-1)$ cell of Jacobi matrix (which is the algebraic complement of the matrix). From the analysis of the formula (2) it is obvious that the cell of Jacobi matrix, that contains the first $n-2$ rows and $n-2$ cells, is not different from the general case. The elements of the main diagonal are calculated as

$$a_{i-1}x_{i-1} - 2x_i - S_0^{-1}\sum_{j=1}^{n}\left(a_{j-1}x_{j-1}x_j - x_j^2\right) - x_iS_0^{-1}\left(a_{i-1}x_{i-1} - 2a_i + a_1x_{i+1}\right),$$
$$i = \overline{1, n-2}.$$

The first $(n-1)$ elements of the $(n-1)$th row of Jacobi matrix are calculated as

$$-x_{n-1}S_0^{-1}\left(a_{k-1}x_{k-1} - 2a_k + a_kx_{k+1}\right), k = \overline{1, n-3},$$
$$a_{n-2}x_{n-1} - x_{n-1}S_0^{-1}\left(a_{n-3}x_{n-3} - 2a_{n-2} + a_{n-2}x_{n-1}\right),$$
$$a_{n-2}x_{n-2} - 2x_{n-1} - S_0^{-1}\sum_{j=1}^{n}\left(a_{j-1}x_{j-1}x_j - x_j^2\right) - x_{n-1}S_0^{-1}\left(a_{n-2}x_{n-2} - 2x_{n-1}\right),$$

and the elements of the $(n-1)$th cell as

$$-x_{n-1}S_0^{-1}\left(a_{n-2}x_{n-2} - 2x_{n-1}\right).$$

Thus $(n-1)\times(n-1)$ cell that is considered, is the Jacobi matrix of $(n-1)$-dimensional model of open Eigen's hypercycle at the point formed by discarding the last coordinates (which are zero) of n-dimensional model's "point-descendant". Hence, $n-1$ eigenvalues of the Jacobi matrix at the "points-descendant" of n-dimensional model are determined from this cell. Thus, the theorem is proved. □

Corollary 3.1 *$n-k$ eigenvalues of the Jacobi matrix at the "points-descendants" where the last k coordinates are zero, are the same as for $(n-k)$-dimensional model, $(k-1)$ of the rest k ones are determined by the formula (4), and the last one can be calculated as*

$$a_{n-k}x_{n-k} - S_0^{-1}\sum_{j=1}^{n-k}\left(a_{j-1}x_{j-1}x_j - x_j^2\right). \tag{6}$$

Proof of Corollary 3.1 is similar to the proof of Theorem 3.2.

Theorem 3.3 *If a stationary point with the last zero coordinate of n-dimensional model of open Eigen's hypercycle is stable, then the "point-descendant" of higher dimension model is stable too and the intervals of parameters, for which the points are stable, are the same. Otherwise, the "point-descendant" is unstable.*

Proof. Consider the stationary point of n-dimensional model where the last $k(k \geq 2)$ coordinates are zero. According to Corollary 3.1 $n-k$ eigenvalues of the Jacobi matrix at this point are the same as for $(n-k)$-dimensional model at the corresponding point. Thus, if the stationary point of $(n-k)$-dimensional model is stable, then $(n-k)$ eigenvalues are negative. According to formulas (4) and (5) other k ones are calculated as

$$\lambda_1 = a_{n-k}x_{n-k} - S_0^{-1}\sum_{j=1}^{n-k}\left(a_{j-1}x_{j-1}x_j - x_j^2\right),$$
$$\lambda_i = -S_0^{-1}\sum_{j=1}^{n-k}\left(a_{j-1}x_{j-1}x_j - x_j^2\right), i = \overline{2,k}.$$

As only nonnegative sector of phase space is considered, then the difference $\lambda_1 - \lambda_i = a_{n-k}x_{n-k}, i = \overline{1,k-1}$ is positive. Thus the inequality $\lambda_1 \geq \lambda_i$ is correct. Thus, if the eigenvalue λ_1 is negative, then all the other eigenvalues $\lambda_i (i = \overline{2,k})$ are negative too. It means that if the stationary point with the last zero coordinates of $(n-k+1)$-dimensional model is stable, then the "point-descendant" of n-dimensional model is stable too. Moreover, the interval of parameters, for which the point is stable, is not changed. Thus, the theorem is proved. □

Theorem 3.4 *If the stationary point of $(n-1)$-dimensional model of open Eigen's hypercycle is stable, then the coresponding "point-descendant" of n-dimensional model is stable when the inequality is correct:*

$$\frac{x_{n-2}}{x_{n-1}} > \frac{a_{n-1}+1}{a_{n-2}}.$$

Proof. Consider the stationary "point-descendant" of (n)-dimensional model with only one (the last) zero coordinate. Then according to Theorem 3.2 $n-1$ eigenvalues of Jacobi matrix at this point are defined as the eigenvalues of Jacobi matrix at the corresponding point of $(n-1)$-dimensional system, and one eigenvalue is $\lambda = a_{n-1}x_{n-1} - S_0^{-1}\sum_{j=1}^{n-1}\left(a_{j-1}x_{j-1}x_j - x_j^2\right)$. If this point of $(n-1)$-dimensional system is stable, then $(n-1)$ eigenvalues are negative.

Consider the eigenvalue λ. Note that the coordinates of the stationary point are determined by the system

$$a_{k-1}x_{k-1} - x_k - S_0^{-1}\sum_{j=1}^{n}\left(a_{j-1}x_{j-1}x_j - x_j^2\right) = 0, 1 \leq k \leq n-1,$$

here k are the numbers of nonzero coordinates. Therefore, we can write the expression

$$\lambda = a_{n-1}x_{n-1} - \left(a_{n-2}x_{n-2} - x_{n-1}\right).$$

Then, the eigenvalue λ is negative, if the following inequality is correct

$$\frac{x_{n-2}}{x_{n-1}} > \frac{a_{n-1}+1}{a_{n-2}}.$$

The theorem is proved. □

Obviously if coordinate x_{n-2} of the point from Theorem 3.4 is zero, then this point is unstable.

Example 3.1 It is obvious that there is a subset

$$\left\{ (x_1, \dots, x_k, 0 \dots, 0) | \, x_j = N \prod_{i=1}^{j-1} a_i, j = \overline{1,n}, 1 < k < n \right\}$$

of the set of stationary points of model (1). Using Theorems 3.3 and 3.4 it is easy to show that each point of this set is unstable.

4 The Two-dimensional Model of Open Eigen's Hypercycle

It was determined in [10] that the two-dimensional model of open Eigen's hypercycle has 6 stationary points: $(0,0)$, $(0,S_0)$, $(N,0)$, $(S_0,0)$, $\left(\frac{S_0+N}{a_1+2}, \frac{S_0(a_1+1)-N}{a_1+2}\right)$, (N, a_1N). The Lyapunov direct method is used for definition of their type and stability. The results are presented in Table 1.

Points	$S_0 \in$			
	$\left(0, \frac{1}{a_1+1}\right)$	$\left(\frac{1}{a_1+1}, 1\right)$	$(1, a_1+1)$	$(a_1+1, +\infty)$
$(0, S_0)$	Unstable node	Unstable node	Unstable node	Unstable node
$(N, 0)$	Unstable node	Unstable node	Saddle	Saddle
$(S_0, 0)$	Stable node	Saddle	Unstable node	Unstable node
$\left(\frac{S_0+N}{a_1+2}, \frac{S_0(a_1+1)-N}{a_1+2}\right)$	Saddle	Stable node	Stable node	Saddle
(N, a_1N)	Saddle	Saddle	Saddle	Stable node

Table 1: The stability of the stationary points.

The method described in [3] is used for definition of behavior of trajectories near complex (degenerate) stationary point. Thus, $(0,0)$ is a complex stationary point of "saddle-node" type for any positive values of the parameters; $(N,0)$ if $S_0 = N$; $(S_0,0)$ if $S_0 = N(a_1+1)^{-1}$; (N, a_1N) if $S_0 = (a_1+1)N$.

Theorem 4.1 *There are no limit cycles in the phase portrait of two-dimentional model of open Eigen's hypercycle.*

Proof. It is easy to show that points $(0,0)$, $(0,S_0)$, $(N,0)$, $(S_0,0)$, $\left(\frac{S_0+N}{a_1+2}, \frac{S_0(a_1+1)-N}{a_1+2}\right)$ are on the integral lines $x_1=0$, $x_2=0$, $x_1+x_2=S_0$. So there is no a limit cycle around these points. As for the point (N, a_1N), it is saddle or node-saddle if $\frac{S_0}{N} \in (0, a_1+1]$ (there is no a limit cycle around this point). If $\frac{S_0}{N} \in (a_1+1, +\infty)$ then it is a stable node. Consider this case. If $\frac{S_0}{N} \in (a_1+1, +\infty)$ then (N, a_1N) is inside the triangle formed by the integral lines $x_1=0$, $x_2=0$, $x_1+x_2=S_0$.

Use Dulac theorem. Take $F(x_1,x_2)=x_1^{-2}x_2^{-2}$ as Dulac function, then

$$\frac{\partial(PF)}{\partial x_1}+\frac{\partial(QF)}{\partial x_2}=-\frac{NS_0-x_1(N-S_0a_1)}{S_0x_1^2x_2^2}.$$

Here P and Q are the left-hand sides of equations of the two-dimensional model of open Eigen's hypercycle. As we consider only the triangle, then $x_1 \leqslant S_0$. Hence

$$-\frac{NS_0-x_1(N-S_0a_1)}{S_0x_1^2x_2^2} \leqslant -\frac{NS_0-S_0(N-S_0a_1)}{S_0x_1^2x_2^2}=-\frac{S_0a_1}{x_1^2x_2^2}.$$

This expression has a constant sign in the triangle, hence there is no a limit cycle in the triangle. Therefore there is no a limit cycle in the phase portrait. The theorem is proved. □

There is only one attractor, namely node, in the system for any positive values of the parameters. The stable point is always in the first quarter of the phase portrait. If $0 < S_0 < (a_1+1)^{-1}N$, only one association is able to exist in the ecosystem. When $S_0=(a_1+1)^{-1}N$, there is a bifurcation (if we consider only the first quarter). It is interpreted as the inclusion of the second association in the ecological system and it defines a new stage of succession process.

If $(a_1+1)^{-1}N < S_0 < (a_1+1)N$, $\left(\frac{S_0+N}{a_1+2}, \frac{S_0(a_1+1)-N}{a_1+2}\right)$ is a stable point. Note that the first association is dominant, if $a_1<1$. If $a_1>1$, the first or the second one is dominant depending on the size of the ecological niche.

If $S_0 > (a_1+1)N$, there is an excess of resources in the system. Both associations reach maximum capacity. Moreover the first association is dominant if $a_1<1$. Otherwise the second association is dominant.

5 The Three-Dimensional Model of Open Eigen's Hypercycle

It was determined that there are 11 stationary points of phase space of three-dimensional model of open Eigen hypercycle: P_1 : $(0,0,0)$, P_2 : $(N,0,0)$, P_3 : $(N, a_1N, 0)$, P_4 : (N, a_1N, a_1a_2N), P_5 : $(S_0,0,0)$, P_6 : $(0,S_0,0)$, P_7 : $(0,0,S_0)$, P_8 : $\left(\frac{N+S_0}{a_1+2}, \frac{S_0(a_1+1)-N}{a_1+2}, 0\right)$, P_9 : $\left(\frac{S_0+N}{2}, 0, \frac{S_0-N}{2}\right)$, P_{10} : $\left(0, \frac{S_0}{a_2+2}, \frac{S_0(a_2+1)}{a_2+2}\right)$, P_{11} : $\left(\frac{S_0+N(a_2+2)}{a_1a_2+a_1+a_2+3}, \frac{(a_1+1)S_0+N(a_1-1)}{a_1a_2+a_1+a_2+2}, \frac{(a_1a_2+a_2+1)S_0-N(a_1+a_2+1)}{a_1a_2+a_1+a_2+3}\right)$.

Using Theorems 3.1, 3.2 and 3.4 it can be shown that points P_1 and P_2 are complex (degenerate) stationary points; point P_3 is a saddle with two-dimension unstable subspace if $S_0/N \in (0, a_1+1)$, or two-dimension stable sub-space if $S_0/N \in (a_1+1, +\infty)$; point P_5 is a stable node if $S_0/N \in (0, (a_1+1)^{-1})$, a saddle with two-dimension stable subspace

if $S_0/N \in ((a_1+1)^{-1}, 1)$, and an unstable node if $S_0/N \in (1, +\infty)$; point P_6 is unstable node; point P_8 is stable node if $S_0/N \in \left((1+a_1)^{-1}, \frac{1+a_1+a_2)}{1+a_2+a_1a_2}\right)$, a saddle with two-dimension stable subspace if $S_0/N \in (0, (a_1+1)^{-1}) \cup \left(\frac{1+a_1+a_2)}{1+a_2+a_1a_2}, 1+a_1\right)$, and a saddle with two-dimension unstable subspace if $S_0/N \in (1+a_1, +\infty)$.

The Lyapunov method is used for definition of the type and stability of the last five stationary points: point P_7 is an unstable point; point P_{10} is a saddle with two-dimension unstable subspace if $\begin{cases} S_0/N \in \left(\frac{1-a_1}{1+a_1}, 1\right) \cup (1, +\infty), \\ a_1 \in (0,1), \end{cases} \cup \begin{cases} S_0/N \in (0,1) \cup (1, +\infty), \\ a_1 \in [1, +\infty), \end{cases}$ and a saddle with two-dimension stable subspace if $\begin{cases} S_0/N \in \left(0, \frac{1-a_1}{1+a_1}\right) \cup (1, +\infty), \\ a_1 \in (0,1), \end{cases}$ point P_{11} is a stable stationary point if $S_0/N \in \left(\frac{1+a_1+a_2}{1+a_2+a_1a_2}, 1+a_1+a_1a_2\right)$, an unstable point with two-dimension unstable subspace if $\begin{cases} S_0/N \in \left(0, \frac{1-a_1}{1+a_1}\right) \cup (1, +\infty), \\ a_1 \in (0,1), \end{cases}$ an unstable point with two-dimension stable subspace if $\begin{cases} S_0/N \in \left(\frac{1-a_1}{1+a_1}, \frac{1+a_1+a_2}{1+a_2+a_1a_2}\right), \\ a_1 \in (0,1), \end{cases} \cup$ $\begin{cases} S_0/N \in \left(0, \frac{1+a_1+a_2}{1+a_2+a_1a_2}\right), \\ a_1 \in [1, +\infty), \end{cases} \cup S_0/N \in (1+a_1+a_1a_2, +\infty)$; point P_4 is a stable stationary point if $S_0/N \in (1+a_1+a_1a_2, +\infty)$, and an unstable stationary point if $S_0/N \in (0, 1+a_1+a_1a_2)$.

The bifurcation diagram is shown in Figure 1 (a) , b)) on the basis of the analysis of stationary points. If $a_2 = 1$, the curve 3 and line 2 merge. Solid curves illustrate bifurcation values of parameters.

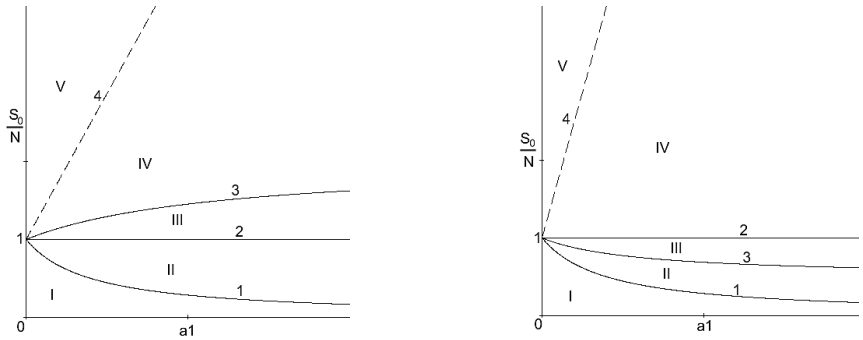

a) $a_2 \in (0,1)$ b) $a_2 \in (1, +\infty)$

Figure 1: Sections of the parametric surfaces $\left(1.S_0/N = (1+a_1)^{-1},\ 2.S_0/N = 1,\ 3.S_0/N = (1+a_1+a_2)/(1+a_2+a_1a_2),\ 4.S_0/N = 1+a_1+a_1a_2\right)$.

Point P_5 is a stable stationary point for the values of the parameters from region I ($0 < S_0/N < (1+a_1)^{-1}$). In this case the size of ecological niche is so small, that only one association is able to exist in the ecosystem. When $(1+a_1)^{-1} < S_0/N < \frac{1+a_1+a_2}{1+a_2+a_1a_2}$, point P_8 appears in the first octant (regions II and III in case a) or region II in case b)). In this case the second association can compete with the less demanding first one. If $S_0/N > \frac{1+a_1+a_2}{1+a_2+a_1a_2}$, the size of the ecological niche is so big, that three associations are

able to coexist in the biogeocoenose (region IV in case a) or regions III and IV in case b)). Note, that they use all resourses if $\frac{1+a_1+a_2}{1+a_2+a_1a_2} < S_0/N < 1+a_1+a_1a_2$ (point P_{11} is stable); there is an excess of resourses if $S_0/N > 1+a_1+a_1a_2$ (point P_4 is stable, region V). So, the appearance of each new association in the system corresponds to the bifurcation of the first octant of phase space. During the bifurcations the stationary points that correspond to the neighboring states of ecological systems, merge and "exchange stability".

6 Conclusion

The main focus in this paper is to study the evolution of biogeocoenose during primary succession. It can be seen from the study of two- and three-dimentional models that there are self-organizing processes in the system. When ecological niche reaches certain size (it is smaller than the limit of occurrence of resources excess), new association is included in the system. Thus, under the influence of the flow of matter and energy the ecosystem evolves. A control parameter is the size of the ecological niche.

Note that similar process is described in the papers on theoretical ecology [18]: first, poor soil is ocuppied by lichens, further by mosses, grass and etc. Moreover, climatic conditions determine the maximum number of primary succession stages and flora forms soil, and thus it determines the time of transition to a new stage.

Note that the described dynamics is typical for natural ecological systems: volcano in Kamchatka [13], sulfur deposits in Lviv region, Ukraine [6], coal mining dumps of Donetsk and Chervonograd industrial areas, Ukraine [4], wetland [24], Glacier Bay, Alaska [9].

Also we can observe a discrete change of state of the ecological system, although the process is described by the continuous model. Discreteness of the process is explained by the presence of bifurcation phenomena in nonlinear models.

References

[1] Aaviksoo, A. Simulating Vegetation Dynamics and Land Use in a Mire Landscape Using a Markov Model. *Landscape and Urban Planning* **31** (1995) 129–142.

[2] Aleksandrov, Yu.A., Chen Y. and Platonov A.V. Permanence and Ultimate Boundedness for Discrete-Time Swithed Model of Population Dynamics. *Nonlinear Dynamics and Systems Theory* **14** (1) (2014) 1–10.

[3] Andronov, A.A., Leontovich, E.A., Gordon, I.I. and Mayer, A.G. *Qualitative Theory of the Dynamic Systems of the Second Order*. Moscow: Mir, 1966. [Russian]

[4] Artamonov, V.M., Vartynova, O.A. and Zhukov, S.P. The comparative and ecological characteristics of coal mining dumps of Donetsk and Chervonogradska industry areas. *Problems of ecology* **1-2** (2008) 99–103. [Ukrainian]

[5] Bellefleur, P. Markov model of forest-type secondary succession in coastal British Columbia. *Canadian Journal of Forest Research* **11** (1) (1981) 18–29.

[6] Bilonoha, V.M. The dynamics of the individual parameters and population structure of the calamagrostis epigeios (L.) roth (poaceae) during the primary succession on excavated substrates by sulfur mining company in Lviv region. *Scientific Principles of Biodiversity Conservation* **10** (1) (2012) 31–40. [Ukrainian]

[7] Buzykin, A.I. *Modeling Elements of Forest Ecosystems.* Krasnoyarsk: V.N. Sukachev Institute of Forest and Wood, USSR Academy of Sciences, 1985. [Russian]

[8] Chakrabarti, C.G., Ghosh, S. and Bhadra, S. Non-equilibrium Thermodynamics of Lotka-Volterra Ecosystems: Stability and Evolution. *Journal of Biological Physics* **21** (1995) 273–284.

[9] Chapin, F.S., Walker, L.R., Fastie, C.L. and Sharman, L.C. Mechanisms of Primary Succession Following Deglaciation at Glacier Bay, Alaska. *Ecological Monographs* **64** (2) (1994) 149–175.

[10] Chernyshenko, S.V. *Nonlinear Analysis of Forest Ecosystems Dynamics.* Dnipropetrovsk: Dnipropetrovsk University Press, 2005. [Russian]

[11] Connell, J. and Slatyer, R. Mechanisms of succession in natural communities and their role in community stability and organization. *American Naturalist* **111** (1977) 1119–1143.

[12] Culver, D.C. 1981. On Using Horn's Markov Succession Model. *The American Naturalist* **117** (4) (1981) 572–574.

[13] Dirksen, V.G. and Dirksen, O.V. Reconstruction of Plant Recovery After Catastrophic Eruption of Kuril Lake-Ilinskaya 7700 ^{14C} Yrs BP in South Kamchatka *Bulletin of KRAUNTS. Series of earth science* **3** (2004) 57-85. [Russian]

[14] Eigen, M. and Schuster, P. *The Hypercycle. A Principle of Natural Self-organization* Springer-Verlag, Berlin, Heidelberg, New York, 1979.

[15] Guts, A.K. and Vololchenkova, L.A. *Cybernetics of Forest Ecosystems catastrophes.* Omsk: Publishing Center KAN, 2012. [Russian]

[16] Kogan, A.B., Naumov, N.P., Rezabek, B.G. and Chorajan, O.G. *Biological Cybernetics.* Moscow: Vysshaja shkola, 1977. [Russian]

[17] Kumar, R and Freedman H.I. Mathematical Analysis in a Model of Obligate Mutualism with Food Chain Populations. *Nonlinear Dynamics and Systems Theory* **2** (1) (2002) 25-44.

[18] Kuznetsov, A.E. and Gradova, N.B. *Scientific Basis of Ecobiotechnology* Moscow: Mir, 2006. [Russian]

[19] Leps, J. and Prach, K. A Simple Mathematical Model of the Secondary Succession of Shrubs. *Folia Geobotanica & Phytotaxonomica* **16** (1) (1981) 61–72.

[20] Lippe, E., De Smidt, J.T. and Glenn-Lewin, D.C.Markov Models and Succession: A Test from a Heathland in the Netherlands. *Journal of Ecology* **73** (3) (1975) 775–791.

[21] Liu, J., Chung, K.W. and Chan H.S.Y. An Ordinary Differential Equation Model of Succession of Korean Pine Broadleaf Forest. *Journal of Biological Systems* **5** (3) (1997) 375–388.

[22] Logofet, D.O. Markov chains as models of succession: a new perspective of the classical paradigm *Forestry* **2** (2010) 46–59.

[23] Logofet, D.O. and Lesnaya, E.V. The mathematics of Markov models: what Markov chains can really predict in forest successions. *Ecological Modelling* **126** (2000) 285–298.

[24] Noon, K.N. A model of created wetland primary succession *Landscape and Urban Planning* **34**,(2) (1996) 97–123.

[25] Rabvotnov, A.T. *Phytocenology.* Moscow: MGU Press, 1992. [Russian]

[26] Sukachev, V.N. *Bases of Forest Typology and Biogeocenology.* Leningrad: Nauka, 1972. [Russian]

[27] Sumina, O.I. Multivariate models of primary vegetation succession ecotopic on heterogeneous territories (illustrated career forest-tundra). *Advances in Current Natural Sciences* **11** (1) (2012) 112–116. [Russian]

[28] Tucker, B.C., and Anand, M. The Application of Markov Models in Recovery and Restoration. *International Journal of Ecology and Environmental Sciences* **30** (2004) 131–140.

[29] Weis, J.J., Cardinale,B.J., Forshay,K.J. and Ives,A.R. Effects of Species Diversity on Community Biomass Production Change Over the Course of Succession. *Ecology* **88** (2007) 929–939.

[30] Whittaker, R.H. A consideration of climax theory: The climax as population patterns. *Ecological Monographs* **21** (1) (1953) 41–78.

Nonlinear Dynamics and Systems Theory, **15** (4) (2015) 428–440

Observer Based Output Tracking Control for Bounded Linear Time Variant Systems

B. Iben Warrad, M.K. Bouafoura and N. Benhadj Braiek *

Laboratory of Advanced Systems, Polytechnic High School of Tunisia, University of Carthage, BP 743, 2078 La Marsa

Received: September 19, 2015; Revised: October 30, 2015

Abstract: In this paper, we propose a new approach to design a reduced observer based state feedback control for bounded linear time variant systems by means of shifted *Legendre* polynomials. The main objective is to force the controlled *LTV* system output to follow that of a linear reference model. On these grounds, augmented state modeling and useful Kronecker product properties are applied. Hence, an optimization problem is derived. Once the observation and control gains are determined by solving the latter problem, the stability of the closed loop system is checked through LMIs conditions. Simulation results illustrate the pertinence of the proposed method.

Keywords: *LTV systems; state observer; tracking; shifted Legendre polynomials, LMIs.*

Mathematics Subject Classification (2010): 93B50, 93C05.

1 Introduction

Modeling a physical process is a crucial step toward its analysis and adapted control synthesis. Indeed, the chosen mathematical model should be accurate enough in order to describe correctly dynamics of the system evolution. Moreover, most physical systems are described by nonlinear models which are not easy to study. A simplification alternative consists in linearizing the systems around some operating points, the procedure remains a very conservative approach. A global method consists in a linearization along a trajectory, that often leads to a linear time varying system (LTV) [2]. Thus, this type of models offer a good compromise between simplicity and ability to reproduce with fidelity the behavior of some real processes namely, highway vehicle [1], electronic circuit design [3] and biochemical systems [8]. Accordingly, several studies have focused on poles and zeros definition for these particular systems [4], also problems related to the controllability

* Corresponding author: mailto:Naceur.Benhadj@ept.rnu.tn

© 2015 InforMath Publishing Group/1562-8353 (print)/1813-7385 (online)/http://e-ndst.kiev.ua

and observability analysis [9], the identification [13,14], the stability analysis [7] and the control [11,12] of LTV systems have been the subject of many publications.

Orthogonal functions are a well developed mathematical tool for dynamic systems analysis and control. In fact, it had been firstly introduced for optimal control [6] and identification [16] of LTI systems. Lately, in literature there appeared extended works to cover nonlinear systems identification [20], stabilization analysis [27] and optimal control [25]. LTV systems have been also among the fields of application of that wise approximation tool, namely, for model order reduction [22], state analysis [23], identification [15] and optimal control [24]. Indeed, the projection of the state differential equation of the dynamic system over an orthogonal basis and introducing useful properties of the latter tool such as operational matrices jointly used with the *Kronecker* product may transform the time depending differential equation into stationary algebraic relations.

In this work, shifted Legendre polynomials are basically used to deduce an observer based state feedback control, the latter tool may have advantages over other orthogonal functions. This was shown by examples [16] where shifted Legendre polynomials converge to the exact solution of a differential equation faster than the other types of orthogonal functions, as, for example Walsh functions, Hermite and Laguerre polynomials. We underline that the derived control law has to ensure, not only stability but also a performance level dictated by a linear reference model used for tracking purposes, which is effectively the main contribution of the proposed study compared to major methods in literature which focused only on stabilization problem [17]. Consequently, a mathematical development will be exposed which is based on the use of interesting properties of shifted Legendre polynomials. The final result is given as a nonlinear criterion whose minimization with optimization Toolbox routines of MATLAB leads to the desired control gains. The last step is to check the asymptotic stability of the closed loop system through Bounded Real Lemma.

The paper is organized as follows. In Section 2, we introduce the studied systems and explain the main objective of the work. In Section 3, the proposed development for a reduced observer based control law applied to time variant linear systems using shift Legendre polynomials is carried out. In Section 4, stability analysis is handled using existing LMIs results for polytopic systems. In Section 5, the effectiveness of the developed method is checked out by a DC motor benchmark.

2 Problem Statement

In this work we consider the linear time variant system described by the following state equations:

$$\begin{cases} \dot{x}(t) = A(t)x(t) + B(t)u(t), \\ y(t) = Cx(t), \\ x(0) = x_0, \end{cases} \tag{1}$$

where $u \in \mathbb{R}^m$ is the control vector, $x \in \mathbb{R}^n$ is the state vector and $y \in \mathbb{R}^l$ is the output vector. Matrices $A(t)$, $B(t)$, C and the vector $x(t)$ have the following forms:

$$A(t) = \begin{bmatrix} A_{11}(t) & A_{12}(t) \\ A_{21}(t) & A_{22}(t) \end{bmatrix}, B(t) = \begin{bmatrix} B_1(t) \\ B_2(t) \end{bmatrix}, x(t) = \begin{bmatrix} x_1(t) \\ x_2(t) \end{bmatrix}, C = \begin{bmatrix} I_l & O_1 \end{bmatrix}$$

with

$$O_1 = 0(l, n-l), x_1(t) \in \mathbb{R}^l, B_1(t) \in \mathbb{R}^{l,m}.$$

System (1) matrices could be written as $\forall t \geqslant 0$, $A(t) = [a_{ij}(t)]$ and $B(t) = [b_{ij}(t)]$ and each term verifies the following boundedness:

$$\underline{a_{ij}} \leqslant a_{ij}(t) \leqslant \overline{a_{ij}} \quad and \quad \underline{b_{ij}} \leqslant b_{ij}(t) \leqslant \overline{b_{ij}}, \tag{2}$$

where $\underline{a_{ij}}$, $\underline{b_{ij}}$ and $\overline{a_{ij}}$, $\overline{b_{ij}}$ are some constant values corresponding respectively to the minimum and maximum of $a_{ij}(t)$ and $b_{ij}(t)$.

We assume that such system satisfies the controllability and observability conditions [9]. Our objective is then to design both reduced order observer and state feedback control law in order to ensure desired performances for the controlled system.

2.1 The state observer structure

We choose to design a reduced order observer which reproduces the non measurable state component $x_2(t)$. Such observer is then described by state model of the following form:

$$\begin{cases} \dot{w}(t) = (A_{22}(t) - L_r A_{12}(t))w(t) + (B_2(t) - L_r B_1(t))u(t) \\ +((A_{22}(t) - L_r A_{12}(t))L_r + (\bar{A}_{21}(t) - L_r A_{11}(t)))y(t), \\ \hat{x}_2(t) = w(t) + L_r y(t). \end{cases} \tag{3}$$

In these equations $w(t) \in \mathbb{R}^{n-l}$ is the state observer vector and $\hat{x}_2(t)$ is the observation of $x_2(t)$. L_r is the gain of the order observer.

Let us define the observation error by:

$$\varepsilon_r(t) = x_2(t) - \hat{x}_2(t). \tag{4}$$

It comes out then:

$$\dot{\varepsilon}_r(t) = \dot{x}_2(t) - \dot{\hat{x}}_2(t) = (A_{22}(t) - L_r A_{12}(t))\,\varepsilon_r(t). \tag{5}$$

The observation gain L_r is determined such that the observation error has the same dynamics as a chosen observation reference model described by a linear state equation

$$\dot{\varepsilon}_{r,ref}(t) = M_r \varepsilon_{r,ref}(t), \tag{6}$$

where M_r is a $((n-l) \times (n-l))$ matrix chosen such that the observer be faster than the controlled system.

2.2 Strategy of control

The control strategy that we plan to develop uses the desired output $y_c(t)$, measured and observed components of the state vector ($y(t)$ and $\hat{x}_2(t)$). It can be expressed in the following form:

$$u(t) = N y_c(t) - K_1 x_1(t) - K_2 \hat{x}_2(t) \tag{7}$$

with

$$N \in \mathbb{R}^{m \times m}, K_1 \in \mathbb{R}^{m \times l} \quad and \quad K_2 \in \mathbb{R}^{m \times (n-l)}.$$

We can express the control law by the following equation:

$$u(t) = N y_c(t) - K_1 x_1(t) - K_2 \hat{x}_2(t) = N y_c(t) - K_1 x_1(t) - K_2 x_2(t) + K_2 \varepsilon_r(t). \tag{8}$$

The gain matrices N, K_1 and K_2 are determined such that the controlled system presents the same behavior of a chosen reference linear model:

$$\begin{cases} \dot{z}(t) = Ez(t) + Fy_c(t), \\ y_r(t) = Gz(t), \end{cases} \tag{9}$$

where $y_c \in \mathbb{R}^m$ is the input vector, $z \in \mathbb{R}^r$ is the state vector and $y_r \in \mathbb{R}^l$ is the output vector.

3 Proposed Observation and Control Approach

By taking into account, equations (1) and (8), state variables could be written as folows:

$$\begin{cases} \dot{x}_1(t) = (A_{11}(t) - B_1(t)K_1)x_1(t) + (A_{12}(t) - B_1(t)K_2)x_2(t) + B_1(t)Ny_c(t) + B_1(t)K_2\varepsilon_r(t), \\ \dot{x}_2(t) = (A_{21}(t) - B_2(t)K_1)x_1(t) + (A_{22}(t) - B_2(t)K_2)x_2(t) + B_2(t)Ny_c(t) + B_2(t)K_2\varepsilon_r(t), \\ y(t) = x_1(t). \end{cases} \tag{10}$$

The augmented state is defined by the concatenation of states related to the original system and the observation error:

$$\tilde{x}(t) = \begin{bmatrix} x_1(t) \\ x_2(t) \\ \varepsilon_r(t) \end{bmatrix}.$$

Hence, equations of the closed loop system take the following form:

$$\begin{cases} \dot{\tilde{x}}(t) = \tilde{A}(t)\tilde{x}(t) + \tilde{B}(t)y_c(t), \\ \tilde{y}(t) = \tilde{C}\tilde{x}(t), \end{cases} \tag{11}$$

with

$$\tilde{A}(t) = \begin{bmatrix} \tilde{a}_{11} & \tilde{a}_{12} & \tilde{a}_{13} \\ \tilde{a}_{21} & \tilde{a}_{22} & \tilde{a}_{23} \\ 0(n-l,l) & 0(n-l,n-l) & \tilde{a}_{33} \end{bmatrix}, \tilde{B}(t) = \begin{bmatrix} B_1(t)N \\ B_2(t)N \\ O_2 \end{bmatrix}, \tilde{C} = \begin{bmatrix} I_l & O_3 \end{bmatrix},$$

where

$$\begin{array}{l} \tilde{a}_{11} = A_{11}(t) - B_1(t)K_1, \tilde{a}_{12} = A_{12}(t) - B_1(t)K_2, \tilde{a}_{21} = A_{21}(t) - B_2(t)K_1, \\ \tilde{a}_{22} = A_{22}(t) - B_2(t)K_2, \tilde{a}_{13} = B_1(t)K_2, \tilde{a}_{23} = B_2(t)K_2, \tilde{a}_{33} = A_{22}(t) - L_rA_{12}(t), \\ O_2 = 0(n-l,m), O_3 = 0(l,2(n-l)). \end{array}$$

The projection of the matrices $A_{11}(t)$, $A_{12}(t)$, $A_{21}(t)$, $A_{22}(t)$, $B_1(t)$ and $B_2(t)$ in a basis of $shifted$ Legendre polynomials truncated to an order N (See Section 7.3 of the Appendix) can be written as:

$$\begin{array}{l} A_{11}(t) = \sum\limits_{i=0}^{N-1} A_{11,iN}s_i(t), A_{12}(t) = \sum\limits_{i=0}^{N-1} A_{12,iN}s_i(t), A_{21}(t) = \sum\limits_{i=0}^{N-1} A_{21,iN}s_i(t), \\ A_{22}(t) = \sum\limits_{i=0}^{N-1} A_{22,iN}s_i(t), B_1(t) = \sum\limits_{i=0}^{N-1} B_{1,iN}s_i(t), B_2(t) = \sum\limits_{i=0}^{N-1} B_{2,iN}s_i(t). \end{array} \tag{12}$$

We can deduce now the projection of the matrice $\tilde{A}(t)$ and $\tilde{B}(t)$ in the same basis of shifted *Legendre* polynomials truncated to an order N, with:

$$\tilde{A}_{iN} = \begin{bmatrix} \tilde{a}_{11,iN} & \tilde{a}_{12,iN} & \tilde{a}_{13,iN} \\ \tilde{a}_{21,iN} & \tilde{a}_{22,iN} & \tilde{a}_{23,iN} \\ 0(n-l,l) & 0(n-l,n-l) & \tilde{a}_{33,iN} \end{bmatrix}, \tilde{B}_{iN} = \begin{bmatrix} B_{1,iN}N \\ B_{2,iN}N \\ O_2 \end{bmatrix},$$

where

$\tilde{a}_{11,iN} = A_{11,iN} - B_{1,iN}K_1, \tilde{a}_{12,iN} = A_{12,iN} - B_{1,iN}K_2, \tilde{a}_{21,iN} = A_{21,iN} - B_{2,iN}K_1,$
$\tilde{a}_{22,iN} = A_{22,iN} - B_{2,iN}K_2, \tilde{a}_{13,iN} = B_{1,iN}K_2, \tilde{a}_{23,iN} = B_{2,iN}K_2,$
$\tilde{a}_{33,iN} = A_{22,iN} - L_r A_{12,iN}.$

The control law defined by the equation (8) has to carry the dynamics of the closed loop system to reproduce as perfectly as possible that of a reference model which may be defined as follows:

$$\begin{cases} \dot{\tilde{z}}(t) = \tilde{E}\tilde{z}(t) + \tilde{F}y_c(t), \\ \tilde{y}_r(t) = \tilde{G}\tilde{z}(t), \end{cases} \tag{13}$$

with

$$\tilde{z} = \begin{bmatrix} z \\ \varepsilon_{ref} \end{bmatrix}, \tilde{E} = \begin{bmatrix} E & O_4 \\ O_4^T & M_r \end{bmatrix}, \tilde{F} = \begin{bmatrix} F \\ O_5 \end{bmatrix}, \tilde{G} = \begin{bmatrix} G & O_6 \end{bmatrix},$$

$O_4 = 0(n_r, n-l)$, $O_5 = 0(n-l, m)$ and $O_6 = 0(l, n_r + n - 2l)$, where n_r is the order of the reference model defined by the equation (9).

The integration of the equation (11) on the time interval $[0, t]$ leads to:

$$\tilde{x}(t) - \tilde{x}(0) = \int_0^t \tilde{A}(\tau)x(\tau)d\tau + \int_0^t \tilde{B}(\tau)y_c(\tau)d\tau, \tag{14}$$

where $\tilde{x}(0)$ denotes the initial conditions vector.

The projection of the state vector $\tilde{x}(t)$ and the order output $y_c(t)$ on the basis of shifted *Legendre* polynomials leads to:

$$\tilde{X}_N S_N(t) - \tilde{X}_{0N} S_N(t) = \int_0^t \sum_{i=0}^{N-1} \tilde{A}_{iN} s_i(t) \tilde{X}_N S_N(t) + \int_0^t \sum_{i=0}^{N-1} \tilde{B}_{iN} s_i(t) y_{cN} S_N(t) \tag{15}$$

Introducing now the product operational matrix (See Section 7.2 of Appendix) in equation (15) yields:

$$\tilde{X}_N S_N(t) - \tilde{X}_{0N} S_N(t) = \int_0^t \sum_{i=0}^{N-1} \tilde{A}_{iN} \tilde{X}_N M_i S_N(t) + \int_0^t \sum_{i=0}^{N-1} \tilde{B}_{iN} y_{cN} M_i S_N(t). \tag{16}$$

The use of the integration operational matrix (See Section 7.2 of the Appendix) yields:

$$\tilde{X}_N S_N(t) - \tilde{X}_{0N} S_N(t) = \sum_{i=0}^{N-1} \tilde{A}_{iN} \tilde{X}_N M_i P_N S_N(t) + \sum_{i=0}^{N-1} \tilde{B}_{iN} y_{cN} M_i P_N S_N(t). \tag{17}$$

Simplifying by the vector $S_N(t)$ and making use of the *vec* operator, which transforms a matrix structure into a vector one and the specific property [21]

$$vec(ABC) = \left(C^T \otimes A\right) vec(B), \tag{18}$$

equation (17) could be written as follows:

$$\begin{aligned} vec(\tilde{X}_N) - vec(\tilde{X}_{0N}) &= \sum_{i=0}^{N-1} \left((M_i P_N)^T \otimes \tilde{A}_{iN} \right) vec(\tilde{X}_N) \\ &+ \sum_{i=0}^{N-1} \left((M_i P_N)^T \otimes \tilde{B}_{iN} \right) vec(y_{cN}), \end{aligned} \tag{19}$$

it comes out:

$$vec(\tilde{X}_N) = \begin{bmatrix} \left[I_{((n-l)+n)\times N} - \sum_{i=0}^{N-1} \left((M_i P_N)^T \otimes \tilde{A}_{iN} \right) \right]^{-1} \times \\ \left[vec(\tilde{X}_{0N}) + \left[\sum_{i=0}^{N-1} \left((M_i P_N)^T \otimes \tilde{B}_{iN} \right) \right] vec(y_{cN}) \right] \end{bmatrix}. \tag{20}$$

In the same way the projection of the closed loop reference model (13), and the use of the operational matrix of integration yield:

$$vec(\tilde{Z}_N) = \begin{bmatrix} \left[I_{(n_r+(n-l))\times N} - \sum_{i=0}^{N-1} \left({P_N}^T \otimes \tilde{E} \right) \right]^{-1} \times \\ \left[vec(\tilde{Z}_{0N}) + \left[\sum_{i=0}^{N-1} \left({P_N}^T \otimes \tilde{F} \right) \right] vec(y_{cN}) \right] \end{bmatrix}. \tag{21}$$

The condition permitting to have a similar behavior of the controlled system (11) and reference model (13) can be written mathematically as follows:

$$\tilde{y}(t) = \tilde{y}_r(t) \Leftrightarrow \tilde{C}\tilde{X}(t) = \tilde{G}Z(t) \Leftrightarrow \left(I_N \otimes \tilde{C} \right) vec(\tilde{X}_N) = \left(I_N \otimes \tilde{G} \right) vec(\tilde{Z}_N). \tag{22}$$

It comes out:

$$\begin{aligned} &\begin{bmatrix} \left(I_N \otimes \tilde{C} \right) \left[I_{((n-l)+n)\times N} - \sum_{i=0}^{N-1} \left((M_i P_N)^T \otimes \tilde{A}_{iN} \right) \right]^{-1} \times \\ \left[vec(\tilde{X}_{0N}) + \left[\sum_{i=0}^{N-1} \left((M_i P_N)^T \otimes \tilde{B}_{iN} \right) \right] vec(y_{cN}) \right] \end{bmatrix} \\ &= \begin{bmatrix} \left(I_N \otimes \tilde{G} \right) \left[I_{(n_r+(n-l))\times N} - \sum_{i=0}^{N-1} \left({P_N}^T \otimes \tilde{E} \right) \right]^{-1} \times \\ \left[vec(\tilde{Z}_{0N}) + \left[\sum_{i=0}^{N-1} \left({P_N}^T \otimes \tilde{F} \right) \right] vec(y_{cN}) \right] \end{bmatrix}. \end{aligned} \tag{23}$$

Notice that

$$\tilde{Z}_{0N} = \begin{bmatrix} Z_{0N} \\ \varepsilon_{r,ref,0N} \end{bmatrix} = \begin{bmatrix} I_{n_r} \\ O_4^T \end{bmatrix} Z_{0N} + \begin{bmatrix} O_4 \\ I_{n-l} \end{bmatrix} \varepsilon_{r,ref,0N}$$

and

$$\tilde{X}_{0N} = \begin{bmatrix} X_{0N} \\ \varepsilon_{r,0N} \end{bmatrix} = \begin{bmatrix} X_{1,0N} \\ X_{2,0N} \\ \varepsilon_{r,0N} \end{bmatrix} = \begin{bmatrix} I_l \\ O_7 \end{bmatrix} X_{1,0N} + \begin{bmatrix} O_8 \\ I_{n-l} \\ O_9 \end{bmatrix} X_{2,0N} \begin{bmatrix} O_{10} \\ I_{n-l} \end{bmatrix} \varepsilon_{r,0N},$$

where $O_7 = 0(2(n-l), l)$,$O_8 = 0(l, n-l)$, $O_9 = 0(n-l, n-l)$ and $O_{10} = 0(n, n-l)$.

In order to simplify the control problem, let us consider null initial condition for the reference model ($Z_{0N} = 0$) and null initial condition for the measurable components state part ($X_{1,0N} = 0$).

Moreover, intial conditions of the observation error, which are a priori unkown, should meet those of the reference observation error model in order to minimize the distance between both models ($\varepsilon_{r,0N} = \varepsilon_{r,ref,0N}$). Consquently, equation (23) could be written as follows:

$$\left[\begin{array}{l} \left(I_N \otimes \tilde{C}\right)\left[I_{((n-l)+n)\times N} - \sum_{i=0}^{N-1}\left((M_i P_N)^T \otimes \tilde{A}_{iN}\right)\right]^{-1} \times \\ \left[\begin{array}{l} \left(I_N \otimes \begin{bmatrix} O_8 \\ I_{n-l} \\ O_9 \end{bmatrix}\right) vec(X_{2,0N}) + \left(I_N \otimes \begin{bmatrix} O_{10} \\ I_{n-l} \end{bmatrix}\right) vec(\varepsilon_{r,ref,0N}) \\ + \left[\sum_{i=0}^{N-1}\left((M_i P_N)^T \otimes \tilde{B}_{iN}\right)\right] vec(y_{cN}) \end{array}\right] \end{array}\right] = \tag{24}$$

$$\left[\begin{array}{l} \left(I_N \otimes \tilde{G}\right)\left[I_{(n_r+(n-l))\times N} - \sum_{i=0}^{N-1}\left({P_N}^T \otimes \tilde{E}\right)\right]^{-1} \times \\ \left[\left(I_N \otimes \begin{bmatrix} O_4 \\ I_{n-l} \end{bmatrix}\right) vec(\varepsilon_{r,ref,0N}) + \left[\sum_{i=0}^{N-1}\left({P_N}^T \otimes \tilde{F}\right)\right] vec(y_{cN})\right] \end{array}\right].$$

The relation (24) can be written as:

$$\Delta_1 vec(y_{cN}) + \Delta_2 vec(X_{2,0N}) + \Delta_3 vec(\varepsilon_{r,ref,0N}) = 0, \tag{25}$$

where

$$\Delta_1 = \left[\begin{array}{l} \left[\begin{array}{l} \left(I_N \otimes \tilde{C}\right)\left[I_{((n-l)+n)\times N} - \sum_{i=0}^{N-1}\left((M_i P_N)^T \otimes \tilde{A}_{iN}\right)\right]^{-1} \times \\ \left[\sum_{i=0}^{N-1}\left((M_i P_N)^T \otimes \tilde{B}_{iN}\right)\right] \end{array}\right] \\ -\left[\left(I_N \otimes \tilde{G}\right)\left[I_{(n_r+(n-l))\times N} - \sum_{i=0}^{N-1}\left({P_N}^T \otimes \tilde{E}\right)\right]^{-1}\left[\sum_{i=0}^{N-1}\left({P_N}^T \otimes \tilde{F}\right)\right]\right] \end{array}\right],$$

$$\Delta_2 = \left[\left(I_N \otimes \tilde{C}\right)\left[I_{((n-l)+n)\times N} - \sum_{i=0}^{N-1}\left((M_i P_N)^T \otimes \tilde{A}_{iN}\right)\right]^{-1}\left(I_N \otimes \begin{bmatrix} O_8 \\ I_{n-l} \\ O_9 \end{bmatrix}\right)\right],$$

$$\Delta_3 = \left[\begin{array}{l} \left[\left(I_N \otimes \tilde{C}\right)\left[I_{((n-l)+n)\times N} - \sum_{i=0}^{N-1}\left((M_i P_N)^T \otimes \tilde{A}_{iN}\right)\right]^{-1}\left(I_N \otimes \begin{bmatrix} O_{10} \\ I_{n-l} \end{bmatrix}\right)\right] \\ -\left[\left(I_N \otimes \tilde{G}\right)\left[I_{(n_r+(n-l))\times N} - \sum_{i=0}^{N-1}\left({P_N}^T \otimes \tilde{E}\right)\right]^{-1}\left(I_N \otimes \begin{bmatrix} O_4 \\ I_{n-l} \end{bmatrix}\right)\right] \end{array}\right]$$

In order to verify such relation for any initial conditions $X_{2,0N}$, $\varepsilon_{r,ref,0N}$ and for any output order y_{cN}, we must ensure:

$$\Delta_1 = 0, \quad \Delta_2 = 0 \quad \textit{and} \quad \Delta_3 = 0.$$

However, these conditions could not be totally realized. Hence, we have to look for a pseudo-solution of this problem by minimizing the norms of matrices Δ_1, Δ_2 and Δ_3, denoted respectively δ_1, δ_2 and δ_3, using optimization MATLAB routines.

4 Stability Analysis of Closed Loop System

Once observation control parameters L_r, N, K_1 and K_2 are determined, the LTV model defined by the equation (11) can be expressed in the following polytopic form such as $\mathrm{M} = \left[\tilde{\mathrm{A}} \middle| \tilde{\mathrm{B}}\right]$ belongs to a polytope of matrices M defined by [5]:

$$M = \left\{ \mathrm{M} = \left[\tilde{A}(\theta) \middle| \tilde{B}(\theta)\right] / M(\theta) = \sum_{i=1}^{v} \left(\theta_i \left[\tilde{A}_i \middle| \tilde{B}_i\right]\right) \right\},$$

where

$$\theta \in \Theta = \left\{ \theta = \begin{bmatrix} \theta_1 \\ \theta_2 \\ \vdots \\ \theta_v \end{bmatrix} / \sum_{i=1}^{v} \theta_i = 1 \right\}.$$

The closed loop system (11) is mean square asymptotically stable with an H_∞ disturbance attenuation γ if and only if there exists a $(n + (n-l)) \times (n + (n-l))$ matrix $P \succ 0$ such that $i = 1 \ldots v$, [10]:

$$\begin{bmatrix} \tilde{A}_i^T P + P\tilde{A}_i & P\tilde{B}_i & \tilde{C}^T \\ \tilde{B}_i^T P & -\gamma^2 I_m & 0 \\ \tilde{C} & 0 & -I_p \end{bmatrix} \prec 0. \tag{26}$$

5 Simulation Example

Let us consider the separated excitation DC motor described by the following equation [26]:

$$\begin{cases} \frac{d\Omega(t)}{dt} = -\frac{f\Omega(t)}{J} + \frac{K_m \Phi(t) I(t)}{J}, \\ \frac{dI(t)}{dt} = -\frac{K_e \Phi(t)\Omega(t)}{L} - \frac{RI(t)}{L} + \frac{V(t)}{L}, \\ x(0) = \begin{bmatrix} 0 & 0.2 \end{bmatrix}^T, \end{cases}$$

where $y = \Omega(t)$ denotes rotational speed of rotor as measured output, $I(t)$ and $V(t)$ are respectively the current and voltage of rotor, $\Phi(t)$ is the rotor flux. For this example, we will assume the values for the physical parameters given in Table 1.

The rotor flux is considered as a time depending function defined by the following relation:

$$\Phi(t) = \Phi_0(1 + 0.1\sin(\pi t))$$

with $\Phi_0 = 1$.

The considered reference model of the controlled system is a second order system characterized by the following parameter matrices:

$$E = \begin{bmatrix} -10.5 & -2.4 \\ 2 & -14.75 \end{bmatrix}, F = \begin{bmatrix} 0 \\ 1.5 \end{bmatrix}, G = \begin{bmatrix} 0 & 10.15 \end{bmatrix}.$$

The reference model of the observation error is characterized by the matrix:

$$M_r = -5.$$

Table 1: Motor parameters.

L: rotor inductance	0.5 H
R: rotor resistance	2 Ω
K_e: electromotive force against	0.1 $NmWb^{-1}A^{-1}$
K_m: electromagnetic torque	0.1 $NmWb^{-1}A^{-1}$
J: rotor and load inertias	0.006 $kgm^{-2}s^{-2}$
f: viscous friction coefficient	0.01 Nms

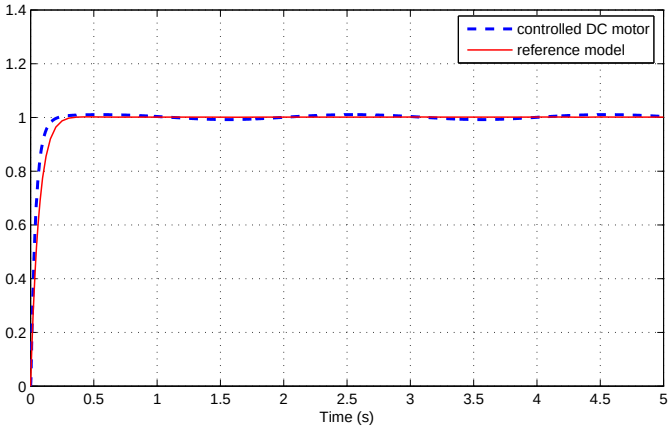

Figure 1: Step response of controlled DC motor and the considered reference model.

For N = 10 (number of elementary SLPs functions) and T=5s, the obtained control gains are the following:

$$N = 175.3, \quad K_1 = 158.6, \quad K_2 = 160.5, \quad \mathrm{L_r} = 1.8.$$

The norms of matrices Δ_1, Δ_2 and Δ_3 are given by the following:

$$\delta_1 = 0.0446, \quad \delta_2 = 0.0298, \quad and \quad \delta_3 = 0.0335.$$

Figure 1 illustrates step responses of controlled DC motor and the considered reference model over an interval $[0, T]$. Figure 2 shows the free motion of the current of rotor and the observer. The asymptotic stability with an H_∞ disturbance attenuation γ of the closed loop system is verified by the feasible solution of the LMI defined in relation (26). Obtained LMI variables were:

$$\gamma = 2.3547,$$

$$P = \begin{bmatrix} 0.8258 & 0.0418 & 0.0278 \\ 0.0418 & 0.0114 & 0.0048 \\ 0.0278 & 0.0048 & 0.0100 \end{bmatrix}.$$

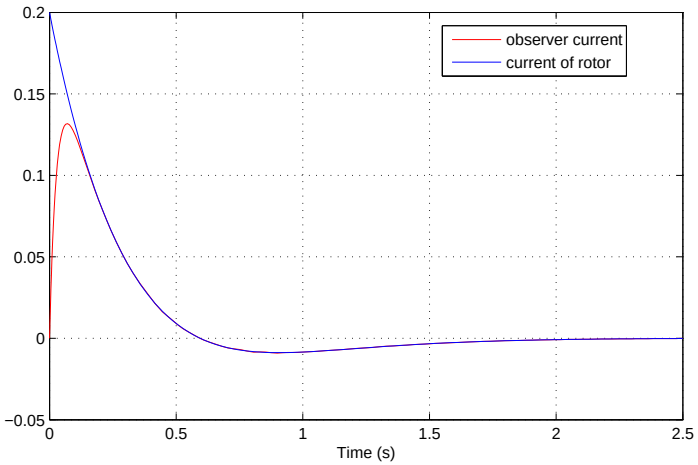

Figure 2: Free motion of the current of rotor and the observer.

6 Conclusions

In this paper, a new analytical approach was introduced for the synthesis of a reduced observed feedback control for linear time variant systems by using shift Legendre polynomials as an approximation tool. The use of the operational matrix of integration and operational matrix of product has allowed the transformation of differential equations into algebraic ones depending on gains of regulators. The main contribution of the paper can be summarized as the system performance guaranty jointly with stability which is obviously ensured. This is done by tracking a linear reference model. The effectiveness of the developed method is checked out by a DC motor benchmark. The simulations results obtained show clearly the accuracy of the synthesized control law. In future works, we intend to extend our development to handle the synthesis of observed state feedback control for nonlinear systems via orthogonal functions.

7 Appendix

7.1 Legendre polynomials

Legendre polynomials denoted by LPs in litterature, have been the most used ones in continuous control problems due to their high accuracy and a unit weighting function. That is why we use them in our work. They are defined over the time interval $\tau \in [-1, 1]$ and given by the recursive formula [18]:

$$(n+1)\,P_{n+1}(\tau) = (2n+1)\,\tau P_n(\tau) - nP_{n-1}(\tau),\ \ for \quad n = 1, 2, \cdots \tag{27}$$

with $P_0(\tau) = 1$ and $P_1(\tau) = \tau$.

In order to obtain orthogonal Legendre polynomials on the interval $[0, t_f]$, the following change of variable is performed:

$$\tau = \frac{2t}{t_f} - 1 \quad with \quad 0 \leq t \leq t_f \tag{28}$$

for $0 \leq t \leq t_f$, the shifted Legendre polynomials, denoted by SLPs, $s_n(t)$ are thus given by:

$$(n+1)\, s_{n+1}(t) = (2n+1)\left(\frac{2t}{t_f} - 1\right) s_n(t) - n s_{n-1}(t) \tag{29}$$

with $s_0(t) = 1$ and $s_1(t) = \frac{2t}{t_f} - 1$.

The principle of orthogonality of shifted Legendre polynomials is expressed by the following equation [19]:

$$\int_0^{t_f} s_i(t) s_j(t) dt = \frac{t_f}{2i+1} \delta_{ij}. \tag{30}$$

So, any integrable function on $0 \leq t \leq t_f$ can be developed into a series of shifted Legendre polynomials with a truncation to an order N under the following relation:

$$f(t) \cong \sum_{i=0}^{N-1} f_i s_i(t) = F_N S_N(t) \tag{31}$$

with

$$F_N = \left[\begin{array}{cccc} f_0 & f_1 & \cdots & f_{N-1} \end{array} \right]$$

and

$$S_N(t) = \left[\begin{array}{cccc} s_0(t) & s_1(t) & \cdots & s_{N-1}(t) \end{array} \right]^T.$$

7.2 Operational matrices

In the SLPs case, the operational matrix of integration P_N could be built through the following recurrent relation:

$$\int_0^t s_n(\tau) d\tau = \frac{t_f}{2} \times \frac{1}{2n+1} (s_{n+1}(t) - s_{n-1}(t)) \tag{32}$$

and

$$\int_0^t s_0(\tau) d\tau = \frac{t_f}{2} (s_0(t) + s_1(t)). \tag{33}$$

Hence, the following algebraic relation for integral calculus could be stated:

$$\int_0^t S_N(t) dt \cong P_N S_N(t). \tag{34}$$

The operational vectors of product K_{ij} have constant coefficients and verify the property [20]:

$$\forall i, j \in \{0, 1, \ldots, N-1\}, s_i(t) s_j(t) \cong K_{ij}^T S_N(t). \tag{35}$$

From the relationship (35), we can readily get the operational matrix of product:

$$M_{iN} = \left[\begin{array}{c} K_{i,0}^T \\ \vdots \\ K_{i,N-1}^T \end{array} \right] \tag{36}$$

that allows the approximation:

$$s_i(t)S_N(t) \cong M_{iN}S_N(t). \tag{37}$$

7.3 Matrix functions approximation

Any time dependent matrix function $A(t) \in \mathbb{R}^{n\times m}$ given by $A(t) = [a_{ij}(t)]$ where $a_{ij}(t)$ are integrable over an interval $0 \leq t \leq t_f$ can be developed into a series of shifted Legendre polynomials with a truncation to an order N under the following relation:

$$A(t) \cong \sum_{i=0}^{N-1} A_{iN}s_i(t), \tag{38}$$

where $A_{iN} \in \mathbb{R}^{n\times m}$ for $i \in \{0, 1, ..., N-1\}$ are matrices with constant coefficients.

References

[1] Benton, R.E. and Smith, D. A static-output-feedback design procedure for robust emergency lateral control of a highway vehicle. *IEEE Transactions on Control Systems Technology* **13** (2005) 618–623.

[2] Marinescu, B. Output feedback pole placement for linear time-varying systems with application to the control of nonlinear systems. *Automatica* **64** (2010) 1524–1530.

[3] Darabi, H. Ibrahim, B. and Rofougaran, A. An analog GFSK modulator in 0.35-μ m CMOS. *IEEE Journal of Solid-State Circuits* **39** (2004) 2292–2296.

[4] Marinescu, B. and Bourlès, H. An intrinsic algebraic setting for poles and zeros of linear time-varying systems. *Systems & Control Letters* **58**(4) (2009) 248–253.

[5] Bosche, J. and El Hajjaji, A. An Output Feedback Controller Design for Lateral Vehicle Dynamic. *The International Federation of Automatic Control*, Seoul, Korea, 2008, 6–11.

[6] Chen, CF. and Hsiao, CH. Design of piecewise constant gains for optimal control via Walsh functions. *IEEE Trans. Automatic Control* **20**(5) (1975) 596–603.

[7] Pastravanu, O. and Matcovschi, M.H. Linear time-variant systems: Lyapunov functions and invariant sets defined by Holder norms. *Journal of the Franklin Institute* **347** (2010) 627-640.

[8] Zak, D.E. Stelling, J. and Doyle III, F.J. Sensitivity analysis of oscillatory (bio)chemical systems. *Computers and Chemical Engineering* **29** (2005) 663–673.

[9] Silverman, L.M. and Meadows, H.E. Controllability and observability in time-variable linear systems. *SIAMJ Control and optimization* **5** (1967) 64–73.

[10] Boyd, D. El Ghaoui, L. Peron, E. and Bala-krishnan, V. Linear Matrix Inequalities in System and Control Theory. *SIAM Society for Industrial and Applied Mathematics*, Philadelphia, 1994.

[11] Amato, F. Mattei, M. and Pironti, A. Solution of the state feedback singular H^∞ control problem for linear time-varying systems. *Automatica* **36** (2000) 1469–1479.

[12] Marino, R. and Tomei, P. Adaptive control of linear time-varying systems. *Automatica* **39** (2003) 651–659.

[13] Maciej, N. Identification of time-varying systems with abrupt parameter changes. *Automatica* **30** (1994) 447–459.

[14] Lozano, R. Dimogianopoulos, D. and Mahony, R. Identification of linear time-varying systems using a modified least-squares algorithm. *Automatica* **36** (2000) 1009–1015.

[15] Mouroutsos, S.G. and Paraskevopoulos, P.N. Identification of time-varying linear systems using orthogonal functions. *Journal of the Franklin Institute* **320** (1985) 249–258.

[16] Paraskevopoulos, P.N. Legendre series approach to identification and analysis of linear systems. *IEEE Trans. Automatic Control* (1985) 585–589.

[17] Zhoua, B. Caib,G.B. and Duana, G.R. Stabilisation of time-varying linear systems via Lyapunov differential equations. *Int. J. Control* **86** (2003) 332–347.

[18] Gradshteyn, I.S. and Ryzhik, I.M. Tables of Integrals, Series and Products, New York, *Academic Press*, 1979.

[19] Hwang, C. and Guo, T.Y. Transfer Function Matrix Identification in MIMO Systems via Shifted Legendre Polynomials. *Int. J. Control* **39** (1984) 807–814.

[20] Rottela, F. and G. Dauphin-Tanguy, G. Non-linear systems identification and optimal control. *Int. J. Control* **48** (1988) 525–544.

[21] Brewer, J.W. Kronecker products and matrix calculus in systems theory. *Trans. IEEE Circ. and Syst. CAS* **48** (1978).

[22] Ayadi, B. and Benhadj Braiek, N. Orthogonal Functions Approach for Model Order Reduction of LTI and LTV Systems. *Nonlinear Dynamics and Systems Theory* **13** (2013) 115–134.

[23] Hsiao, C. and Wang, W. State analysis and optimal control of linear time-varying systems via Haar wavelets. *Optimal Control Applications and Methods* **19** (1998) 423–433.

[24] Razzaghi, M. Optimal control of linear time-varying systems via Fourier series. *Journal of Optimization Theory and Applications* **65** (1990) 375–384.

[25] Mohan, B. M. and Sanjeeb Kumar Kar, Optimal Control of Nonlinear Systems via Block Pulse Functions and Legendre Polynomials. *Differential Equations and Dynamical Systems* **20** (2012) 149–159.

[26] Rotella, F. Ayadi, M. and Carrillo, F.J. Control and trajectory tracking by flatness of a time-variant stator flux motor. *Control Applications. Proceedings of the 2002 International Conference* **1** (2002) 102–107.

[27] Belhaouane, M.M. and Benhadj Braiek, N. Design of Stabilizing Control for Synchronous Machines via Polynomial Modelling and Linear Matrix Inequalities Approach. *International Journal of Control, Automation, and Systems – IJCAS* **9** (3) (2011) 425–436.

Nonlinear Dynamics and Systems Theory, **15** (4) (2015) 441–442

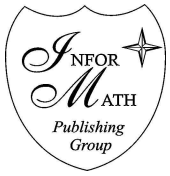

Contents of Volume 15, 2015

© 2015 InforMath Publishing Group/1562-8353 (print)/1813-7385 (online)/http://e-ndst.kiev.ua

Volume 15 **Number 3** **March 2015**

Volume 15 **Number 4** **March 2015**

CAMBRIDGE SCIENTIFIC PUBLISHERS

AN INTERNATIONAL BOOK SERIES
STABILITY OSCILLATIONS AND OPTIMIZATION OF SYSTEMS

Stability Analysis of Nonlinear Systems under Structural Perturbations
Stability, Oscillations and Optimization of Systems: 2014, Volume 8, 252 pp.
ISBN 978-1-908106-37-7 £55 /$100 /€ 80

A.A. Martynyuk
Institute of Mechanics, National Academy of Sciences of Ukraine, Kyiv, Ukraine
V.G. Miladzhanov
Andizhan University, Andizhan, O'zbekiston

This book focuses on some problems of stability theory of nonlinear large-scale systems. The purpose of this book is to describe some new applications of Liapunov matrix-valued functions method to the stability of evolution problems governed by nonlinear continuous systems, discrete-time systems, impulsive systems and singularly perturbed systems under nonclassical structural perturbations. The authors take a challenging and original approach based on concept of structural perturbations combined with direct Liapunov's method. This new approach will lead to results that cannot be obtained by standard theories of stability in the field.

The **Stability Analysis of Nonlinear Systems under Structural Perturbations** addresses to specialists in dynamical systems, applied differential equations, and the stability theory. It may be useful for graduated students in mathematics, control theory, and mechanical engineering.

CONTENTS

Please send order form to:
Cambridge Scientific Publishers
PO Box 806, Cottenham, Cambridge CB4 8RT Telephone: +44 (0) 1954 251283
Fax: +44 (0) 1954 252517 Email: janie.wardle@cambridgescientificpublishers.com
Or buy direct from our secure website: www.cambridgescientificpublishers.com